Title
Molecular Organic Geochemical Records of Late Ordovician Biospheric Evolution

Author
Rohrssen, Megan

Publication Date
2013

Peer reviewed|Thesis/dissertation

UNIVERSITY OF CALIFORNIA
RIVERSIDE

Molecular Organic Geochemical Records of Late Ordovician Biospheric Evolution

A Dissertation submitted in partial satisfaction
of the requirements for the degree of

Doctor of Philosophy

in

Geological Sciences

by

Megan Kimberly Rohrssen

December 2013

Dissertation Committee:

Dr. Gordon D. Love, Chairperson
Dr. Timothy W. Lyons
Dr. Woodward W. Fischer

The Dissertation of Megan Kimberly Rohrssen is approved:

Committee Chairperson

University of California, Riverside

Acknowledgments

Thank you, Gordon for introducing me to this field, in all its potential and pitfalls, and for giving me tools to work in it.

Thank you to my committee members Tim Lyons and Woody Fischer, and co-authors David Fike and Seth Finnegan. Anything written here that's worth reading probably is so because of your help. I am grateful to the entire faculty in UCR Earth Sciences for helping build such a positive environment, and for being so generous with your time and knowledge.

Thank you Chao Li for so much patience in helping me grow less afraid of breaking things by teaching me to fix them. Mark Williams, thank you for putting up with my novice mentorship at the beginning and dissertation angst towards the end. Thanks, Steve Bates for all the help with the lab, like figuring out the dozen ways to break a rock powdering machine. Thank you Lidya Tarhan, Lucas Joel, Natascha Riedinger, Kayla Kroll, Jacqui Gilchrist, Eli Brewer, Julian Lozos, Cassy Rose, Amy Kelly, Corrie Neighbors, Kenny Ryan, Leanne Hancock, Robyn Dahl, Sarah Henry, and Joanna Oseguera for comradeship, commiseration, and occasional cat-sitting. Thank you Carina Lee and Emily Haddad (and Alex Zumberge, even though you just started!) for taking over the lab so ably. Thank you Rosemarie Bisquera and Daniel Garson for help with lab work.

Thank you Louise DeHayes, John Herring, Jennifer Reising, Laurie Graham, RC Sutton, Melody Powell, and Sheila Mabee for somehow keeping the department running despite our best efforts, including but not limited to garbled purchase orders, forgotten forms, and stomping on giant bubble wrap while you were trying to work. Thank you Paula Matheus-Carnevali, Alison Murray, Kevin Hand, Dan Berisford and

the whole Icy Worlds field team. Thank you to Max Coleman and Ben Brunner for introducing me to UCR, which wouldn't have happened if not for that SURF way back when.

Thank you SoCal Ultimate community (especially Riverside pick-up/Inland Empire Strikes Back, and the ladies of Viva) for introducing me to silly games and Korean BBQ, for friendship and something to do besides work. Thank you, Harrisons, for accepting me from the start, and for all the unsolicited advice.

To my parents, grandparents, and family: nature or nurture, it's all your fault.

To Benjamin.

Finally, C.O. One of us needed to stay near home. I think you got the harder job.

Thank you.

ABSTRACT OF THE DISSERTATION

Molecular Organic Geochemical Records of Late Ordovician Biospheric Evolution

by

Megan Kimberly Rohrssen

Doctor of Philosophy, Graduate Program in Geological Sciences
University of California, Riverside, December 2013
Dr. Gordon D. Love, Chairperson

Lipid biomarkers are recalcitrant organic natural products that have potential to provide information about the major contributors to sedimentary organic matter in past environments, about geochemical conditions during deposition, and about the thermal history of rocks. Because tiny, non-mineralizing cells of microbes and of Paleozoic primary producers have low fossilization potential, lipid biomarkers are one of the few ways to acquire information about the base of marine food webs in deep time. Further, the intricate linkages between microbial communities and environmental conditions (nutrients, dissolved oxygen) provide greater context for interpreting the macrofossil record.

The Late Ordovician has received the most attention as a mass extinction linked to climate change. We compiled stratigraphic lipid biomarker records of microbial communities to better understand both the baseline and response to changing environmental conditions in the Late Ordovician. This information will be of use in assessing the causes of climatic change, extinction, and impacts of inferred cooling on marine geochemistry.

We present results from thermally well-preserved strata from the Laurentian Taconic foreland (Anticosti Island), mid-continent (Cincinnati Arch, eastern Iowa), and

western continental margin (Vinini Formation), as well as the Baltic shelf (Estonia, Sweden). Lipid biomarker distributions, primarily hopane/sterane ratios, document strong relationships between nutrient availability and the balance of primary production between bacteria and algae, with bacteria favored in oligotrophic waters and algae predominating in waters influenced by upwelling or runoff. The Hirnantian glacial maximum presents both spikes in hopane/sterane and a decrease in average ratio below the pre-Hirnantian mean, perhaps related to disruption of eukaryotic productivity and increased nutrient availability, respectively. Compounds derived from aerobic methanotrophic bacteria (3β-methylhopane) occur in high relative abundance across the paleotropics throughout the studied interval. The positive relationship between aerobic methanotroph markers and paleotemperature proxies implies increased methane cycling during warm intervals, an important positive feedback on climate during extended intervals of Early Paleozoic time.

Contents

List of Figures

List of Tables

Chapter 1

Introduction

1.1 The Late Ordovician Glacial Maximum and Mass Extinction

Interest in climate change has risen dramatically over the past few decades with recognition of anthropogenic CO_2 as a driver of climate. Marine ecosystems and nutrient cycles are expected to change with higher pCO_2 and warmer temperatures, due to several factors including ocean acidification, inhibition of nitrification at lower pH, reduced solubility of gasses at higher temperature, and increased activity of microorganisms at higher temperatures. However the nature of, and interactions among, those changes is difficult to predict either through modeling or laboratory-scale experiments. Fortunately, crustal rocks record outcomes of ancient global-scale climate changes with which to test hypotheses regarding relationships between climate, nutrient cycles, and the biosphere that goes back at least 600 million years. One period of Earth's history that is likely to prove very informative with respect to the effects of climate change is the Late Ordovician, approximately 450 to 443 Ma.

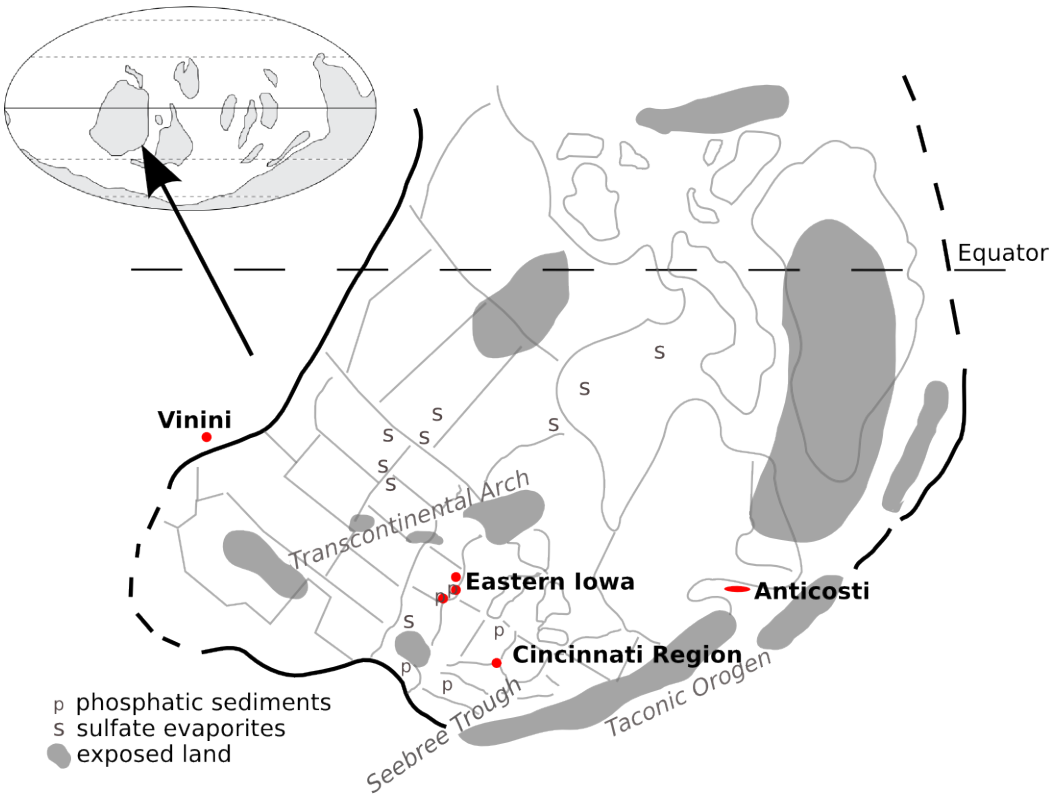

Figure 1.1: Map of Late Ordovician paleogeography, inset modified from Cocks and Torsvik (2002) and Laurentia map modified from Raatz and Ludvigson (1996).

Ordovician climate was long thought to be predominantly warm due to high pCO_2 (Berner and Kothavala, 2001; Yapp and Poths, 1992), although sedimentological (e.g. Frakes et al., 1992), inorganic and organic geochemical evidence support earlier, Middle to Late Ordovician age cooling (Came et al., 2007; Trotter et al., 2008; Finnegan et al., 2011), and pCO_2 at the lower end of Berner's carbon mass balance modeling (5-8x PAL, Pancost et al., 2013). In either case, Ordovician seas were significantly different from modern: atmospheric oxygen was likely still much lower than present-day, dissolved inorganic oxidant availability (i.e. sulfate) remained low relative to modern levels (Gill et al., 2007) and a large proportion of continental landmass was covered by shallow seas (Fig. 1.3). The combination of warm temperatures, extensive epeiric seas, and low dissolved inorganic oxidant concentrations likely made intervals of the Late Ordovician predisposed to the development of quasiestuarine circulation and formation of extensive oxygen minimum zones (OMZs) (e.g. Witzke, 1987). Enhanced denitrification within Late Ordovician OMZs may have driven nitrogen limitation of marine ecosystems (Finney et al., 2007; LaPorte et al., 2008; but see also Saltzman at a., 2005) in addition to possible direct effects of low sulfate availability (Ratti et al., 2011). If reduced seawater pH due to elevated pCO_2 inhibits nitrification (Beman et al., 2011), this may have further compounded nitrogen limitation in Lower Paleozoic marine realms. Limiting nutrients may have switched to phosphorous-limitation during intervals characterized by carbon isotope volatility and perhaps cooler global conditions (e.g. Saltzman, 2005). Information about microbial community structure during the Lower Paleozoic warm periods should reflect a stable, warm, low-oxidant regime that may be applicable to other periods in Earth's history such as the Cenozoic hot-house to ice-house transition or Cretaceous ocean anoxic events.

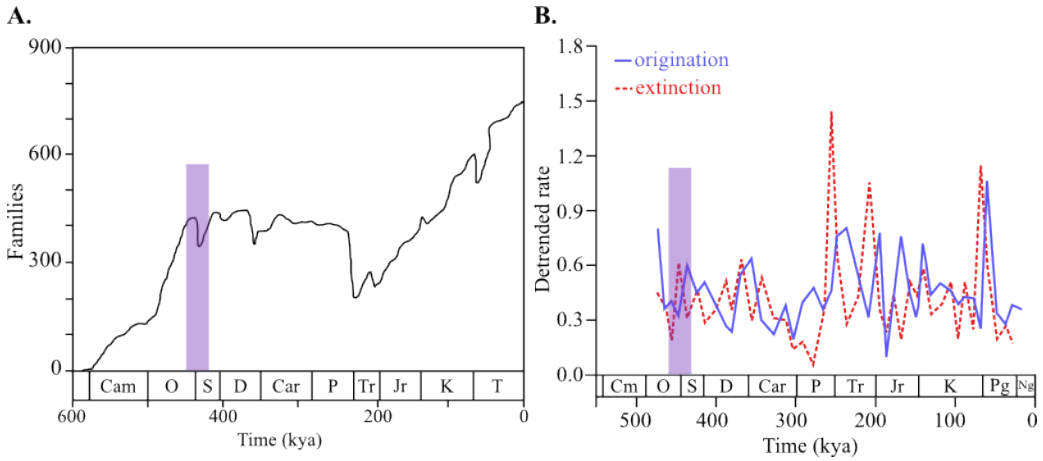

Figure 1.2: Figure 1.4. A. Phanerozoic marine invertebrate families (modified from Raup and Sepkoski, 1982) and B. detrended Phanerozoic origination and extinction rates (modified from Alroy, 2008). The Late Ordovician - Early Silurian in both figures is highlighted by the vertical purple bar.

The Middle Ordovician "hothouse" was moderated by Late Ordovician cooling, the extent and timing/episodicity of which are becoming more apparent (Melchin et al., 2013). Recent recalibration of the Ordovician timeseries and integration with carbon isotope data hint at parallels in the rate of change between Late Ordovician cooling and the late Cenozoic greenhouse to icehouse transition (Smith et al., 2011). Unlike the late Cenozoic, growth and retreat of extensive continental ice sheets at high southern latitude in the Hirnantian (444.68 - 443.41Ma, GTS 2009) (Sadler et al. 2009; Brenchley et al., 1994; Finnegan et al., 2011) was accompanied by the two-phased extinction of an estimated 84 percent of marine invertebrate species (Figure 1.4; Raup and Sepkoski, 1982; Hallam and Wignall, 1997) and a positive carbon isotope excursion of 3-6 permil (Hirnantian Isotopic Carbon Excursion, HICE, Brenchley et al., 1994). Glacio-eustatic regression had particularly strong impact on both the habitat and fossil record of marine organisms in epeiric seas and compounded environmental (temperature, transgression of anoxic bottom water) forcings in driving a "common cause" for the Late Ordovician mass extinction (Finnegan et al., 2011). The Late Ordovician and Early-Middle Silurian

remain periods of elevated extinction rates even when approached with more elaborate statistical techniques (e.g. Alroy, 2008), however both methods miss the nuance available through non-binned datasets (Sadler and students of GEO206b, 2013). Intermittent glaciations, extinctions, and carbon isotope excursions continued through Silurian times (Page et al., 2007), a shift in climatic/geochemical baseline beginning in the Early Katian and persisting for some 40 million years, in notable contrast to the model of a brief glacial in the midst of a long, stable, warm period.

1.2 Molecular Organic Geochemistry in Geobiology

Lipid biomarker analyses are presently flourishing in studies of present-day and Cenozoic systems, particularly the recent expansion of paleotemperature proxies into marine and terrestrial climate reconstructions. The use of biomarkers in "deep time," however, is limited to a few groups doing restricted studies mainly on the Cretaceous-Paleogene or Permian-Triassic extinction intervals, or pushing the boundaries of organic geochemistry in, often, overmature Precambrian rocks. This leaves hundreds of millions of years' unexplored time spanning several interesting turning points in the co-evolution of life and the Earth.

The structure and isotopic composition of lipid biomarkers reflect the taxonomy and metabolic strategies of ancient organisms and help constrain paleoenvironmental conditions (of oxicity, salinity, etc) in aquatic settings (Table 1.1 for examples). These molecular fossils have proven ability to track the evolution of marine microbial communities and ocean redox conditions through the Phanerozoic (e.g. Grantham and Wakefield, 1988; Schwark and Empt, 2006; Pancost et al., 1998). Biomarker stratigraphies, in combination with inorganic geochemical proxies, such as S, N, and C stable

isotopes, trace element abundances and iron mineral speciation, can yield important information about the response of marine microbial communities to environmental perturbations (e.g. oceanic anoxic events), such as the onset or cessation of oligotrophic conditions (e.g. due to nitrate limitation), eutrophication (e.g. due to upwelling or restricted circulation), or photic zone euxinia (PZE, Summons and Powell, 1986). For example, studies of biomarkers from the Permo-Triassic mass extinction have provided significant insight into mechanisms of extinction (e.g. photic zone euxinia, Grice et al., 2005) and detected major environmental changes leading up to the extinction (Cao et al., 2009).

Parameter	**Implication/interpretation**
Source Organisms	
oleanane	angiosperm (flowering) plants, Cretaceous and younger
highly branched isoprenoids	diatoms, Mesozoic and younger
carbon preference index	higher plants: odd over even in C_{27}-C_{31} *n*-alkanes; *Gloeocapsamorpha prisca*: odd over even in C_{15}-C_{19} *n*-alkanes
24-*iso*-propylcholestane	(demo)sponges
24-*n*-propylcholestane	pelagophyte algae, marine deposition
3β-methylhopanes	methanotrophic bacteria, acetic acid bacteria
2α-methylhopanes	cyanobacteria, soil bacteria (when accompanied by high gammacerane)
isorenieratane	green sulfur bacteria, photic zone euxinia
okenane	purple sulfur bacteria, photic zone euxinia
Age	
C_{28}/C_{29} sterane ratio	age-related, high values in Mesozoic and younger rocks
dinosteranes	age-related, high values in Mesozoic and younger rocks
Geochemical Conditions	
gammacerane	water column stratification
pristane/phytane	from chlorophyll side chain, reflects redox conditions
homohopane index	preservation of hopane side chain, related to oxygenation
Lithology and Thermal History	
diasterane/regular sterane	lithology (clay content)
sterane ααα*S*/(ααα*S* + ααα*R*)	thermal maturity
hopane αββ*S*/(αββ*S* + αββ*R*)	thermal maturity

Table 1.1: List of selected biomarker parameters reflecting source organisms, geochemical conditions, and post-deposition history. See Peters et al. (2003) and Killops and Killops (2005) for further discussion.

Although lipid biomarkers may contribute a great deal of nuance to understanding of marine conditions, there are pitfalls to working with Paleozoic rocks that must

be addressed. The primary challenge is contamination either recently, through anthropogenic contaminants on the outcrop or in the lab, or naturally, through migration of hydrocarbons in the hundreds of millions of years the rocks have been buried. Fortunately, careful attention to methodology and to cross-checks provided by the lipid biomarkers themselves can prevent or identify contamination. For example, biomarker parameters for source rock composition and thermal maturity (Table 1.1, Figures 1.1, 1.2) must be consistent with independently constrained source rock lithology and thermal history, using methodologies such as RockEval Pyrolysis, conodont alteration index, or vitrinite reflectance. Additionally, Lower Paleozoic biomarkers should not include compounds produced by organisms that had not yet evolved or reached significant abundance, for example, oleanane, which is produced by angiosperms, or dinosteranes, derived from compounds produced by dinoflagellates (Peters et al., 2003). A final check of syngeneity is provided by catalytic hydropyrolysis of exhaustively pre-extracted kerogen, the insoluble majority of sedimentary organic matter (Love et al., 1995). Lipid biomarkers produced by pyrolysis of kerogen should bear expected relationships (i.e similar profile but slightly lower thermal maturity and clay-catalysed rearrangement) to extracted biomarkers as kerogen is immobile in sediments at relevant temperatures and cannot have migrated into the rock during burial.

With careful attention to procedural blanks (Figures 1.3, 1.4), internal and external self-consistency checks, and due consideration of the many factors at play in precursor compound synthesis by source organisms (e.g. the conditions under which cyanobacteria synthesize hopanoids methylated at C-2) molecular organic geochemistry provides a window into relatively under-explored tiers of the biosphere in Paleozoic

A. Sterane carbon numbering and stereochemistry

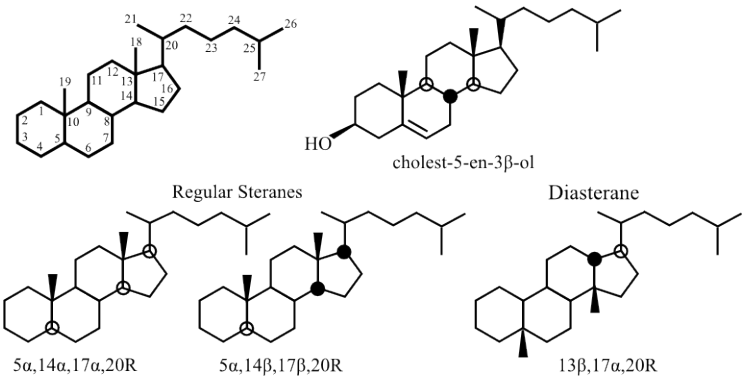

B. MRM-GC-MS sterane elution pattern.

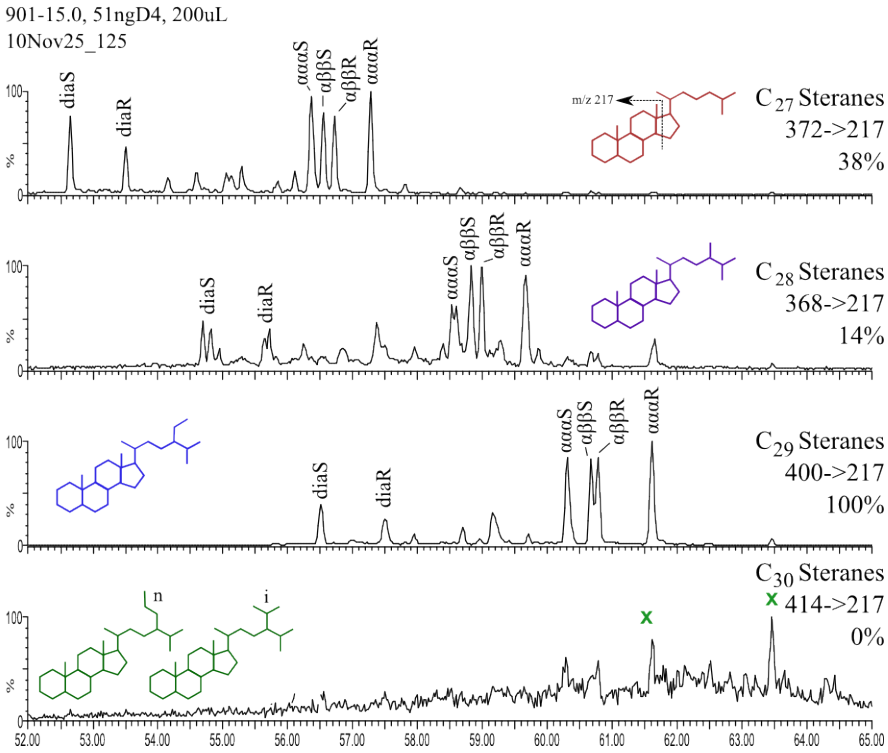

Figure 1.3: A. Steroid carbon numbering and stereochemistry (modified from Killops and Killops, 2005) with B. structures and MRM-GC-MS elution patterns for a saturated hydrocarbon fraction of an sample from Anticosti Island, Canada.

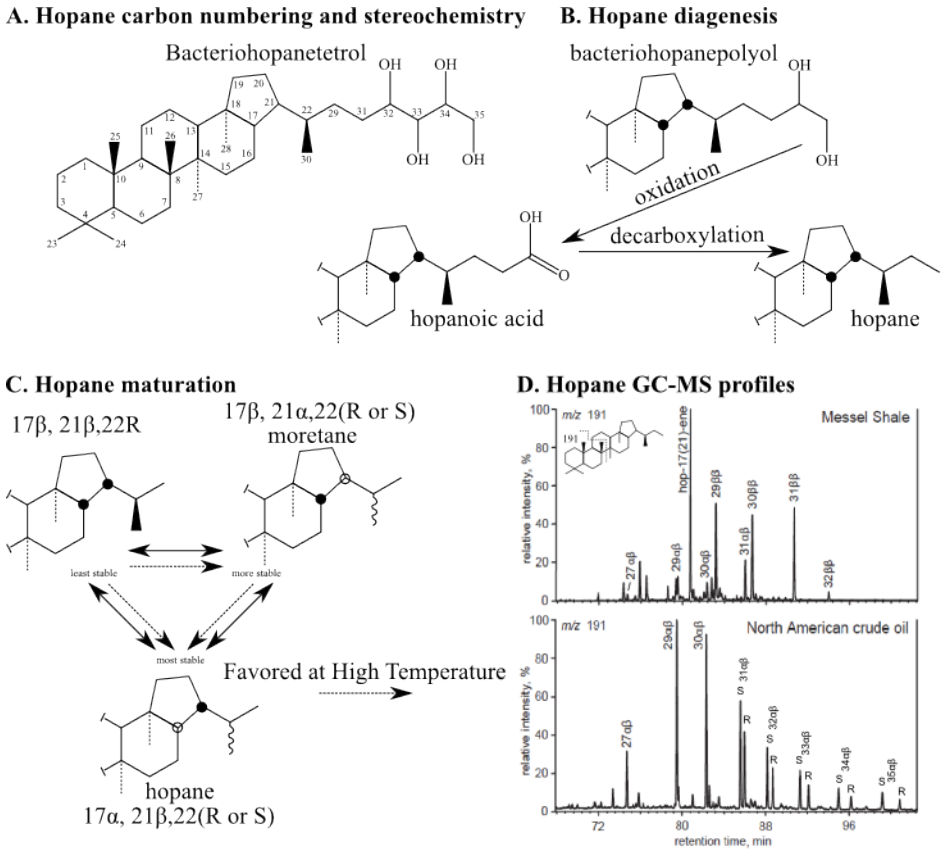

Figure 1.4: A. Hopane structure and carbon numbering (modified from Killops and Killops, 2005); B. Hopane transformations through diagenesis, from biolipid (bacteriohopanepolyol) to geolipid (hopane)(modified from Peters et al., 2003); C. hopane transformations during diagenesis and catagenesis (modified from Seifert and Moldowan, 1980; Killops and Killops, 2005); and D. Comparison of hopane m/z 191 chromatograms between an immature shale (top) and mature oil (bottom) (modified from Gaines et al., 2008.

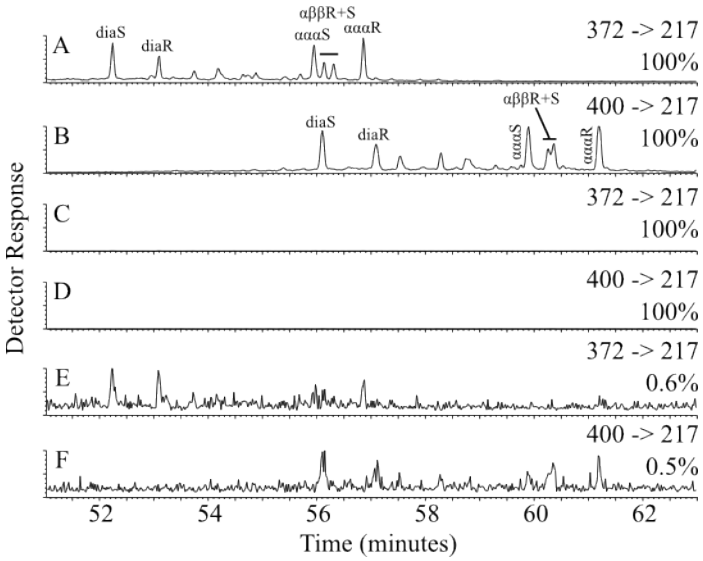

Figure 1.5: MRM-GC-MS for C_{27} steranes (m/z 372 - 217 transition) and C_{29} steranes (m/z 400 - 217 transition) for Anticosti (904-3.0) and a laboratory procedural blank. Percentages indicate signal intensity to Anticosti C_{29} $\alpha\alpha\alpha$R sterane. A. and B. Anticosti C_{27} and C_{29} steranes, C. and D. Procedural blank at same scale, E. and F. Procedural blank magnified by approximately 150.

times.

1.3 Previous Studies of Ordovician Organic Geochemistry

Ordovician rocks and oils have long drawn the interest of organic geochemists due to the "unique compositional characteristics" observed in many Ordovician-sourced oils: a carbon number preference for C_{17} and C_{19} *n*-alkanes; abundant alkylcyclohexanes; low amounts of pristane and phytane; and occasionally low amounts of steranes and hopanes (e.g. Fowler and Douglas, 1984; Fowler et al., 1986; Jacobson et al., 1988). Many of these characteristics are now thought to derive from the enigmatic, extinct microorganism *Gloeocapsamorpha prisca* (Zallesky, 1917) and the particular environmental conditions in which it flourished (Reed et al., 1986; Hoffman et al., 1987; Pancost et al., 1998; Derenne et al., 2002). While the *G. prisca* signature is common among many

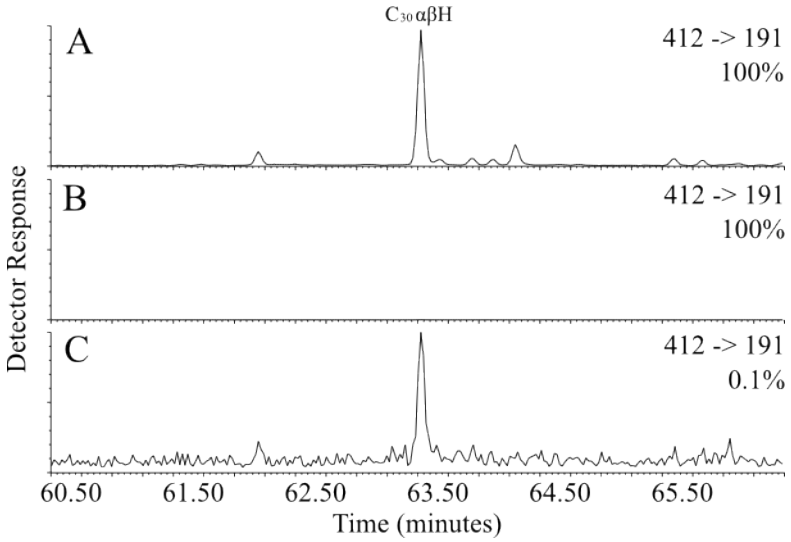

Figure 1.6: Multiple Reaction Monitoring (MRM)-GC-MS chromatograms for C_{30} hopanes (m/z 412 - 191 transition) for Anticosti (904-3.0) and a laboratory procedural blank. Percentages indicate signal intensity relative to Anticosti C_{30} $\alpha\beta$-hopane. A. Anticosti C_{30} $\alpha\beta$-hopane, B. Procedural blank at same scale, C. Procedural blank magnified by approximately 1000.

Ordovician rocks, it is not the only striking feature and becomes less common towards the Late Ordovician. In particular, high amounts of 3β-methylhopane have been detected, although not yet systematically studied, in many Middle and Late Ordovician source rocks and oils. For example, Summons and Jahnke (1990) initially illustrated the identification of methylhopanes in MRM GC-MS using a Middle Ordovician rock extract from Australia, likely because of the high abundance of those compounds in the extract.

Analysis of biomarkers in the late Middle Ordovician Decorah Formation of Iowa has demonstrated the response of marine microbial communities to establishment and cessation of photic zone euxinic conditions attendant upon oceanographic circulation changes (Pancost et al., 1998). In this instance, deposition of the Platteville Formation occurred with more prolific growth of cyanobacteria in an oxygenated water column; circulation stagnated during deposition of the Spechts Ferry Member of the Decorah

Shale leading to water column stratification, as evidenced by a spike in the abundance of gammacerane, and at least intermittent deposition of isorienieratane, indicative of PZE conditions (Table 1.1). With improvement in water column mixing, gammacerane and isorenieratane abundances drop and are replaced by *G. prisca* biomass, the degradation of which is interpreted to have impacted oxygen availability in sediments and preservation of organic matter (Pancost et al., 1998).

Photic zone euxinia appears to have been not an unusual condition in Middle to Late Ordovician seas. However, whether there is a relationship between PZE and the Late Ordovician mass extinction has yet to be established. PZE appears to have been an important factor in preservation of organic matter during deposition of the Late Ordovician hot shales of Jordan (Armstrong et al., 2009), one of three published lipid biomarker studies of Hirnantian rocks to date. However, as the authors note, the Jordan hot shales were deposited in a silled, periglacial basin perhaps unrepresentative of most Late Ordovician environments, and there is insufficient stratigraphic or biomarker detail to discern the duration of PZE or its relationships with bacterial and algal communities in the basin. A study in progress stemming from this thesis considers the abundance of isorenieratane relative to graptolite biostratigraphy to test whether increased levels of isorenieratane are associated with declines in graptolite diversity and/or abundance or at least with a greater proportion of putatively OMZ-inhabiting clades.

1.4 Broader Impacts

This dissertation presents the first systematic lipid biomarker research into Late Ordovician and early Silurian microbial community structure and response to climatic change proximal to the Late Ordovician mass extinction. Broader impacts to

the Lower Paleozoic research community include insight into trophic systems in epicontinental seas, supporting the inferred importance of local circulation systems and modified "layer cake" interpretations of the lithostratigraphy; documentation of substantial change in microbial communities during the Late Ordovician mass extinction, including enhanced algal contribution to sedimentary organic matter during the glaciation either through enhanced productivity or diminished bacterial re-working; and new recognition of the potential role of methane cycling in Lower Paleozoic climate. In the wider view, application of molecular organic geochemistry to intervals in between the Recent and Precambrian helps to strengthen both our understanding of the proxies and the image of the field among geologists.

1.5 References

1. Alroy, J., 2008, Dynamics of origination and extinction in the marine fossil record: Proceedings of the National Academy of Sciences, v. 105, p. 11536-11542.

2. Armstrong, H.A., Abbott, G.D., Turner, B.R., Makhlouf, I.M., Muhammad, A.B., Pedentchouk, N., Peters, H., 2009, Black shale deposition in an Upper Ordovician-Silurian permanently stratified peri-glacial basin, southern Jordan: Palaeogeography, Palaeoclimatology, Palaeoecology, v. 273, p. 368-377.

3. Beman, J.M., Chow, C.-E., King, A.L., Feng, Y., Furhman, J.A., Andersson, A., Bates, N.R., Popp, B.N., Hutchins, D.A., 2011, Global declines in oceanic nitrification rates as a consequence of ocean acidification: Proceedings of the National Academy of Sciences, v. 108, p. 208-213.

4. Berner, R.A., Kothavala, Z., 2001, GEOCARB III: A revised model of atmospheric CO_2 over Phanerozoic time: American Journal of Science, v. 301, p. 182-204.

5. Brenchley, P.J., Marshall, J.D., Carden, G.A.F., Robertson, D.B.R., Long, D.G.F., Meidla, T., Hints, L., Anderson, T.F., 1994, Bathymetric and isotopic evidence for a short-lived Late Ordovician glaciation in a greenhouse period: Geology, v. 22, p. 295-298.

6. Came, R.E., Eiler, J.M., Veizer, J., Azmy, K., Brand, U., Weidman, C.R., 2007, Coupling of surface temperatures and atmospheric CO_2 concentrations during the Paleozoic era: Nature, v. 449, p. 198-201.

7. Cao, C., Love, G.D., Hays, L.E., Wang, W., Shen, S., Summons, R.E., 2009, Biogeochemical evidence for euxinic oceans and ecological disturbance presaging

the end-Permian mass extinction event: Earth and Planetary Science Letters, v. 281, p. 188-201.

8. Cocks, L.R.M., Torsvik, T.H., 2002, Earth geography from 500 to 400 million years ago: a faunal and palaeomagnetic review: Journal of the Geological Society, London, v. 159, p. 631-644.

9. Derenne, S., Metzger, P., Largeau, C., Van Bergen, P.F., Gatellier, J.P., Sinninghe Damste, J.S., de Leeuw, J.W., Berkaloff, C., 1991, Similar morphological and chemical variations of *Gloeocapsomorpha prisca* in Ordovician sediments and cultured *Botryococcus braunii* as a response to changes in salinity: Organic Geochemistry, v. 19, p. 299-313.

10. Epstein, A.G., Epstein, J.B., Harris, L.D., 1976, Conodont color alteration: an index to organic metamorphism. US Government Printing Office, Washington, D.C.

11. Finnegan, S, Bergmann, K., Eiler, J.M., Jones, D.S., Fike, D.A., Eisenman, I., Hughes, N.C., Tripati, A.K., Fischer, W.W., 2011, The magnitude and duration of Late Ordovician-Early Silurian glaciation: Science, v. 331, p. 903-906.

12. Finnegan, S., Peters, S., Fisher, W.W., 2011b, Late Ordovician-Early Silurian selective extinction patterns in Laurentia and their relationship to climate change: 11th International Symposium on the Ordovician System, 9-13 May, Madrid.

13. Finney, S.C., Berry, W.B.N., 1997, New perspectives on graptolite distributions and their use as indicators of platform margin dynamics: Geology, v. 25, p. 919-922.

14. Fowler, M.G., Douglas, A.G., 1984, Distribution and structure of hydrocarbons in four organic-rich Ordovician rocks: Organic Geochemistry, v. 6, p. 105-114.

15. Fowler, M.G., Aboliins, P., Douglas, A.G., 1986, Monocyclic alkanes in Ordovician organic matter: Organic Geochemistry v. 10, p. 815-823.

16. Frakes, L.A., Francis, J.E., Syktus, J.I., 1992, Climate Modes of the Phanerozoic, Cambridge, UK, Cambridge University Press, 274 p.

17. Gaines, S.M., Eglinton, G., Rullkotter, J., 2008, Echos of Life: What fossil molecules reveal about Earth History, Oxford University Press, 376 p.

18. Gill, B.C., Lyons, T.W., Saltzman, M.R., 2007, Parallel, high-resolution carbon and sulfur isotope records of the evolving Paleozoic marine sulfur reservoir: Palaeogeography, Palaeoclimatology, Palaeoecology, v. 256, p. 156-173.

19. Gill, B.C., Lyons, T.W., Saltzman, M.R., 2005, Parallel, high-resolution carbon and sulfur isotope records of the Late Ordovician and Late Carboniferous records of two different glacial episodes: American Geophysics Union Annual Meeting, San Francisco.

20. Grantham, P.J., Wakefield, L.L., 1988, Variations in the sterane carbon number distributions of marine source rock derived crude oils through geological time: Organic Geochemistry, v. 12, p. 61-73.

21. Grice, K, Cao, C., Love, G.D., Bottcher, M.E., Twitchett, R.J., Grosjean, E., Summons, R.E., Turgeon, S.C., Dunning, W., Jin, Y. 2005, Photic zone euxinia during the Permian-Triassic superanoxic event: Science, v. 307, p. 706-709.

22. Guthrie, J.M., Pratt, L.M., 1995, Geochemical character and origin of oils in Ordovician reservoir rock, Illinois and Indiana, USA: American Association of Petroleum Geologists Bulletin, v. 79, p. 1631-1649.

23. Guthrie, J.M., 1996, Molecular and carbon isotopic analysis of individual biological markers: evidence for sources of organic matter and paleoenvironmental conditions in the Upper Ordovician Maquoketa Group, Illinois Basin, U.S.A.: Organic Geochemistry, v. 25, p. 439-460.

24. Hallam, A., Wignall, P.B., 1997, Mass extinctions and their aftermath: Oxford University Press, Inc. New York, U.S.A. 320 pp.

25. Hammarlund, E.U., Dahl, T.W., Harper, D.A.T., Bond, D.P.G., Nielsen, A.T., Bjerrum, C.J., Schovsbo, N.H., Schnlaub, H.P., Zalasiewicz, J.A., Canfield, D.E., 2012, A sulfidic driver for the end-Ordovician mass extinction: Earth and Planetary Science Letters, v. 331-332, p. 128-139.

26. Hoffmann, C.F., Foster, C.B., Powell, T.G., Summons, R.E., 1987, Hydrocarbon biomarkers from Ordovician sediments and the fossil alga *Gloeocapsomorpha prisca* Zalessky 1917: Geochimica et Cosmochimica Acta, v. 51, p. 2681-2697.

27. Jacobson, S.R., Hatch, J.R., Teerman, S.C., Askin, R.A., 1988, Middle Ordovician organic matter assemblages and their effect on Ordovician-derived oils: American Association of Petroleum Geologists Bulletin, v. 72, p. 1090-1100.

28. Johnson, C.M., McLennan, S.M., McSween, H.Y., Sumons, R.E., 2013, Smaller, better, more: Five decades of advances in geochemistry: Geological Society of America Special Paper 500, p. 1-44.

29. Killops, S.D., Killops, V.J., 2005, Introduction to Organic Geochemistry. 2nd ed: Blackwell Publishing, Ltd. Oxford, 393 pp.

30. LaPorte, D.F., Holmden, C., Patterson, W.P., Loxton, J.D., Melchin, M.J., Mitchell, C.E., Finney, S.C., Sheets, H.D., 2009, Local and global perspectives on carbon and nitrogen cycling during the Hirnantian glaciation: Palaeogeography, Palaeoclimatology, Palaeoecology, v. 276, p. 182-195.

31. Love, G.D., Snape, C.E., Carr, A.D., Houghton, R.C., 1995, Release of covalently-bound alkane biomarkers in high yields from kerogen via catalytic hydropyrolysis: Organic Geochemistry, v. 23, p. 981-986.

32. Melchin, M.,J., Mitchell, C.E., Holmden, C., Storch, P., 2013. Environmental changes in the Late Ordovician-Early Silurian: Review and new insights from black shales and nitrogen isotopes: Geological Society of America Bulletin, v. 125, p. 1635-1670.

33. Page, A.A., Zalasiewicz, J.A., Williams, M., Popov, L.E., 2007, in Williams, M., Haywood, A.M., Gregory, F.J., and Schmidt, D.N. (eds.), Were transgressive black

shales a negative feedback modulating glacioeustasy in the Early Palaeozoic Icehouse?: Deep Time Perspectives on Climate Change: Marrying the Signal from Computer Models and Biological Proxies. The Micropalaeontological Socity, Special Publications. The Geological Society, London, p. 123-156.

34. Pancost, R.D., Freeman, K.H., Patzkowsky M.E., Wavrek, D.A., Collister, J.W., 1998, Molecular indicators of redox and marine photoautotroph composition in the late Middle Ordovician of Iowa, U.S.A.: Organic Geochemistry, v. 29, p. 1649-1662.

35. Pancost, R.D., Freeman, K.H., Herrmann, A.D., Patzkowsky, M.E., Ainsaar, L., Martma, T., 2013, Reconstructing Late Ordovician carbon cycle variations: Geochimica et Cosmochimica Acta, v. 105, p. 433-454.

36. Peters, K.E., Walters, C.C., Moldowan, J.M., 2003, The Biomarker Guide, 2nd edition: Cambridge University Press, Cambridge. 1132 pp.

37. Pope, M.C., Steffen, J.B., 2003, Widespread, prolonged late Middle to Late Ordovician upwelling in North America: A proxy record of glaciation?: Geology, v. 31, p. 63-66.

38. Raatz, W.D., Ludvigson, G.A., 1996, Depositional environments and sequence stratigraphy of Upper Ordovician epicontinental deep water deposits, eastern Iowa and southern Minnesota: Geological Society of America Special Paper, v. 306, p. 143-159.

39. Ratti, S., Knoll, A.H., Giordano, M., 2011, Did sulfate availability facilitate the evolutionary expansion of chlorophyll a+c phytoplankton in the oceans?: Geobiology, v. 9, p. 310-312.

40. Raup, D.M., Sepkoski, J.J., 1982, Mass extinctions in the marine fossil record: Science, v. 215, p.1501-1503.

41. Reed, J.D., Illich, H.A., Horsfield, B., 1986, Biochemical evolutionary significance of Ordovician oils and their sources: Organic Geochemistry, v. 10, p. 347-358.

42. Rohrssen, M., Love, G., Fisher, W., Finnegan, S., Fike, D., 2013, Lipid biomarkers record fundamental changes in the microbial community structure of tropical seas during the Late Ordovician Hirnantian glaciation: Geology, v. 41, p. 127-130.

43. Sadler, P.M., Cooper, R.A., Melchin, M., 2009, High-resolution, early Paleozoic (Ordovician-Silurian) time scales: Geological Society of America Bulletin, v. 121, p. 887-906.

44. Sadler, P., students of GEO206b in Montanez, I.P. and Isaacson, P.E., 2013, A 'sedimentary record' of opportunities: The Sedimentary Record, v. 11, p. 4-8.

45. Saltzman, M.R., 2005, Phosphorous, nitrogen, and the redox evoluton of the Paleozoic oceans: Geology, v. 33, p. 573-576.

46. Schwark, L., Empt, P., 2006, Sterane biomarkers as indicators of Palaeozoic algal evolution and extinction events: Palaeogeography, Palaeoclimatology, Palaeoecology, v. 240, p. 225-236.

47. Seifert, W., Moldowan, J.M., 1980, The effect of thermal stress on source-rock quality as measured by hopane stereochemistry: Physics and Chemistry of the Earth, v. 12, p. 229-237.

48. Smith, M.E., Singer, B.S., and Simo, T., 2011, A time like our own? Radioisotopic calibration of the Ordovician greenhouse to icehouse transition: Earth and Planetary Science Letters, v. 311, p.3 64-374.

49. Summons, R.E., Powell, T.G., 1986, *Chlorobiaceae* in Palaeozoic seas revealed by biological markers, isotopes and geology: Nature, v. 319, p. 763-765.

50. Summons, R.E., Jahnke, L.L., 1990, Identification of the methylhopanes in sediments and petroleum: Geochimica et Cosmochimica Acta, v. 54, p. 247-251.

51. Summons, R.E., Bradley, A.S., Jahnke, L.L., Waldbauer, J.R., 2006, Steroids, triterpenoids and molecular oxygen: Philosophical Transactions of the Royal Society, v. 361, p. 951-968.

52. Trotter, J.A., Williams, I.S., Barnes, C.R., Lecuyer, C., Nicoll, R.S., 2008, Did cooling oceans trigger Ordovician biodiversification? Evidence from conodont thermometry: Science, v. 321, p. 550-554.

53. Vandenbroucke, T.R.A., Armstrong, H.A., Williams, M., Paris, F., Sabbe, K., Zalasiewicz, J.A., Nlvak, J., Verniers, J., 2009, Epipelagic chitinozoan biotopes map a steep latitudinal temperature gradient for earliest Late Ordovician seas: Implications for a cooling Late Ordovician climate: Palaeogeography, Palaeoclimatology, Palaeoecology, v. 294, p. 202-219.

54. Witzke, B.J., 1987, Models for circulation patterns in epicontinental seas applied to Paleozoic facies of North American craton: Paleoceanography, v. 2, p. 229-248.

55. Yapp, C.J., Poths, H., 1992, Ancient atmospheric CO_2 pressures inferred from natural goethites: Nature, v. 355, p. 342-344.

Chapter 2

Lipid biomarkers record fundamental changes in the microbial community structure of tropical seas during the Late Ordovician Hirnantian glaciation

Megan Rohrssen 1, Gordon D. Love 1, Woodward W. Fischer 2, Seth Finnegan 2, 3, and David A. Fike 4

1 Department of Earth Sciences, University of California, Riverside, California 92521, USA 2 Department of Geological and Planetary Sciences, California Institute of Technology,Pasadena, California 91125, USA 3 Department of Integrative Biology, University of California, Berkeley, California 94720, USA 4 Department of Earth and Planetary Sciences, Washington University, St. Louis, Missouri 63130, USA

Published in Geology, 2013, v. 41, p. 127-130.

2.1 Abstract

The Late Ordovician mass extinction was linked to climate cooling and glaciation of Gondwana during the terminal Ordovician Hirnantian Stage (444.7 - 443.4 Ma). Extinction patterns have been well described for many marine taxa, but much less is known about marine microbial communities through this interval. To elucidate the structure of microbial communities in tropical marine basins through the Late Ordovician, we analyzed lipid biomarkers in thermally well-preserved strata from the Taconic foreland (Anticosti Island, Canada), the Cincinnati Arch, and western continental margin (Vinini Formation, Nevada, US). Despite clear oceanographic differences, lipid biomarker profiles show similarities between these three localities. Major shifts in biomarker distributions of Anticosti Island and the Vinini Formation, mainly hopane/sterane ratios, record changes in the balance of bacterial versus algal primary production. Bacterial contributions to sedimentary organic matter were highest during warm intervals, both before and after Hirnantian cooling. In particular, 3β-methylhopane s, likely sourced from aerobic methanotrophic bacteria, occur in high relative abundance (many times the Phanerozoic average) across Laurentia throughout most of the interval studied. 3β-methylhopane abundances also reveal an overall positive relationship with paleotemperature proxies, implying increased methane cycling during warm intervals. These results suggest that enhanced methane cycling could have provided an important positive feedback on climate during extended intervals of Early Paleozoic time.

2.2 Introduction

Near the end of Late Ordovician time, climatic and environmental changes drove one of the most severe mass extinctions of the Phanerozoic Eon. Atmospheric pCO_2 was perhaps 8 - 16 times pre-industrial levels (Berner and Kothavala, 2001; Yapp and Poths, 1992), and predominantly warm surface seawater temperatures appear to have characterized much of Ordovician time. This warm climate state was interrupted by Late Ordovician cooling, the magnitude and timing of which remain subject to debate (e.g., Pope and Steffen, 2003; Brenchley et al., 1994; Trotter et al., 2008; Finnegan et al., 2011). Expansion and retreat of continental ice sheets at high southern latitude in the Hirnantian stage (444.68 - 443.41 Ma) was accompanied by a perturbation to the global carbon cycle manifest as a 3 - 6 permil positive carbon isotope excursion (Brenchley et al., 1994).

Global reconstructions suggest that eustatic sea level was at or near Phanerozoic high-stand during much of Late Ordovician time (e.g., Hallam, 1992), and many continents were inundated by epeiric seaways. These warm, shallow seas often hosted diverse faunas but may have had idiosyncratic circulation patterns in which oxygen minimum zones (OMZs) would expand to influence large areas of epicontinental seafloor (Witzke, 1987; Finney et al., 2007; LaPorte et al., 2009). The broad distribution of epeiric sea habitats and their sensitivity to both record bias and environmental forcings (e.g., eustatic sea level, temperature, bottom water O_2 concentrations) have been implicated in the common cause driver (Newell, 1949; Peters, 2006; Finnegan et al., 2012) and two-phased expression of the Late Ordovician mass extinction (Sheehan, 2001; Hallam and Wignall, 1997).

Although there has been progress in understanding patterns of faunal extinc-

tion through Late Ordovician time, far less is known about the microbial community dynamics that underpinned food webs and catalyzed biogeochemical cycles. Lipid biomarkers track important evolutionary, microbial, and environmental transitions associated with mass extinctions such as the Permo-Triassic (Cao et al., 2009; Grice et al., 2005) and end Cretaceous (Sepulveda et al., 2009; Kuypers et al, 2001), and have proven informative regarding the response of microbial communities to environmental change during earlier Ordovician events (Pancost et al., 1998, 1999; Armstrong et al., 2009). Previous studies have noted that high hopane/sterane ratios, low amounts of acyclic isoprenoids, and large amounts of methylhopanes are typical of Ordovician oils and source rocks (e.g., Reed et al., 1986; Fowler and Douglas, 1984; Guthrie and Pratt, 1995; Jacobson et al., 1988; Hoffman et al., 1987; Summons and Jahnke, 1990) – these features have yet to be investigated in stratigraphic framework or integrated with independent proxy information to understand their paleoenvironmental significance.

Here we present a lipid biomarker profile from western Anticosti Island, Quebec, Canada to construct a record of marine microbial community structure through the Hirnantian interval in a tropical carbonate ramp setting. Additional stratigraphic data from the U.S.-Midcontinent (Cincinnati region) and from the western margin of Laurentia (Vinini Formation at Vinini Creek) were studied to assess the temporal, environmental, and spatial extent of the patterns observed on Anticosti Island (Figure 2.1).

Strata exposed in outcrop on Anticosti Island, Quebec, Canada record deposition of a storm-influenced tropical carbonate ramp in the rapidly subsiding Taconic Foreland basin (Long, 2007), and provide one of the most complete records of the Hirnantian interval on Laurentia. Detailed investigations of Anticosti Island sedimentary geology,

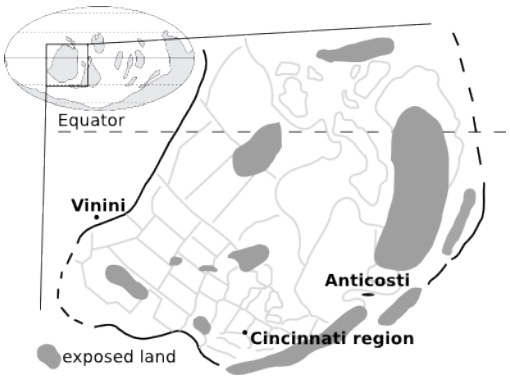

Figure 2.1: Late Ordovician paleogeography and locations of studied Laurentian sections. Paleogeography modified from Cocks and Torsvik, (2002). Laurentian map modified from Raatz and Ludvigson, 1996.

biostratigraphy, paleontology (e.g., Long, 2007; Desrochers et al., 2010; Delabroye et al., 2011; Achab et al., 2011; Copper, 2001), and chemostratigraphy (e.g., Orth et al., 1986; Long, 1993; Jones et al., 2011; Young et al., 2010) provide excellent context for lipid biomarker study. Most importantly, surface outcrops on western Anticosti Island have telenite reflectance values (0.8 - 1.0 percent) indicative of organic thermal maturities in the early to mid oil window (Bertrand, 1990). Because Anticosti rocks crop out along a paleodepth gradient, with deeper-water and more stratigraphically complete deposition at the western end of the island, data composited from western Anticosti exposures yield the greatest stratigraphic coverage (Figure 2.2). Anticosti's paleotropical setting affords a partial control for the influence of temperature if, as predicted, tropical regions express a smaller interglacial-glacial temperature change than regions at mid- and high latitudes. The carbonate-rich epeiric depositional environment of both Anticosti and the Cincinnati region in the Late Ordovician likely represents much of the vast shallow seaways that covered large areas of most Late Ordovician continents.

The Katian-age Whitewater, Liberty, and Waynesville Formations of the Cincinnati region of the United States (e.g., Holland, 1993; South Gate Hill) were deposited

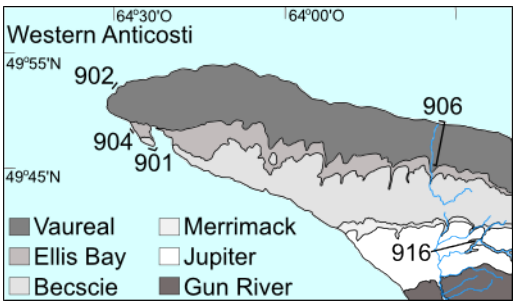

Figure 2.2: Map of sampling localities on Western Anticosti Island, Quebec, Canada. Numbers denote sites and correspond to sample names in tables.

on a shallow mixed carbonate/clastic ramp in an epeiric sea setting. Contemporaneous collection of samples for biomarker analysis with samples for δ^{13}C and δ^{18}O analyses on Anticosti Island (Jones et al., 2011) and for clumped isotope paleothermometry on Anticosti and in the Cincinnati region (Finnegan et al., 2011) allow direct examination of stratigraphic relationships between lipid biomarker data and these independent proxies. As on Anticosti Island, extensive literature regarding sequence stratigraphy and isotope chemostratigraphy exists for the Cincinnati region (e.g. Holland, 1993; Bergstrom et al., 2010; Frey, 1987; Holland and Patzkowsky, 2007). Hirnantian omission/erosion in the Cincinnati region precludes comparison with Hirnantian-age rocks from Anticosti, however biostratigraphic correlation of Katian-age deposits in both locations allows for approximate stratigraphic comparison of lipid biomarker fingerprints and trends across approximately 2,000 km.

The Katian to Hirnantian-age Vinini Formation (exposed in the Roberts Mountains of Nevada) was deposited on the passive margin of Western Laurentia in a putative upwelling zone, so described on the basis of high organic carbon content and the presence of phosphatic sediments (Finney et al., 1999). The Vinini Formation exposed in outcrop in the Monitor Range records deposition under shallower water, more proximal conditions than the Vinini Creek section (Finney et al., 1999; Holmden et al.,

2012). Although Monitor Range hand samples were available, these were not selected for biomarker analysis on the basis of visual inspection, which clearly shows extensive fractures and alteration, along with unusual carbonate textures (data not shown). Recent $\delta^{44/40}$Ca analyses indicate that the Monitor Range sections were impacted by submarine groundwater discharge (Holmden et al., 2012). Revisitation of these samples as an investigation into potential effects of submarine groundwater discharge on lipid biomarkers could provide an interesting exercise for future work.

Biostratigraphic and chemostratigraphic data presently offer several non-unique correlations between these units. Under either correlation scenario - biostratigraphic (Figure 2.7) or chemostratigraphic (Figure 2.8) - the lipid biomarker results show restructuring of microbial communities and carbon cycling pathways during Late Ordovician cooling.

2.3 Methods

2.3.1 Sample Collection

Anticosti Island and Cincinnati region samples were collected by the authors contemporaneously with samples collected for carbon, oxygen, and clumped isotope analyses presented elsewhere (Jones et al., 2011; Finnegan et al., 2011) under the same sample nomenclature. As a result, the stratigraphic relationships among these samples are very well constrained. Anticosti Island sampling locations are presented in Figure 2.2. Vinini Formation samples were donated by Dr. Stan Finney (California State University, Long Beach) from collections he and colleagues, particularly Dr. John Cooper (dec.), made during excavation of the trench at Vinini Creek. The stratigraphic positions of these samples are derived from Dr. Cooper's notes and the graptolite biostratigraphy

they assembled (Finney et al., 1999; Storch et al., 2011). Cincinnati region samples were collected at the South Gate Hill outcrop near Cedar Grove, Indiana (Holland, 1993).

2.3.2 Sample Preparation and Analytical Methods

Outcrop samples of Anticosti and Cincinnati region carbonates, marls, and carbonaceous shales were trimmed and the inner portions cut into pieces. The inner pieces were then ultrasonically washed with ultrapure water, methanol, dichloromethane, hexane, and dichloromethane again, prior to powdering in a ceramic or zirconia puck mill (SPEX 8510 Shatterbox). The puck mill was cleaned between samples by powdering two batches of fired sand (850^{o}C, overnight) followed by rinses with the same sequence of solvents described above. Samples were powdered in two aliquots, with the first discarded and the second collected for extraction. Fired sand procedural blanks were crushed with each batch of samples and processed identically to sample powders to monitor background levels of biomarker analytes. In addition to the powder reserved for lipid biomarker analyses, a split was collected for inorganic geochemical analyses.

Lipid biomarkers were extracted from 30-40 g of rock powder in a Microwave Accelerated Reaction System (CEM corp.) with dichloromethane and methanol (9:1 v/v) at 100^{o}C for 15 minutes. Elemental sulfur was removed from the total extract with HCl-activated, solvent washed copper pellets prior to silica gel column chromatography. Total extracts were fractionated with hexane, hexane:dichloromethane (1:1 v/v), and dichloromethane:methanol (3:1 v/v) to elute saturated hydrocarbons, aromatic hydrocarbons, and polar (N, S, and O-containing) compounds, respectively.

Gas chromatography-mass spectrometry (GC-MS) analyses of saturated (Figure 2.3) and aromatic hydrocarbons was conducted with an Agilent 7890A, equipped with a DB-1MS capillary column (60 m x 0.25 mm, 0.25 um film) and run with He as

carrier gas. The temperature program for GC-MS full scan and selected ion monitoring was 60°C (2 min), ramp to 250°C at 20°C/min, to 325°C at 2°C/min, and hold at 325°C for 20 min.

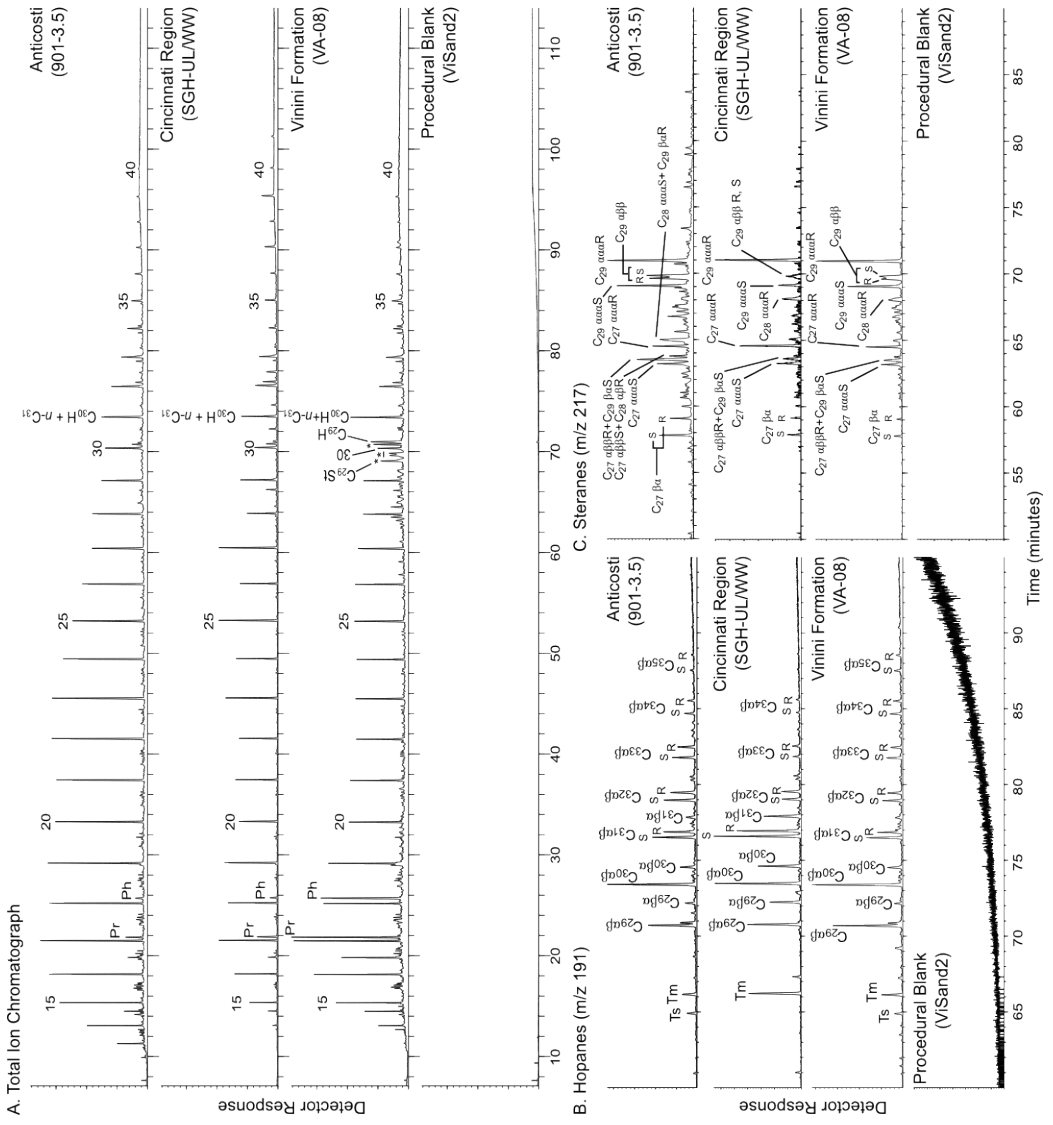

Figure 2.3: A. Total ion chromatograms (TIC) of saturated hydrocarbons and selected ion monitoring (SIM) chromatograms of B. hopanes (m/z 191) and C. steranes (m/z 217) from Anticosti (901-3.5), the Cincinnati region (SGH-UL/WW), the Vinini Formation (VA-08), and a laboratory procedural blank using pre-combusted sand. TIC signal is normalized to Vinini Formation sample signal, SIMs are normalized to most abundant compound in each trace.

Multiple reaction monitoring (MRM) GC-MS of saturated hydrocarbons (Figures 1.5, 1.6) was carried out with a Waters AutoSpec Premier mass spectrometer

equipped with an Agilent 7890A gas chromatograph and DB-1MS coated capillary column (60 m x 0.25 mm, 0.25 um film) using He for carrier gas. MRM-GC-MS measurements were conducted with a temperature program of 60°C for 2 min, heating to 315°C at 4°C/min with a final hold at 315°C for 35 min. Biomarker compounds were identified based on retention time and published mass spectra and quantified in MRM-GC-MS by comparison with a deuterated C_{29} sterane internal standard (d4-$\alpha\alpha\alpha$-24-ethylcholestane (20R), Chiron Laboratories, AS), assuming equal response factors between sample compounds and the internal standard. Individual yields of hopane and sterane diastereoisomers found in laboratory procedural blanks were typically less than 0.1 ng of individual compounds and polycyclic alkane biomarker MRM-GC-MS signal (hopanes, steranes, methylsteranes, methylhopanes, tricyclic terpanes, Table 2) from rock samples was typically at least 2-3 orders of magnitude higher in total than those detected in blanks (i.e. less than 0.03 ng C_{29} $\alpha\alpha\alpha$R sterane/g extracted sand blank vs less than 10 ng C_{29} $\alpha\alpha\alpha$R sterane/g TOC in samples) (Table 3).

2.3.3 Syngeneity of Lipid Biomarkers

Lipid biomarkers from Anticosti samples exhibit several features that support a syngenetic origin: lithology- and maturity-dependent biomarker parameters consistent with rock composition and burial history, and biomarker ratios characteristic of Early Paleozoic rocks (Table 2.1, Figure 2.3). A dominance of C_{29} steranes versus the C_{28} and C_{27} analogs, as observed in all rocks analyzed in our investigation, is the typically recognized sterane signal for Lower Paleozoic marine rocks and oils (Grantham and Wakefield, 1988). In addition, Anticosti, Cincinnati region, and the Vinini formation bitumens included here lack compounds produced by organisms that were not prominent in Lower Paleozoic environments, namely dinosteranes (marine dinoflagellates) and

oleananes (angiosperms).

2.3.4 Inorganic Geochemical Analyses

Total inorganic carbon (TIC) and total carbon (TC) were determined using an Eltra CS-500 carbon-sulfur analyser, with total organic carbon (TOC) obtained through subtraction (TC-TIC = TOC). Nitrogen isotope analyses were conducted on residues from HCl dissolution of carbonates weighed into silver capsules and combusted using a Costech Elemental Analyser coupled to a Delta Advantage in the Facility for Isotope Ratio Mass Spectrometry, at the University of California Riverside.

2.4 Results and Discussion

2.4.1 Microbial Community Structure Prior to Hirnantian Cooling

The ratio of (C_{27}-C_{35}) hopanes to (C_{27}-C_{29}) steranes provides a basic but informative measure of the relative contributions of bacteria and eukaryotes to sedimentary organic matter. Hopanes are the hydrocarbon fossil products of biohopanoids produced by diverse groups of bacteria, while steranes are derived from sterols common to all eukaryotes and absent in all but a very few bacteria (e.g., Summons et al., 2006).

Prior to the positive $\delta^{13}C$ excursion and glacial maximum, Anticosti and Cincinnati region bitumens yield Hopane/Sterane (H/St) ratios around an average baseline of ca. 4.06.0 (Figure 2.4, Table 1), significantly elevated above the Phanerozoic marine average range of 0.52.0 (Peters et al., 2003). Such elevated H/St ratios are commonly attributed to high levels of bacterial versus eukaryotic productivity and have been associated with significant environmental perturbations, such as the Permian-Triassic mass extinction (Cao et al., 2009), although also to high rates of bacterial remineralization

of organic matter (c.f. Marynowski et al., 2000). Here, the high H/St background values of pre- $\delta^{13}C$ excursion Anticosti and Cincinnati region bitumens (Figure 2.4) reflect enhanced bacterial contribution to total primary productivity in warm, oligotrophic marine basins and epeiric seas, consistent with limitation of algal production due to extensive denitrification in OMZs (LaPorte et al., 2009). Under these conditions, recycled ammonium, rather than nitrate, would have likely provided a primary nitrogen source (e.g., Higgins et al., 2012, but see also Saltzman et al., 2005). Substantially lower H/St ratios from Vinini Formation bitumens (Figure 2.5) indicate larger amounts of algal production along the northwestern margin of Laurentia associated, consistent with upwelling of nutrient-rich waters driven by western boundary current circulation (Finney et al. 1999).

Nitrogen isotope values of around 0 permil for pre-Hirnantian Vinini Formation total nitrogen have been attributed to quantitative burial of cyanobacterially-fixed nitrogen due to extensive denitrification in an upwelling-induced oxygen minimum zone (LaPorte et al., 2009). LaPorte and colleagues (2009) attribute the shift to heavier $\delta^{15}N_{TN}$ (about 1 permil) during the carbon isotope excursion to contraction of the local OMZ and concomitant lessening of denitrification. Analyses of total nitrogen from upper Ellis Bay Formation (Lousy Cove and Laframboise Members) HCl-decarbonated residues yield $\delta^{15}N_{TN}$ values of 3.2 to 3.9 permil (average 3.6, Figure 2.6). Heavier $\delta^{15}N_{TN}$ from Anticosti carbonates may reflect additional importance of isotopically heavy nitrogen species in oligotrophic seas (c.f. Stueken, 2013), and points to the alternative, or additional, possibility that a gradient in nitrogen isotopes was present between Ordovician epeiric seas and shelves, as has been demonstrated for Mesoproterozoic margins (Stueken, 2013). One consequence of a gradient in $\delta^{15}N$ is that, similarly to ϵ Nd

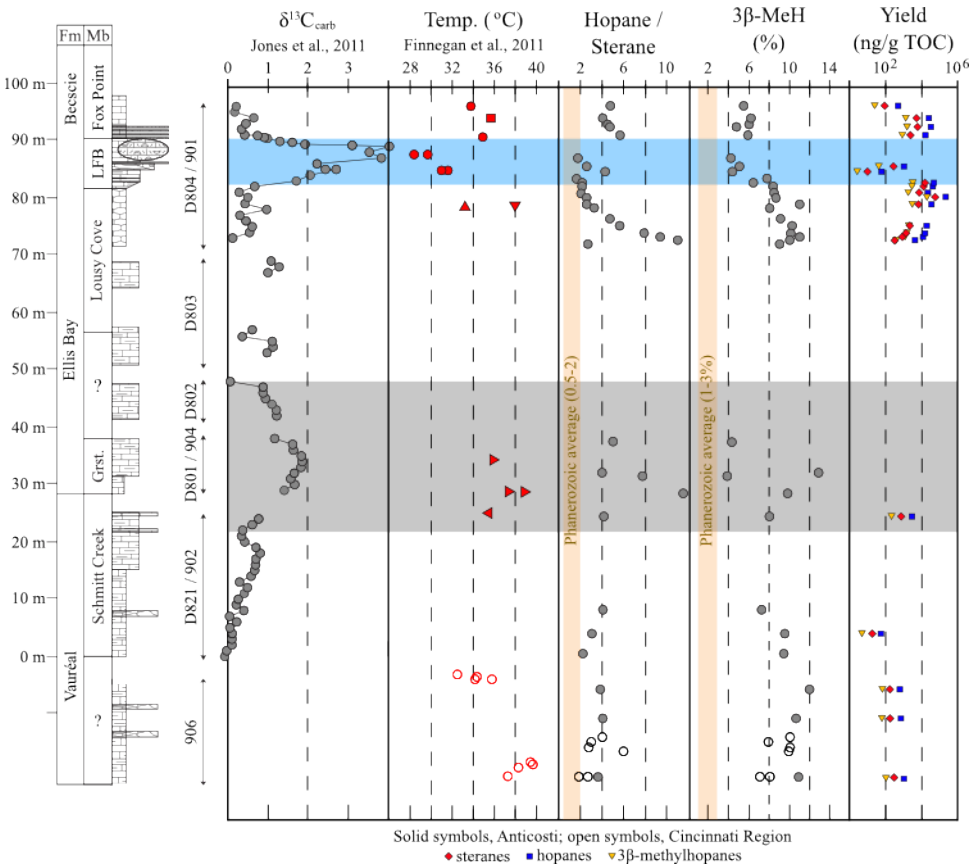

Figure 2.4: Lipid biomarker composite stratigraphic records from Western Anticosti Island, Canada (filled circles), and the Cincinnati region of the U.S.A. (open circles) plotted with stable carbon ($\delta^{13}C_{carb}$, Jones et al., 2011) and nitrogen ($\delta^{15}N_{org}$) isotope profiles from Anticosti Island, and clumped isotope paleothermometry estimates of sea surface temperatures (Finnegan et al., 2011). Vertical bars indicate the Phanerozoic marine averages for hopane/sterane and 3β-methylhopane index [C_{31} 3β-methylhopane /(C_{30} $\alpha\beta$-hopane + C_{31} 3β-methylhopane) x 100]. Hopane/sterane ratio and yields in ppb of total organic carbon for C_{27}-C_{35} hopanes, C_{27}-C_{29} steranes, and (2α- + 3β)- C_{30}-C_{36} methylhopanes. Abbreviations: LFB, Laframboise Member; Grst. Mb., Grindstone Member; TOC, Total Organic Carbon; MeH, methylhopane.

(Holmden et al., 2013), variations in $\delta^{15}N$ may be at least partially driven by sea level change, potentially confounding interpretations regarding nitrogen cycling in sections with indicators of substantial water depth variations. In this context the possible very small shift to less-enriched $\delta^{15}N_{TN}$ on Anticosti during the glacial maximum is more likely to reflect a change in nitrogen cycling or supply than to the change in sea level, as regression might be expected to result in even more positive values.

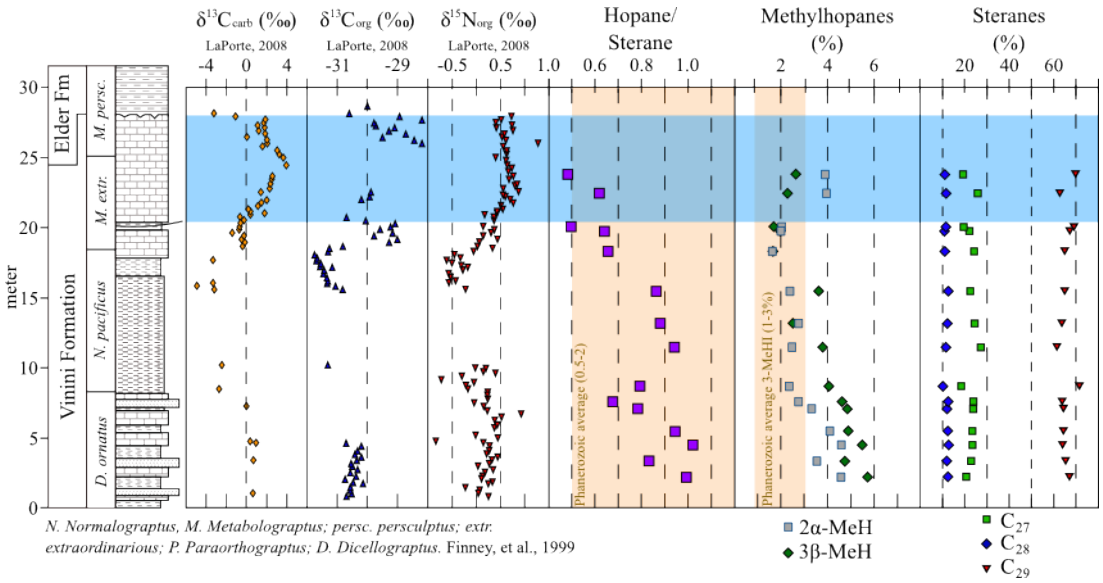

Figure 2.5: A selected lipid biomarker stratigraphic record from the Vinini Formation of Nevada, U.S.A. (Finney et al., 1999; Storch et al., 2011) plotted with nitrogen and carbon isotope records from LaPorte et al., 2009. The horizontal gray bar delineates the Hirnantian $\delta^{13}C$ excursion; the vertical bar is the Phanerozoic average 3β-methylhopane index. Steranes plotted as percentage of total C_{27}-C_{29} (regular steranes + diasteranes). n.b. *Metabolograptus persculptus* and *M. extraordinarious* were recently transferred from the *Normalograptus* genus (Melchin et al., 2011).

Anticosti Island bitumens also contain unusually high amounts of a series of C_{30}-C_{36} 3β-methylhopane (3-MeH, Figures 2.4, 2.6)molecules thought to derive primarily from microaerophilic Type I methanotrophic proteobacteria, as well as some acetic acid bacteria (Welander et al., 2013; Farrimond et al., 2004). The marine, carbonate-buffered depositional conditions of both Anticosti and the Cincinnati region suggests

that acetic acid bacteria are unlikely contributors of 3-MeH as such environments are likely outside their physiological tolerances. Although terrestrial derivation cannot be fully excluded, compounds brought in with runoff should show a strong, self-consistent relationship to sea level change and lithology (e.g. shoreline encroachment during regression would increase the proportion of 3-MeH if they were terrestrially-derived, a result which is not observed). Methanotroph origins for 3-MeH are further supported by the identification of ^{13}C-depleted hopanes and 3-MeH in some ancient rocks (e.g., Ruble et al., 1994). While 3-MeH are found in nearly all rocks, they are rarely present in amounts greater than the Phanerozoic average range of 1-3 percent of C_{30} $\alpha\beta$-desmethylhopane. Interestingly, one of the examples initially used to demonstrate detection and identification of 3-MeH was an Ordovician rock from Australia (Goldwyer formation, Summons and Jahnke, 1990). Anomalously high amounts of 3-MeH have also been detected in bitumens from the Permo-Triassic of South China (Cao et al., 2009), during intervals where sulfur isotopic records indicate extremely low water column sulfate concentrations (Luo et al., 2010).

Results from our Laurentian locations suggest that elevated 3-MeH abundances were a widespread phenomenon in Ordovician seas. 3-MeH indices of 4 - 12 percent (Figures 2.4, 2.6) occur in Anticosti extracts and are greater than 7.2 percent in Cincinnati region bitumens, more than 2,000 km away. Although not as high, Vinini Formation 3-MeH indices (1.7 - 5.7 percent, Figure 2.5) also reach values well above the Phanerozoic average (1 - 3 percent; Cao et al., 2009), and highlight the widespread nature of the signal (Figures 2.1, 2.7, Table 1). Although diagenetic modeling and carbon isotope analyses suggest that classical seep structures and carbon isotope signatures might be absent in low-sulfate intervals of the Lower Paleozoic because of reduced influence of AOM (Bristow and Grotzinger, 2013), the presence of elevated 3-MeH across such broad

geographic scales is more parsimoniously explained by enhanced diagenetic methane cycling on at least a regional scale (consistent, as we propose, with lessened activity of AOM), than by the coincidence of sampling near seeps or advection of methane through both epeiric and western margin settings.

We hypothesize that high 3-MeH abundances were a consequence of warm temperatures in Late Ordovician tropical surface seawater (e.g., Finnegan et al. 2011). High temperatures would have decreased the solubility of O_2 in seawater, and perhaps along with more limited supply of electron acceptors like nitrate and sulfate (e.g., Gill et al., 2007; LaPorte et al., 2009; Hammarlund et al. 2012), promoted greater fermentative recycling of organic matter and an enhanced methane cycle (Luo et al., 2010). Methane produced in shallow sediments and not oxidized through AOM could promote growth of aerobic methanotrophic bacteria, including those which produce 3-MeH.

Sterane carbon number distributions provide useful insight into changes in algal primary production across Phanerozoic time (Grantham and Wakefield, 1988; Schwark and Empt, 2006). The C_{27}-C_{30} steranes in Anticosti Island, Cincinnati region, and Vinini Formation bitumens are dominated by C_{29} isomers (Table 2.1) – biomarkers characteristic of green algae (Volkman, 1986) and typical of Lower Paleozoic marine settings (Grantham and Wakefield, 1988). The small cell size and ability to grow on a variety of nitrogen species possessed by many green algal clades suits them to oligotrophic marine conditions (Parker et al., 2008).

2.4.2 Responses to Hirnantian Cooling

Broad changes in microbial communities and methane cycling took place during Hirnantian time and through the mass extinction intervals (Copper, 2001) and carbon

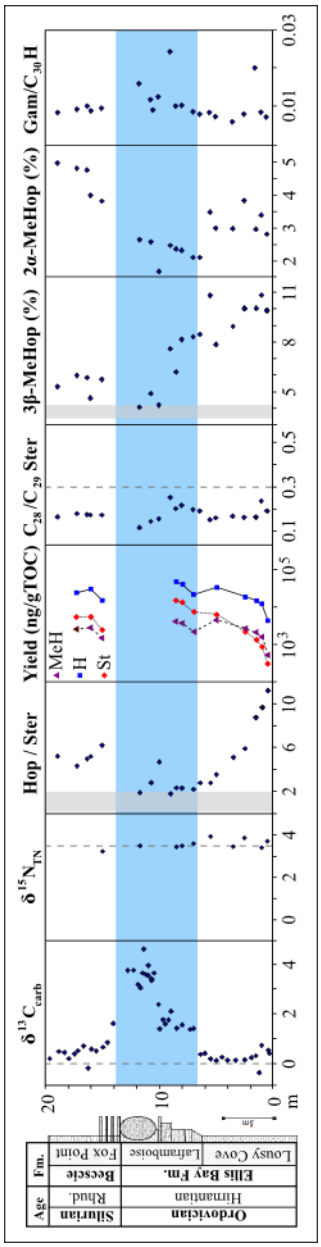

Figure 2.6: Lipid biomarkers through the Hirnantian glacial maximum exposed in outcrop at Anse aux Fraise (901), Anticosti Island with carbon isotope data from Jones et al. (2011). Yields for C_{27}-C_{35} hopanes, C_{27}-C_{29} steranes, and (2α- + 3β)- C_{30}-C_{36} methylhopanes are in ppb of total organic carbon. The vertical gray bar denotes the Phanerozoic averages of 0.5 to 2 for H/St, and 1 - 3 percent for 3β-methylhopane index in marine sedimentary rocks . The horizontal blue bar outlines the canonical carbon isotope excursion. Fm., Formation; Rhudd, Rhuddanian; Hop/Ster, hopane/sterane, H, hopane; St, sterane; MeHop, methylhopane; Gam, gammacerane.

isotope excursion on Anticosti Island (Figures 2.4, 2.6). We observe a large excursion in H/St from an average of H/St around 4 in the Vaural Formation to H/St 12.8 in the Lousy Cove Member, followed by a decline to lower values, all prior to the δ^{13}C excursion in the Laframboise Member. The initiation of the H/St excursion is poorly constrained due to lack of outcrop, but the decline to H/St values less than those of the Vaural Formation is clearly defined (Figures 2.4, 2.6). The decrease in H/St is not coupled to a significant change in lithofacies, as the trajectory stabilizes before deposition of the basal portion of the bioherm-bearing Laframboise member and is not accompanied by a trend in either carbonate or organic carbon content (Jones et al., 2011). This decline in H/St occurs during a reduction in acritarch diversity (Delabroye et al., 2011), possibly reflecting emergence of a lower diversity, higher abundance (bloom-like) algal ecosystem. The lowest H/St values observed on Anticosti occur during a glacial maximum recognized from both sedimentary (Desrochers et al., 2010) and paleoclimate proxy data (Finnegan et al., 2011).

Absolute concentrations of steranes, hopanes, and methylhopanes relative to total organic carbon reveal that all compound classes increase in yield during the decline in H/St and prior to the δ^{13}C excursion (Table 2, Figure 2.6). The increase in yields of these cyclic hydrocarbons could reflect release from kerogen during early-oil window catagenesis (Farrimond et al., 1998) and/or the preferential enrichment of recalcitrant polycyclic alkanes versus linear and branched hydrocarbons during more oxic diagenetic conditions. In either case, the observed rate of increase in sterane abundance is significantly higher than for hopanes as H/St declines (Figure 2.6, Table 2). Consequently a changing eukaryotic (algal) sterane contribution is the major control on the observed H/St ratios. The relative increase in algal production, and hence lower H/St, during the glacial maximum may be explained by an increase in algal production beyond the

capacity of the increase in bacterial respiration of algal organic matter following the H/St excursion, possibly due to a physiological response of algae to cooler temperatures during the peak of Hirnantian glaciation. Alternatively, alleviation of nitrogen limitation by contraction of denitrifying oxygen minimum zones (LaPorte et al., 2009) may have allowed algae to recover rapidly from low levels in the Lousy Cove Member and thrive during the Hirnantian glacial maximum.

High rates of bacterial anaerobic respiration of organic matter at warmer temperatures may explain the elevated H/St through the Late Ordovician, however increased bacterial respiration of algal organic matter due to increased temperature cannot be invoked for the H/St excursion, which takes place during stable or cooling temperatures (Finnegan et al., 2011; Trotter et al., 1998). If bacterial respiration were solely responsible for the low levels of steranes during the H/St excursion, then the interval with the greatest oxidant availability should have the highest H/St. In fact, the H/St is lowest during the interval with the coolest, shallowest and therefore probably best oxygenated water column. Taken together, the increase in total yields, especially of steranes, and lack of evidence for an increase in bacterial respiration rates accompanying the H/St excursion suggest that algal production was selectively impacted during deposition of at least the Lousy Cove Member of the Ellis Bay Formation. These findings are more consistent with a Hirnantian age for the whole Ellis Bay, or with protracted Late Ordovician environmental perturbation, than with the Hirnantian being restricted to the Laframboise member.

Sterane distributions generally remain very stable throughout the studied interval and show a C_{29} sterane dominance during both warm and cool intervals on Anticosti Island as well as in the Vinini Formation (Figure 2.7, Table 2.1). By contrast, microfossil analyses demonstrate that plankton experienced conspicuous extinction over this

interval (Delabroye et al., 2011); this apparent discordance is likely due to the differential sensitivity of the morphological and molecular fossil records to taxonomic level and uncertainties in Paleozoic microfossil phylogenetic affinities (Delabroye et al., 2011). Although a change in sterane distribution towards C_{29} sterane predominance does accompany later mass extinctions, e.g. Permo-Triassic, Cretaceous-Paleogene (Schwark and Empt, 2006), no such trend is observed on Anticosti (Figure 2.6). The relative stability of sterane carbon number patterns through our time series, and dominance of C_{29} steranes, reveals that despite clear plankton extinctions, eukaryotic primary production was dominated by green algae throughout the glaciation and carbon cycle perturbation. A lack of major change in dominant algal taxa is consistent with the lack of permanent macrofaunal ecological turnover in the Late Ordovician mass extinction (Droser et al., 2000). Another possible explanation for stasis in sterane carbon number distribution is that the algal community was already in a Lower Paleozoic "state" in which there was no shifting towards a "more primitive" community because the algal portion of marine primary production was already dominated by green-lineage algae well-suited to warm, oligotrophic conditions and other algae had not yet diversified to provide any other possible state besides variations in the relative amounts of algal and (cyano)bacterial primary producers.

The decline in H/St ratio is followed by a decrease in 3-MeH index from 8 - 11 percent to 4 - 6 percent (Fig. 2.4, Fig. 2.6). This decrease initiates in the Lousy Cove Member, with a drop in the basal Laframboise Member that corresponds to both a significant facies (and eustatic sea level) change (Copper, 2001; Desrochers et al., 2010) and declining sea surface temperature estimates (Finnegan et al. 2011). A similar, though somewhat smaller, trend in 3-MeH index is observed in the Vinini Formation, which declines from 5.7 to 2.6 percent (Figure 2.5). We interpret this pattern as a reduction

in methanogenesis and concomitant methanotrophy due to cooling-driven increases in seawater O_2 concentrations with resultant OMZ contraction (LaPorte et al., 2009) and increased oxidant budgets in shallow sediments. In this fashion, a reduction in methane cycling would have added an important positive feedback on Hirnantian cooling.

A series of C_{31}-C_{36} 2α-methylhopane (2-MeH) also present a nadir during the maximum carbon isotope excursion and sea level low-stand (Figure 2.6). The 2-MeH indices for Anticosti fall within the range commonly observed for marine rocks on Phanerozoic age, changes in their abundance through the sea level fall and rebound may provide some insight into source organisms. Hopanes methylated at C-2 have received particular attention from geobiologists through their inferred association with oxygenic photosynthetic cyanobacteria. Discovery of an anaerobic soil bacterium (Rhodopseudomonas palustris) observed to produce 2-MeH (Rashby et al., 2007) prompted broader investigation. Genes encoding for enzymes needed to produce hopanes from squalane (Pearson and Rusch, 2009), as well as genes for hopane A-ring methylases (Welander et al., 2010; Welander and Summons, 2012), have since been detected in a wide range of bacteria, however it remains to be seen which and how many of these organisms possess all of the needed steps in the pathway and produce 2-MeH, either in environmental samples or in vitro. Although cyanobacterial sources of 2-MeH are well-documented, in modern environments all known 2-MeH synthesizing cyanobacteria inhabit freshwater environments. Some assistance in differentiation among these potential sources may come from other lipids. In the case of *R. palustris*, tetrahymanol – a pentacyclic isoprenoid with a geolipid product (gammacerane) of similar preservation potential to hopanes – is produced in addition to 2-MeH. Thus, if we posit that soil bacteria such as *R. palustris* are the sources of 2-MeH in Anticosti extracts and apply a uniformitarian view of biosynthesis, gammacerane should describe similar trends, a feature which is not observed (Figure

2.6). Additionally, compounds derived from soil (whether from cyanobacteria or proteobacteria) might be expected to reach maximum abundance during the shallowest sea level, when shorelines are closest to the depositional environment, a pattern also not observed for 2-MeH. Together, the lack of correlation between 2-MeH and gammacerane, and inverse relationship between 2-MeH and sea-level, are most consistent with a marine, cyanobacterial origin for 2-MeH.

Yields diminish, a small unresolved complex mixture appears, and normal isomer patterns of homohopanes and steranes are disrupted within the biohermal interval, perhaps reflecting a "real" increase in degradation of organic matter or else contamination by fluids migrating through the more-porous, locally recrystallized bioherms. In either case, it is difficult to interpret the results from this interval with confidence; data from the biohermal interval of the Laframboise member are therefore excluded.

2.4.3 Silurian Recovery

Lipid biomarker profiles in the lowermost Silurian Becscie Formation on Anticosti Island reflect a return to microbial communities similar to those preceding the Hirnantian glacial maximum (Figures 2.4, 2.6). Although our Silurian sample coverage is not extensive due to more prevalent grainstone lithologies, a H/St ratio of 5.6 in a sample from the Aeronian Merrimack Formation suggests that bacteria once again made a significantly higher contribution to primary productivity relative to algae compared with typical Phanerozoic marine rocks and oils. The Silurian bitumens also record high 3-MeH indices, implying that methane cycling was again enhanced during the warm period (Finnegan et al., 2011) that followed the Hirnantian glacial maximum (Figures 2.4, 2.6).

2.4.4 Correlation

Anticosti Island and Cincinnati region samples were collected by the authors contemporaneously with samples collected for carbon, oxygen, and clumped isotope analyses presented elsewhere (Jones et al., 2011; Finnegan et al., 2011) under the same sample nomenclature. As a result, the stratigraphic relationships among these samples are very well constrained. Anticosti Island sampling locations are presented in Figure 2.2. Vinini Formation samples were donated by Dr. Stan Finney (California State University, Long Beach) from collections he and colleagues, particularly Dr. John Cooper (dec.), made during excavation of the trench at Vinini Creek. The stratigraphic positions of these samples are derived from Dr. Cooper's notes and the graptolite biostratigraphy they assembled (Finney et al., 1999; Storch et al., 2011). Cincinnati region samples were collected at the South Gate Hill outcrop near Cedar Grove, Indiana (Holland, 1993). Although the absolute chronology of the graptolite-depauperate Ellis Bay formation, and therefore its relationship to the Vinini Formation, remains a work in progress, the linkage between lipid biomarker samples and clumped isotope paleotemperature calculations is robust.

Correlation among sites within Laurentia as well as across paleocontinents is hampered by rampant endemism and strong environmental associations of many biostratigraphically useful Paleozoic taxa. Different, though no less pernicious, challenges exist for chemostratigraphic correlation: Late Ordovician carbon isotope stratigraphies bear multiple excursions of varying magnitude and geographic extent (see, e.g. Delabroye and Vecoli, 2010; Holmden et al., 2013), doubtless reflecting a spectrum of local to global carbon cycling effects (Brenchley et al., 1994; Kump et al., 1999; Melchin and

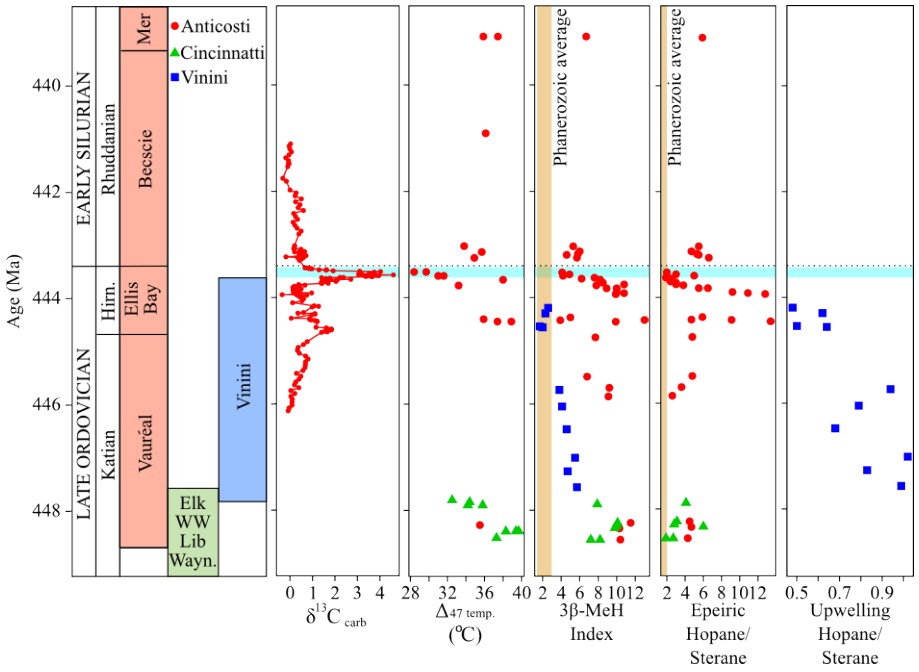

Figure 2.7: Correlation scheme for lipid biomarker stratigraphic records from Western Anticosti Island, Canada, the Cincinnati region of the U.S.A. and Vinini Formation of Nevada, U.S.A. plotted with a stable carbon isotope ($\delta^{13}C_{carb}$) profile from Anticosti Island (Jones et al., 2011) and clumped isotope paleothermometry estimates of sea surface temperatures (Finnegan et al., 2011) in which the entire Ellis Bay Formation is assigned to the Hirnantian Stage.

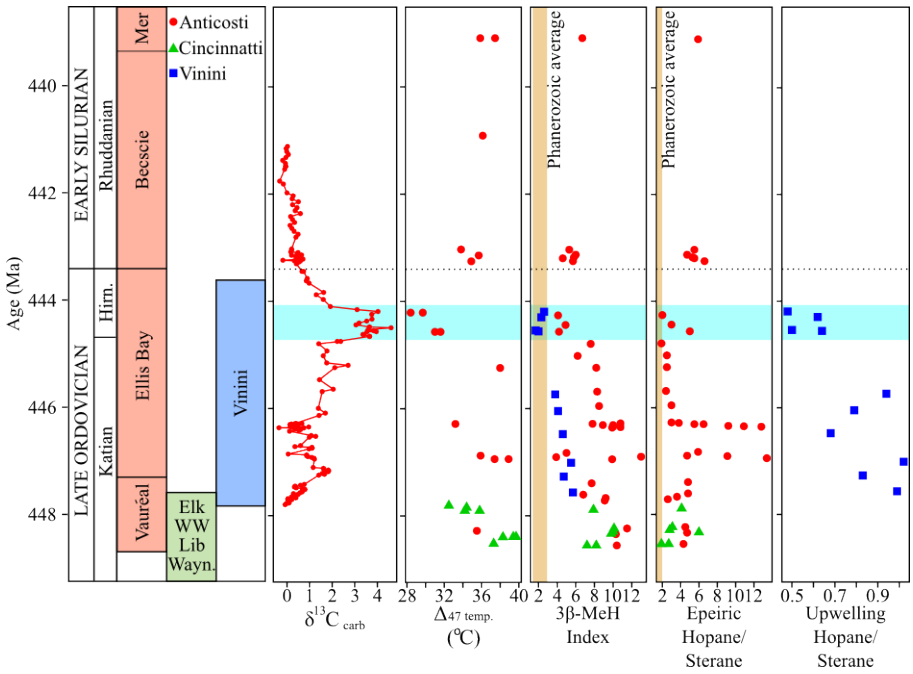

Figure 2.8: Correlation scheme for lipid biomarker stratigraphic records from Western Anticosti Island, Canada, the Cincinnati region of the U.S.A. and Vinini Formation of Nevada, U.S.A. plotted with a stable carbon isotope (ca) profile from Anticosti Island (Jones et al., 2011) and clumped isotope paleothermometry estimates of sea surface temperatures (Finnegan et al., 2011) in which only the Laframboise Member of the Ellis Bay Formation is assigned to the Hirnantian Stage.

Holmden, 2006).

In particular, correlation among Anticosti, Cincinnati region, and Vinini Formation samples is complicated by continuing discussion over the age of the Ellis Bay Formation of Anticosti Island, that is, whether the entire Ellis Bay Formation is Hirnantian in age (Figure 2.7), or only its uppermost Member (Laframboise, Figure 2.8). We present a correlation based on graptolite biostratigraphy (Loydell, 2012) and carbon isotope chemostratigraphy (Figure 2.7), as well as an alternative correlation proposed elsewhere (Jones et al., 2011) (Figure 2.8). For our dataset, correlation based on graptolite biostratigraphy results in an offset between the Vinini Formation and Anticosti trends (Figure 2.7) whereas correlation based on carbon isotope chemostratigraphy results in similar timing for the decline in 3-methylhopanes and hopane/sterane ratios between the Vinini Formation and Anticosti (Figure 2.8). More broadly, biomarker evidence for substantial impacts on microbial communities from lower in the Ellis Bay Formation imply, in the case of the Laframboise Member as Hirnantian dating scheme, environmental perturbation well in advance of the glacial maximum and less extensive impacts during the glacial maximum (Figure 2.8). A Hirnantian age for the entire Ellis Bay Formation constrains major perturbations to microbial communities to the Hirnantian (Figure 2.7).

2.5 Conclusions

Biomarker patterns in tropical shallow marine basins through the Hirnantian stage capture a fundamental restructuring of marine microbial communities during this interval of climate change. Bacterial primary production was favored during warm, greenhouse climates and low oxidant, expanded OMZ conditions; eukaryotic production

(mainly by green algae) was tied to regions and intervals of cooler ocean temperatures and contracted OMZ conditions. The coupling of lipid biomarkers with independent paleoenvironmental proxies provides a framework for interpreting systematic changes in 3β-methylhopane abundances, a widespread but previously enigmatic characteristic of Ordovician-aged source rocks. High 3β-methylhopane indices imply enhanced methane cycling under warm, lower oxidant environmental conditions, and outline the existence and mechanics of a positive climate feedback that would have both promoted warm climates, maintaining the expanded OMZs observed in Late Ordovician marine basins, as well as amplified cooling during the Hirnantian glacial maximum.

2.6 Acknowledgments

This work was supported by the Agouron Institute. The authors wish to thank D. Boulet and the Societe des etablissements de plein air du Quebec for assistance with work in Anticosti National Park, Stan Finney (California State University, Long Beach) for donation of the Vinini Formation samples, David Jones (Amherst College) for providing carbon isotope data and help with Anticosti fieldwork, and Kristin Bergmann (Caltech) for help with Cincinnati region fieldwork. The authors also wish to acknowledge the editors of Geology for permission to use previously published material in this Dissertation.

2.7 References

1. Achab, A., Asselin, E., Desrochers, A., Riva, J.F., and Farley, C., 2011, Chitinozoan biostratigraphy of a new Upper Ordovician stratigraphic framework for Anticosti Island, Canada: Geological Society of America Bulletin, v.123, p.186205.
2. Armstrong, H.A., Abbott, G.D., Turner, B.R., Makhlouf, I.M., Muhammad, A.B., Pedentchouk, N., Peters, H., 2009, Black shale deposition in an Upper Ordovician-

Silurian permanently stratified peri-glacial basin, southern Jordan: Palaeogeography, Palaeoclimatology, Palaeoecology, v. 273, p. 368-377.

3. Berner, R.A., and Kothavala, Z., 2001, GEOCARB III: A revised model of atmospheric CO_2 over Phanerozoic time: American Journal of Science, v.301, p.182204.

4. Bertrand, R., 1990, Maturation thermique et histoire de lenfouissement et de la generation des hydrocarbures du bassin de larchipel de Mingan et de lile dAnticosti, Canada: Canadian Journal of Earth Sciences, v.27, p.731741.

5. Birgel, D., Himmler, T., Freiwald, A., Peckmann, J., 2008, A new constraint on the antiquity of anaerobic oxidation of methane: Late Pennsylvanian seep limestones from southern Namibia: Geology, v. 36, p. 543-546.

6. Brenchley, P.J., Marshall, J.D., Carden, G.A.F., Robertson, D.B.R., Long, D.G.F., Meidla, T., Hints, L., and Anderson, T.F., 1994, Bathymetric and isotopic evidence for a short-lived Late Ordovician glaciation in a greenhouse period: Geology, v.22, p.295298.

7. Bristow, T.F., Grotzinger, J.P., 2013, Sulfate availability and the geological record of cold-seep deposits: Geology, v. 41, p. 831-834.

8. Cao, C., Love, G.D., Hays, L.E., Wang, W., Shen, S., and Summons, R.E., 2009, Biogeochemical evidence for euxinic oceans and ecological disturbance presaging the end-Permian mass extinction event: Earth and Planetary Science Letters, v.281, p.188201.

9. Cocks, L.R.M., and Torsvik, T.H., 2002, Earth geography from 500 to 400 million years ago: A faunal and palaeomagnetic review: Journal of the Geological Society, v.159, p.631644.

10. Copper, P., 2001, Reefs during the multiple crises towards the Ordovician-Silurian boundary: Anticosti Island, eastern Canada, and worldwide: Canadian Journal of Earth Sciences, v.38, p.153171.

11. Delabroye, A., Vecoli, M., 2010, The end-Ordovician glaciation and the Hirnantian Stage: A global review and questions about Late Ordovician event stratigraphy: Earth-Science Reviews, v. 98, p. 269-282.

12. Delabroye, A., Munnecke, A., Vecoli, M., Copper, P., Tribovillard, N., Joachimski, M.M., Desrochers, A., and Servais, T., 2011, Phytoplankton dynamics across the Ordovician/Silurian boundary at low paleolatitudes: Correlations with carbon isotopic and glacial events: Palaeoceanography, Palaeoclimatology: Palaeoecology, v.312, p.7997.

13. Desrochers, A., Farley, C., Achab, A., Asselin, E., and Riva, J.F., 2010, A far-field record of the end Ordovician glaciation: The Ellis Bay formation, Anticosti, Island, Eastern Canada: Palaeoceanography, Palaeoclimatology: Palaeoecology, v.296, p.248263.

14. Farrimond, P., Taylor, A., and Telns, N., 1998, Biomarker maturity parameters: The role of generation and thermal degradation: Organic Geochemistry, v.29, p.11811197.

15. Farrimond, P., Talbot, H.M., Watson, D.F., Schulz, L.K., and Wilhelms, A., 2004, Methylhopanoids: Molecular indicators of ancient bacteria and a petroleum correlation tool: Geochimica et Cosmochimica Acta, v.68, p.38733882.

16. Finnegan, S., Bergmann, K., Eiler, J.M., Jones, D.S., Fike, D.A., Eisenman, I., Hughes, N.C., Tripati, A.K., and Fischer, W.W., 2011, The magnitude and duration of Late Ordovician-Early Silurian glaciation: Science, v.331, p.903906.

17. Finnegan, S., Heim, N., Peters, S., and Fisher, W.W., 2012, Climate change and the selective signature of the Late Ordovician mass extinction: Proceedings of the National Academy of Sciences of the United States of America.

18. Finney, S.C., Berry, W.B.N., Cooper, J.D., Ripperdan, R.L., Sweet, W.C., Jacobson, S.R., Soufiane, A., Achab, A., and Noble, P.J., 1999, Late Ordovician mass extinction: A new perspective from stratigraphic sections in central Nevada: Geology, v.27, p.215218.

19. Finney, S.C., Berry, W.B.N., and Cooper, J.D., 2007, The influence of denitrifying seawater on graptolite extinction and diversification during the Hirnantian (latest Ordovician) mass extinction event: Lethaia, v.40, p.281291.

20. Fowler, M.G., and Douglas, A.G., 1984, Distribution and structure of hydrocarbons in four organic-rich Ordovician rocks: Organic Geochemistry, v. 6, p. 105-114.

21. Frey, R.C., 1987, The occurrence of pelecypods in Early Paleozoic epeiric-sea environments, Late Ordovician of the Cincinnati, Ohio area: Palaios, v. 2, p. 3-23.

22. Gill, B.C., Lyons, T.W., and Saltzman, M.R., 2007, Parallel, high-resolution carbon and sulfur isotope records of the evolving Paleozoic marine sulfur reservoir: Palaeogeography, Palaeoclimatology, Palaeoecology, v.256, p.156173.

23. Grantham, P.J., and Wakefield, L.L., 1988, Variations in the sterane carbon number distributions of marine source rock derived crude oils through geological time: Organic Geochemistry, v.12, p.6173.

24. Grice, K, Cao, C., Love, G.D., Bottcher, M.E., Twitchett, R.J., Grosjean, E., Summons, R.E., Turgeon, S.C., Dunning, W., Jin, Y. 2005, Photic zone euxinia during the Permian-Triassic superanoxic event: Science, v. 307, p. 706-709.

25. Guthrie, J.M., and Pratt, L.M., 1995, Geochemical character and origin of oils in Ordovician reservoir rock, Illinois and Indiana, USA: American Association of Petroleum Geologists Bulletin, v. 79, p. 1631-1649.

26. Hallam, A., 1992, Phanerozoic Sea-Level Changes: New York, Columbia University Press, 230 p.

27. Hammarlund, E.U., Dahl, T.W., Harper, D.A.T., Bond, D.P.G., Nielsen, A.T., Bjerrum, C.J., Schovsbo, N.H., Schonlaub, H.P., Zalasiewicz, J.A., and Canfield, D.E., 2012, A sulfidic driver for the end-Ordovician mass extinction: Earth and Planetary Science Letters, v.331, p.128139.

28. Higgins, M.B., Robinson, R.S., Husson, J.M., Carter, S.J., and Pearson, A., 2012, Dominant eukaryotic export production during ocean anoxic events reflects the importance of recycled NH4+: Proceedings of the National Academy of Sciences of the United States of America, v.109, p.22692274.

29. Hoffmann, C.F., Foster, C.B., Powell, T.G., Summons, R.E., 1987, Hydrocarbon biomarkers from Ordovician sediments and the fossil alga *Gloeocapsomorpha prisca* Zalessky 1917: Geochimica et Cosmochimica Acta, v. 51, p. 2681-2697.

30. Holland, S.M., 1993, Sequence stratigraphy of a carbonate-clastic ramp: The Cincinnatian Series (Upper Ordovician) in its type area: Geological Society of America Bulletin, v.105, p.306322.

31. Holland, S.M., and Patzkowsky, M.E., 2007, Gradient ecology of a biotic invasion: Biofacies of the type Cincinnatian Series (Upper Ordovician), Cincinnati, Ohio region, U.S.A.: Palaios, v. 22, p. 392-407.

32. Holmden, C., Panchuk, K., and Finney, S.C., 2012, Tightly coupled records of Ca and C isotope changes during the Hirnantian glaciation event in an epeiric sea setting: Geochimica et Cosmochimica Acta, v. 98, p. 94-106.

33. Holmden, C., Mitchell, C.E., LaPorte, D.F., Patterson, W.P., Melchin, M.J., Finney, S.C., 2013, Nd isotope records of late Ordovician sea-level change– Implications for glaciation frequency and global stratigraphic correlation: Palaeogeography, Palaeoclimatology, Palaeoecology, v. 386, p. 131-144.

34. Jacobson, S.R., Hatch, J.R., Teerman, S.C., Askin, R.A., 1988, Middle Ordovician organic matter assemblages and their effect on Ordovician-derived oils: American Association of Petroleum Geologists Bulletin, v. 72, p. 1090-1100.

35. Jones, D.S., Fike, D.A., Finnegan, S., Fischer, W.W., Schrag, D.P., and McCay, D., 2011, Terminal Ordovician carbon isotope stratigraphy and glacioeustatic sea-level change across Anticosti Island (Qubec, Canada): Geological Society of America Bulletin, v.123, p.16451664.

36. Kump, L.R., Arthur, M.A., Patzkowsky, M.E., Gibbs, M.T., Punkus, D.S., Sheehand, P.M., 1999, A weathering hypothesis for glaciation at high atmospheric pCO_2 during the Late Ordovician: Palaeogeography, Palaeoclimatology, Palaeoecology, v. 152, p. 173-187.

37. Kuypers, M.M.M., Blokker, P., Erbacher J., Kinkel, H., Pancost, R.D., Schouten, S., Sinninghe Damste, J.S., 2001, Massive expansion of marine archaea during a mid-Cretaceous ocean anoxic event: Science, v. 293, p. 92-94.

38. LaPorte, D.F., Holmden, C., Patterson, W.P., Loxton, J.D., Melchin, M.J., Mitchell, C.E., Finney, S.C., and Sheets, H.D., 2009, Local and global perspectives on carbon and nitrogen cycling during the Hirnantian glaciation: Palaeogeography, Palaeoclimatology, Palaeoecology, v.276, p.182195.

39. Long, D.G.F., 1993, Oxygen and carbon isotopes and event stratigraphy near the Ordovician-Silurian boundary, Anticosti Island Quebec: Palaeogeography, Palaeoclimatology, Palaeoecology, v. 104, p., 4959.

40. Long, D.G.F., 2007, Tempestite frequency curves: A key to Late Ordovician and Early Silurian subsidence, seal-level change, and orbital forcing in the Anticosti foreland basin, Quebec, Canada: Canadian Journal of Earth Sciences, v.44, p.413431, doi:10.1139/e06-099.

41. Loydell, D.K., 2012, Graptolite biozone correlation charts: Geological Magazine, v. 149, p. 124-132, doi: 10.1017/S0016756811000513.

42. Luo, G., Kump, L.R., Wang, Y., Tong, J., Arthur, M.A., Yang, H., Huang, J., Yin, H., and Xie, S., 2010, Isotopic evidence for an anomalously low oceanic sulfate concentration following end-Permian mass extinction: Earth and Planetary Science Letters, v.300, p.101111.

43. Marynowski, L., Narkiewicz, M., Grelowski, C., 2000, Biomarkers as environmental indicators in a carbonate complex, example from the Middle to Upper Devonian, Holy Cross Mountains, Poland: Sedimentary Geology, v. 137, p. 187-212.

44. Melchin, M.J., Mitchell, C.E., Naczk-Cameron, A., Fan, J.X., Loxton, J., 2011, Phylogeny and adaptive radiation of the Neograptina (Graptoloida) during the Hirnantian mass extinction and Silurian recovery: Proceedings of the Yorkshire Geological Society, v. 58, p. 281-309.

45. Melchin, M.J., Holmden, C., 2006, Carbon isotope chemostratigraphy in Arctic Canada: Sea-level forcing of carbonate platform weathering and implications for Hirnantian global correlation: Palaeogeography, Palaeoclimatology, Palaeoecology, v. 234, p. 186-200.

46. Newell, N.D., 1949, Periodicity in invertebrate evolution: Geological Society of America Bulletin, v. 60, p. 1911-1912.

47. Orth, C.J., Gilmore, J.S., Quintana, L.R., Sheehan, P.M., 1986, Terminal Ordovician extinction: Geochemical analysis of the Ordovician/Silurian boundary, Anticosti Island, Quebec: Geology, v. 14, p. 433-436.

48. Pancost, R.D., Freeman, K.H., Patzkowsky, M.E., Wavrek, D.A., and Collister, J.W., 1998, Molecular indicators of redox and marine photoautotroph composition in the late Middle Ordovician of Iowa, U.S.A: Organic Geochemistry, v.29, p.16491662.

49. Pancost, R.D., Freeman, K.H., Patzkowsky M.E., 1999, Organic-matter source variation and the expression of a late Middle Ordovician carbon isotope excursion: Geology, v. 27, p. 1015-1018.

50. Parker, M.S., Mock, T., and Armbrust, E.V., 2008, Genomic insights into marine microalgae: Annual Review of Genetics, v.42, p.619645.

51. Pearson, A., Rusch, D.B., 2009, Distribution of microbial terpenoid lipid cyclases in the global ocean metagenome: The ISME Journal, v. 3, p. 352-363.

52. Peters, K.E., Walters, C.C., and Moldowan, J.M., 2003, The Biomarker Guide, 2nd edition: Cambridge, UK, Cambridge University Press, 1132 p.

53. Peters, S.E., 2006, Genus extinction, origination, and the durations of sedimentary hiatuses: Paleobiology, v. 32, p. 387-407.

54. Pope, M.C., and Steffen, J.B., 2003, Widespread, prolonged late Middle to Late Ordovician upwelling in North America: A proxy record of glaciation?: Geology, v.31, p.6366.

55. Raatz, W.D., and Ludvigson, G.A., 1996, Depositional environments and sequence stratigraphy of Upper Ordovician epicontinental deep water deposits, eastern Iowa and southern Minnesota: Geological Society of America. Special Paper, v.306, p.143159.

56. Rashby, S.E., Sessions, A.L., Summons, R.E., Newman, D.K., 2007, Biosynthesis of 2-methylbacteriohopanepolyols by an anoxygenic phototroph: Proceedings of the National Academy of Sciences, v. 104, p. 15099-15104.

57. Reed, J.D., Illich, H.A., and Horsfield, B., 1986, Biochemical evolutionary significance of Ordovician oils and their sources: Organic Geochemistry, v.10, p.347358.

58. Ruble, T.E., Bakel, A.J., and Philp, R.P., 1994, Compound specific isotopic variability in Uinta Basin native bitumens: Paleoenvironmental implications: Organic Geochemistry, v.21, p.661671.

59. Sadler, P.M., Cooper, R.A., Melchin, M., 2009, High-resolution, early Paleozoic (Ordovician-Silurian) time scales: Geological Society of America Bulletin, v. 121, p. 887-906.

60. Saltzman, M.R., 2005, Phosphorus, nitrogen, and the redox evolution of the Paleozoic oceans: Geology, v. 33, p. 573-576.

61. Schwark, L., and Empt, P., 2006, Sterane biomarkers as indicators of Palaeozoic algal evolution and extinction events: Palaeogeography, Palaeoclimatology, Palaeoecology, v.240, p.225236.

62. Sepulveda, J., Wendler, J., Leider, A., Kuss, H.-J., Summons, R.E., Hinrichs, K.-U., 2009, Molecular isotopic evidence of environmental and ecological changes across the Cennomanian-Turonian boundary in the Levant Platform of central Jordan: Organic Geochemistry, v. 40, p. 553-568.

63. Sheehan, P.M., 2001, The Late Ordovician mass extinction: Annual Review of Earth and Planetary Sciences, v.29, p.331364, doi:10.1146/annurev.earth.29.1.331.

64. Storch, P., Mitchell, C.E., Finney, S.C., and Melchin, M., 2011, Uppermost Ordovician (upper Katian - Hirnantian) graptolites of north-central Nevada, U.S.A.: Bulletin of Geosciences, v. 86, p. 301-386.

65. Stueken, E.E., 2013, A test of the nitrogen-limitation hypothesis for retarded eukaryote radiation: Nitrogen isotopes across a Mesoproterozoic basinal profile: Geochimica et Cosmochimica Acta, v. 120, p. 121-139.

66. Summons, R.E., and Jahnke, L.L., 1990, Identification of the methylhopanes in sediments and petroleum: Geochimica et Cosmochimica Acta, v.54, p.247251.

67. Summons, R.E., Bradley, A.S., Jahnke, L.L., and Waldbauer, J.R., 2006, Steroids, triterpenoids and molecular oxygen: Philosophical Transactions of the Royal Society of London. Series B, Biological Sciences, v.361, p.951968.

68. Trotter, J.A., Williams, I.S., Barnes, C.R., Lecuyer, C., Nicoll, R.S., 2008, Did cooling oceans trigger Ordovician biodiversification? Evidence from conodont thermometry: Science, v. 321, p. 550-554.

69. Volkman, J.K., 1986, A review of sterol markers for marine and terrigenous organic matter: Organic Geochemistry, v.9, p.8399, doi:10.1016/0146-6380(86)90089-6.

70. Welander, P.V., Coleman, M.L., Sessions, A.L., Summons, R.E., Newmann, D.K., 2010, Identification of a methylase required for 2-methylhopanoid production and implicatons for the interpretation of sedimentary hopanes: Proceedings of the National Academy of Sciences, v. 107, p. 8537-8542.

71. Welander, P.V., and Summons, R.E., 2013, Discovery, taxonomic distribution, and phenotypic characterization of a gene required for 3-methylhopanoid production: Proceedings of the National Academy of Sciences, v. 109, p. 12905-12910.

72. Witzke, B.J., 1987, Models for circulation patterns in epicontinental seas applied to Paleozoic facies of North American craton: Paleoceanography, v.2, p.229248.

73. Yapp, C.J., and Poths, H., 1992, Ancient atmospheric CO_2 pressures inferred from natural goethites: Nature, v. 355, p. 342-344.

74. Young, S.A., Saltzman, M.R., Ausich, W.I., Desrochers, A., and Kaljo, D., 2010, Did changes in atmospheric CO_2 coincide with latest Ordovician glacial-interglacial cycles?: Palaeogeography, Palaeoclimatology, Palaeoecology, v.296, p.376388.

Sample[1]	Formation	Member	TIC (wt %)	TOC (wt%)	H/St[2]	Gamm[3] / C_{30} αβH	2-MeH I[4] (%)	3-MeH I[4] (%)	C_{27} Sterane[5] (%C_{27}-C_{29})	C_{28} Sterane[5] (%C_{27}-C_{29})	C_{29} Sterane[5] (%C_{27}-C_{29})	C_{28}/C_{29} Steranes
ANTICOSTI												
916-29.1	Merrimack		10.8	<0.1	5.91	0.01	4.4	6.7	27	12	62	0.19
901-18.9	Becscie	Fox Point	10.8	0.54	5.52	0.01	4.0	5.3	23	11	66	0.16
901-17.2	Becscie	Fox Point	10.3	0.39	4.74	0.01	4.0	6.0	24	11	65	0.18
901-16.3	Becscie	Fox Point	11.1	0.15	5.27	0.01	4.0	5.8	24	11	65	0.17
901-16.0	Becscie	Fox Point	10.6	0.23	5.51	0.01	2.9	4.6	25	11	64	0.17
901-15.0	Becscie	Fox Point	11.0	0.39	6.58	0.01	3.5	5.7	25	11	64	0.17
901-11.7	Ellis Bay	Laframboise	10.4	0.09	2.04	0.02	2.3	4.1	17	8	74	0.11
901-10.7	Ellis Bay	Laframboise	10.2	0.48	2.99	0.01	2.4	4.9	21	10	69	0.14
901-10.0	Ellis Bay	Laframboise	10.8	0.20	4.98	0.01	1.3	4.2	24	10	66	0.15
901-9.0	Ellis Bay	Laframboise	8.9	0.10	1.90	0.02	2.2	7.6	25	15	60	0.25
901-8.5	Ellis Bay	Laframboise	7.8	0.15	2.51	0.01	1.7	6.2	27	12	61	0.20
901-8.0	Ellis Bay	Laframboise	7.2	0.16	2.49	0.01	2.1	8.2	27	13	60	0.21
901-7.0	Ellis Bay	Laframboise	7.5	0.33	2.37	0.01	1.9	8.3	28	12	61	0.19
901-6.4	Ellis Bay	Laframboise	8.6	<0.1	2.98	0.01	1.7	8.5	27	12	61	0.19
901-5.5	Ellis Bay	Lousy Cove	n.m.	n.m.	2.98	0.01	3.3	10.8	24	10	66	0.15
901-5.0	Ellis Bay	Lousy Cove	10.2	0.40	3.79	0.01	4.1	7.8	24	10	65	0.16
901-3.5	Ellis Bay	Lousy Cove	8.7	0.29	5.48	0.01	2.7	8.9	27	10	62	0.16
901-2.5	Ellis Bay	Lousy Cove	9.1	0.32	6.54	0.01	3.5	10.0	28	10	62	0.16
901-1.5	Ellis Bay	Lousy Cove	8.8	0.25	9.18	0.02	3.1	10.0	28	10	62	0.16
901-1.0	Ellis Bay	Lousy Cove	8.2	0.16	10.92	0.01	3.5	10.8	31	13	56	0.23
901-0.5	Ellis Bay	Lousy Cove	8.9	0.32	12.82	0.01	3.0	9.9	32	11	57	0.19
904-7.5	Ellis Bay	Grindstone	10.9	<0.1	8.33	0.01	7.5	5.2	26	12	62	0.19
904-3.0	Ellis Bay	Grindstone	5.53	0.17	5.88	0.02	2.6	13.0	35	12	53	0.24
904-2.5	Ellis Bay	Grindstone	9.96	0.13	9.05	0.01	3.9	3.9	31	11	58	0.19
904-0.0	Ellis Bay	Grindstone	7.65	0.15	17.85	0.02	2.4	7.7	34	11	55	0.19

[1]First portion of sample name indicates sampling site (Figure 2.2), remaining digits are meter height in logged section. [2]Hop/Ster is the ratio of 19 C_{27} to C_{35} hopane isomers (Ts, Tm, two C_{28} hopanes, C_{29} to C_{35} αβ-hopanes, and C_{29} to C_{31}βα-hopanes. [3]Gamm, gammacerane. [4]C_{31}2α-methylhopane and C_{31}3β-methylhopane indices calculated as percentages of [C_{31}methylhopane/(C_{31}methylhopane+ C_{30}αβ-hopane)*100]. [5]Diasteranes and regular steranes as a percentage of C_{27}-C_{29} steranes due to the sub-detection limit concentrations of C_{30} steranes.

Table 2.1: Selected lipid biomarker ratios for Anticosti, the Cincinnati Region, and the Vinini Formation.

Table 2.2: Table 2.1 continued.

Sample[1]	Formation	Member	TIC (wt %)	TOC (wt%)	H/St[2]	Gamm[3] / C_{30} αβH	2-MeH I[4] (%)	3-MeH I[4] (%)	C_{27} Sterane[5] (%C_{27}-C_{29})	C_{28} Sterane[5] (%C_{27}-C_{29})	C_{29} Sterane[5] (%C_{27}-C_{29})	C_{28}/C_{29} Steranes
ANTICOSTI (cont.)												
902-21.5	Vaureal	Schmitt Creek	11.0	0.23	4.85	0.01	6.4	7.7	29	12	58	0.21
902-7.5	Vaureal	Schmitt Creek	n.m.	n.m.	4.75	0.02	6.3	6.8	32	12	56	0.21
902-3.6	Vaureal	Schmitt Creek	11.1	0.31	3.59	0.02	5.8	9.2	32	14	54	0.26
902-0.6	Vaureal	Schmitt Creek	8.2	0.30	2.62	0.01	7.5	9.1	39	13	48	0.27
906-56	Vaureal	Lavache	11.2	0.18	4.49	0.01	6.2	11.5	32	14	54	0.26
906-52	Vaureal	Lavache	10.8	0.19	4.73	0.01	5.7	10.3	33	15	52	0.28
906-44	Vaureal	Lavache	9.4	0.37	4.26	0.01	11.3	10.4	32	15	53	0.28
CINCINNATI REGION												
SGH-UL/WW	U. Liberty / L.Whitewater		9.9	<0.1	4.11	0.02	1.9	7.9	33	14	53	0.26
SGH-TOS	Liberty?		11.5	0.20	3.07	0.02	1.9	10.1	48	14	37	0.39
SGH-50.5	Liberty		11.2	0.18	2.83	0.03	1.7	10.0	45	13	42	0.30
SGH-43	Liberty?		1.5	0.20	6.05	0.02	1.3	9.8	31	18	51	0.35
SGH-13A	Waynesville		5.5	0.17	1.86	0.03	2.6	8.2	39	14	47	0.31
SGH-13B	Waynesville		7.6	<0.1	2.71	0.03	3.4	7.2	40	14	45	0.32
VININI FORMATION, NEVADA												
VC-08	Vinini		11.2	0.46	0.48	0.11	3.9	2.6	19	11	70	0.16
VC-05	Vinini		8.4	1.68	0.62	0.10	4.0	2.3	26	12	63	0.18
VC-01	Vinini		8.1	0.54	0.50	0.28	2.0	1.7	19	12	69	0.17
VA-31	Vinini		n.m.	n.m.	0.64	0.08	2.0	2.0	22	11	67	0.16
VA-30	Vinini		n.m.	n.m.	0.66	0.07	1.6	1.7	24	11	65	0.17
VA-27	Vinini		n.m.	n.m.	0.46	0.07	2.4	3.6	23	13	65	0.19
VA-25	Vinini		n.m.	n.m.	0.38	0.08	2.8	2.5	24	12	63	0.19
VA-23	Vinini		0.0	18.39	0.94	0.05	2.5	3.8	27	11	61	0.19
VA-20	Vinini		10.3	2.10	0.79	0.06	2.4	4.1	18	10	71	0.14

[1]First portion of sample name indicates sampling site (Figure 2.2), remaining digits are meter height in logged section. [2]Hop/Ster is the ratio of 19 C_{27} to C_{35} hopane isomers (Ts, Tm, two C_{28} hopanes, C_{29} to C_{35} αβ-hopanes, and C_{29} to C_{31}βα-hopanes. [3]Gamm, gammacerane. [4]C_{31}2α-methylhopane and C_{31}3β-methylhopane indices calculated as percentages of [C_{31}methylhopane/(C_{31}methylhopane+ C_{30}αβ-hopane)*100]. [5]Diasteranes and regular steranes as a percentage of C_{27}-C_{29} steranes due to the sub-detection limit concentrations of C_{30} steranes.

Sample[1]	Formation	Member	TIC (wt %)	TOC (wt%)	H/St[2]	Gamm[3] / C_{30} αβH	2-MeH I[4] (%)	3-MeH I[4] (%)	C_{27} Sterane[5] (%C_{27}-C_{29})	C_{28} Sterane[5] (%C_{27}-C_{29})	C_{29} Sterane[5] (%C_{27}-C_{29})	C_{28}/C_{29} Steranes
VININI FORMATION, NEVADA (cont.)												
VA-18	Vinini		9.9	0.85	0.68	0.04	2.8	4.6	24	12	64	0.20
VA-16	Vinini		n.m.	n.m.	0.37	0.08	3	5	24	12	64	0.19
VA-16gs	Vinini		n.m.	n.m.	0.37	0.09	3	5	24	12	64	0.19
VA-13	Vinini		n.m.	n.m.	0.52	0.06	4.1	4.9	23	12	64	0.19
VA-12	Vinini		10.6	0.14	1.02	0.08	4.6	5.5	23	13	64	0.20
VA-10	Vinini		4.6	1.66	0.83	0.08	3.6	4.7	23	12	65	0.18
VA-08	Vinini		9.6	0.52	0.99	0.08	4.6	5.7	21	12	67	0.19

[1]First portion of sample name indicates sampling site (Figure 2.2), remaining digits are meter height in logged section. [2]Hop/Ster is the ratio of 19 C_{27} to C_{35} hopane isomers (Ts, Tm, two C_{28} hopanes, C_{29} to C_{35} αβ-hopanes, and C_{29} to C_{31}βα-hopanes. [3]Gamm, gammacerane. [4]C_{31}2α-methylhopane and C_{31}3β-methylhopane indices calculated as percentages of [C_{31}methylhopane/(C_{31}methylhopane+ C_{30}αβ-hopane)*100]. [5]Diasteranes and regular steranes as a percentage of C_{27}-C_{29} steranes due to the sub-detection limit concentrations of C_{30} steranes.

Table 2.3: Table 2.1 continued.

Sample	All Steranes (ppb/TOC)	All Hopanes (ppb/TOC)	(2- + 3-) Methylhopanes (ppb/TOC)
901-18.9	89	855	50
901-17.2	5174	30062	2526
901-16.0	5878	39308	2829
901-15.0	2394	19685	1471
901-10.7	271	1215	69
901-8.5	15225	57577	4281
901-8.0	12772	49345	3796
901-6.4	56128	260867	23816
901-5.0	6618	40505	4684
901-2.5	2211	23948	2658
901-1.5	1356	18601	2039
901-1.0	847	15326	1595
901-0.5	312	5548	505

Table 2.4: Yields for selected samples.

Sample	Extracted powder (g)	C_{29} ααα*R* Sterane (ng/g powder)	C_{30} αβ Hopane (ng/g powder)
Lab Blank 1	30.0626	0.01	0.01
Lab Blank 2	5.0060	0.03	0.01
Lab Blank 3	30.0455	0.01	0.02
Lab Blank 4	36.2782	nd	nd
Lab Blank 5	36.0316	0.00	0.00

Table 2.5: Yields for most abundant compounds in blanks.

Chapter 3

Lipid biomarkers from the Late Katian-age Maquoketa Formation of eastern Iowa, U.S.A.

This chapter explores the potential effects of facies changes upon lipid biomarker records of microbial community structure in the Late Ordovician. The intent is to use slightly older rocks than those presented in Chapter 2 in order to determine the stratigraphic extent of elevated 3β-methylhopane and high hopane/sterane ratios, and avoid effects of the most extreme environmental perturbations, i.e. the Hirnantian glacial maximum. A recently proposed stratigraphic correlation scheme suggests that the Maquoketa Formation and upper lithologic units of the Cincinnati Region may overlap with Anticosti Island and Vinini Formation rocks to a much greater extent than anticipated, which may be a complicating factor. In any case, based on the results described in Chapter 2, it was expected that in these Upper Katian rocks: i) hopane/sterane ratios would likely be highest in organic-lean carbonate facies, and lowest in deepwater and/or

upwelling-influenced facies; ii) that 3-MeHI would be highest in shallow, carbonate-dominated settings; and iii) that indicators of redox conditions would track both sea level change and the shallow to deep water depth gradient between the BS-5 and H33 drill cores.

3.1 Abstract

Lipid biomarker records indicate substantial changes in microbial communities during the Hirnantian glacial maximum and mass extinction; to better constrain microbial community structures leading up to the glacial maximum and mass extinction, we have analyzed lipid biomarkers from two cores along a shallow to deep water paleobathymetry and/or sediment supply gradient preserved in the Maquoketa Formation in Iowa, U.S.A. Analyses from a third core, representing an intermediate water depth, are ongoing. We compare these results with previous work to constrain the extent to which changes in microbial communities that are observable during the Late Ordovician mass extinction and cooling event are attributable to regional or global environmental drivers, such as climatic or oceanographic changes, as opposed to local variations in litho- and organo-facies effects. Biomarkers from the Maquoketa Formation are thermally well-preserved, and lack individual compounds and abundance profiles associated with younger contamination (e.g. oleanane from angiosperms, sterane assemblages characteristic of marine algal inputs from Mesozoic and younger organic inputs), and have characteristics typical of Lower Paleozoic-age rock bitumens and oils (e.g. low C_{28}/C_{29} sterane ratios). Lipid biomarker profiles indicate substantial similarities between shallow, oligotrophic carbonate depositional environments across Laurentia. However, the influence of elevated nutrient levels, particularly upon algal biomarker abundance, is

evident also in regions for which lithological evidence indicates active upwelling or condensation, both along the margin of Laurentia and the western side of the epeiric Sebree trough. Comparison among Late Ordovician Laurentian sites for which there is lipid biomarker data available, largely through this study, was performed and notable differences and similarities in biomarker records are discussed in the context of hypotheses regarding local marine circulation and depositional environmental conditions. Discussion of unusual biomarker assemblages obtained from the rock bitumen from a sample of the Middle Ordovician Winneshiek Lagerstatte is included for completeness.

3.2 Introduction

The two-phased extinction of approximately 84 percent of marine invertebrate species in the Late Ordovician is thought to have been driven by impacts of the Hirnantian-Stage glacial maximum (e.g. as reviewed in Sheehan, 2001). In this model, the first phase of extinction resulted from cooling and regression preferentially impacting taxa in shallow epicontinental seas which were near the Phanerozoic maximum in extent. The second phase of extinction transpired at the end of the glacial maximum as glacioeustatic sea level rise brought oxygen-deficient bottom waters over the previously better-oxygenated shelves. Lipid biomarker analysis has previously demonstrated that microbial communities which formed the base of marine ecosystem were impacted by Late Ordovician-age environmental change even in in the paleotropics in both shallow epeiric habitats and deeper water, upwelling-influenced zones (Rohrssen et al., 2013).

In addition to identifying an increase in relative algal biomarker abundance during the Hirnantian glacial maximum and decrease in 3β-methylhopane s most commonly attributed to aerobic methanotrophic bacteria, Rohrssen et al. (2013) clearly indicated

a strong relationship between depositional environment and microbial community structure. Although some features of the biomarker records from Anticosti Island and the Vinini Formation at Vinini Creek are not accompanied by obvious lithological differences, the existence of substantial eustatically-driven facies change accompanying the Hirnantian glacial maximum may complicate extrapolation of lipid biomarker records without better constraint on the relationship between microbial community structure and lithofacies.

There are uniformitarian and empirical reasons to expect that at least some portion of the observed Hirnantian biomarker records may be due to facies migration with regression and transgression rather than to global changes in temperature or nutrient availability:

i) The distributions of macro- and microfauna between deeper and shallower water modern marine environments predict a similar partitioning in ancient environments,which may have been even more extreme in the Lower Paleozoic due to still on-going oxygenation of the deep ocean.

ii) Lipid biomarker proxies vary systematically between the shallow, oligotrophic, carbonate facies of epeiric seas and the more nutrient-replete, deeper waters of marginal upwelling-influenced systems.

iii) The Hirnantian glacial maximum was accompanied by substantial eustatic regression, driving major facies change in nearly all Hirnantian-age sections. Better understanding the suspected relationships between depositional environments and organic geochemical proxies is important for further application of these proxies in the Paleozoic because impacts from sea level change would be most influential in the epeiric settings which comprise the majority of preserved Paleozoic rocks.

The Maquoketa Formation of Eastern Iowa provides an exceptional opportu-

nity to test expected facies versus temporal relationships in lipid biomarker records of evolving microbial community structure. In the Late Ordovician, Iowa was bounded to the paleo-north by exposed highlands of the Transcontinental Arch and separated from the Cincinnati region carbonate platform by a paleo-northeast to southwest trending shelf-break into the deeper waters of the Sebree Trough (Figure 3.1) a depression thought to have connected central Laurentia to the open ocean at this time (Kolata et al., 2001). Deposition of phosphatic and cherty sediments along the wester shelf-break has been attributed to upwelling of nutrients derived from the Sebree Trough (e.g. Witzke, 1987; Raatz and Ludvigson, 1996). Farther to the north, siliciclastics shed from the Transcontinental arch are more abundant, perhaps indicating a concomitant freshwater influx (e.g. Witzke, 1987; Raatz and Ludvigson, 1996), while siliciclastics from the rising Taconics made it past the Jessamine Dome and Sebree Trough only at high-stand (Chetel et al., 2005).

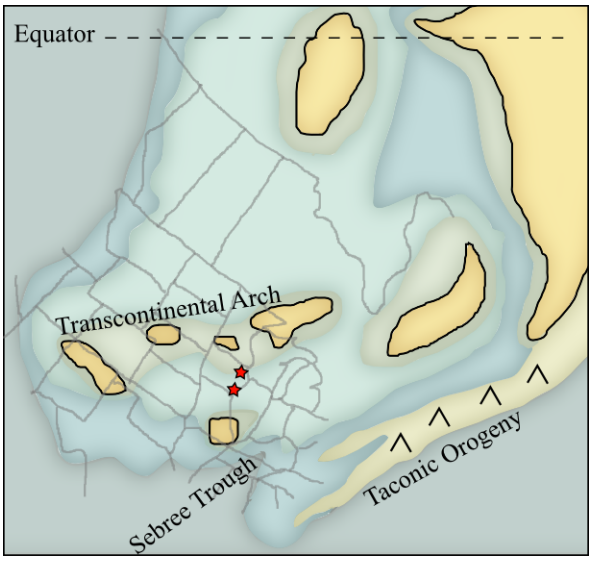

Figure 3.1: Map of central Laurentia in Katian times, modified after Blakey, 2011; Chetel et al., 2005; Witzke, 1980; and Kolata et al., 2001. Exposed land is outlined, present-day geopolitical boundaries indicated by gray lines for reference, and sampling locations indicated by stars.

In addition to the lateral change in facies, the Maquoketa Formation preserves at least two smaller-scale transgressive-regressive couplets, exemplified by the basal Elgin Member and Clermont Member phosphorites (H-33 core). As a result of this paleotopography and Late Ordovician sea level change, samples collected from drill cores BS5 (Clayton County) and H33 (Des Moines County) capture the change in facies from carbonate-rich platform to shale with phosphatic intervals at the shelf-break, through two shallowing-up cycles in roughly contemporaneous deposits (Raatz and Ludvigson, 1996). This substantial contrast in depositional environment through time as well as across the shelf will provide a linkage between epeiric carbonate environments such as Anticosti and the Cincinnati region, and offshore, upwelling-influenced environments such as that preserved in the Vinini Formation. Thus, by comparing biomarkers and lithofacies across cores as well as stratigraphically within each core it should be possible to determine the extents to which lipid biomarkers track both local and broader-scale environmental factors (e.g. stratification, oxidant availability, carbonate versus siliciclastic, temperature, etc.).

These sites taken together allow for differentiation between characteristics of marine microbial communities that appear to be locally governed by water column chemistry (e.g. H/St), or common to the Middle/Late Ordovician (high 3β-methylhopane indices, low 24-*n*-propylcholestanes, and low *Gloeocapsamorpha prisca* Zalessky 1917 markers), and the extent to which these relationships can explain the observed changes due to Hirnantian glacial perturbation. Furthermore, insight into microbial community structure derived from these lipid biomarker analyses contributes to on-going discussion of circulation and water mass properties of ancient epeiric seaways.

3.3 Materials and Methods

3.3.1 Materials

Samples were collected at the Iowa Core Repository (Iowa City, IA) from the Big Springs 5 (BS-5) and H33 drill cores. BS-5 was drilled in Clayton County in 1989 (Iowa Geological and Water Survey GEOSAM well number 30190) and is in the north-central area described by Raatz and Ludvigson (1996). The H33 borehole was drilled in Des Moines County (Iowa Geological and Water Survey GEOSAM well number 27543) and is assigned to Raatz and Ludvigson's (1996) southern facies area. Samples were also collected from SS-15, Jackson County, which was deposited in the shallower reaches of the southern facies belt, near to SS-9, the core examined in that study (Raatz and Ludvigson, 1996). The sample from Graf was collected from a shale interval immediately below the main *Isorthoceras* nautiloid bed at the Graf Roadcut (Stop 5, Witzke et al., 1997) by the authors. Core descriptions, including fossil occurrence data, and Member assignments were done by Brian Witzke (University of Iowa). Although making member assignments in the southeastern Maquoketa is challenging and has used different terminology to reflect uncertainties in correlation (i.e. Upper and Lower Scales Shale, Witzke et al., in Witzke et al., 1997), for clarity we conflate the Upper Scales Shale with the Clermont Member and the Lower Scales with the Elgin Member in these cores.

The sample of Winneshiek Lagerstatte was provided by Huaibao Liu (Iowa Geological Survey), from material collected for paleobiological analysis (Liu et al., 2006). The Winneshiek Lagerstatte material was stored in water after excavation, which may have introduced contamination prior to subsampling for lipid biomarker work.

3.3.2 Biomarker Analysis

Drill cores stored cardboard core boxes were subsampled, wrapped in pre-combusted aluminum foil and stored in cotton sample bags. Individual samples were trimmed using a diamond-blade jewelers' saw (Hilquist) with fresh distilled, deionized water for each sample. Solvent-cleaned, trimmed interior chips of core and outcrop material were then powdered, extracted, and analyzed as described previously (Rohrssen et al., 2013).

Briefly, inner core pieces were ultrasonically washed with ultrapure water, methanol, dichloromethane, hexane, and dichloromethane again, prior to powdering in a ceramic or zirconia puck mill (SPEX 8510 Shatterbox). The puck mill was cleaned between samples by powdering two batches of fired sand (850°C, overnight) followed by rinses with the same sequence of solvents described above. Samples were powdered in two aliquots, with the first discarded and the second collected for extraction. Fired sand procedural blanks were crushed with each batch of samples and processed identically to sample powders to monitor background levels of biomarker analytes.

Lipid biomarkers were extracted from 30-40 g of rock powder in a Microwave Accelerated Reaction System (CEM corp.) with dichloromethane and methanol (9:1 v/v) at 100°C for 15 minutes. Elemental sulfur was removed from the total extract with HCl-activated, solvent washed copper pellets prior to silica gel column chromatography. Total extracts were fractionated with hexane, hexane:dichloromethane (1:1 v/v), and dichloromethane:methanol (3:1 v/v) to elute saturated hydrocarbons, aromatic hydrocarbons, and polar (N, S, and O-containing) compounds, respectively.

Gas chromatography-mass spectrometry (GC-MS) analyses of saturated and aromatic hydrocarbons was conducted with an Agilent 7890A, equipped with a DB-1MS

capillary column (60 m x 0.32 mm, 0.25 um film) and run with He as carrier gas. The temperature program for GC-MS full scan and selected ion monitoring was 60°C (2 min), ramp to 250°C at 20°C/min, to 325°C at 2°C/min, and hold at 325°C for 20 min.

Multiple reaction monitoring (MRM) GC-MS of saturated hydrocarbons was carried out with a Waters AutoSpec Premier mass spectrometer equipped with an Agilent 7890A gas chromatograph and DB-1MS coated capillary column (60m x 0.25 mm, 0.25 um film) using He for carrier gas. MRM-GC-MS measurements were conducted with a temperature program of 60°C for 2 min, heating to 150°C at 10°C/min then 320°C at 3°C/min with a final hold at 320°C for 22 min. Biomarker compounds were identified based on retention time and published mass spectra and quantified in MRM-GC-MS by comparison with a deuterated C29 sterane internal standard (d4-$\alpha\alpha\alpha$-24-ethylcholestane (20R), Chiron Laboratories, AS), assuming equal response factors between sample compounds and the internal standard. Individual yields of hopane and sterane diastereoisomers found in laboratory procedural blanks were typically less than 0.1 ng of individual compounds and polycyclic alkane biomarker MRM-GC-MS signal (hopanes, steranes, methylsteranes, methylhopanes, tricyclic terpanes) from rock samples was typically at least 2-3 orders of magnitude higher in total than those detected in blanks.

3.3.3 Assessment of Biomarker Syngeneity

GC-MS (Figure 3.2, 3.3, 3.4) and MRM-GC-MS (Figures 3.5, 3.7) analysis of saturated hydrocarbon fractions reveal very immature lipid biomarker profiles for Maquoketa Formation bitumens, consistent with their location near the center of the North American Craton and burial history. This result is consistent with previous analyses of Maquoketa Formation core material from Iowa, Illinois, and Indiana which indicate that organic matter in these samples is immature, with T_{max} for the stratigraphically

lowest samples (Guttenberg Formation) around 440°C and most samples in the range of 426-430°C (Guthrie, 1996). The two cores display a slight thermal maturity gradient both down-core and from north to south, perhaps reflecting deeper burial more proximal to the basinal depocenter. Cross-checks of biomarker maturity, lithology, and source age proxies are consistent within the majority of Maquoketa Formation samples.

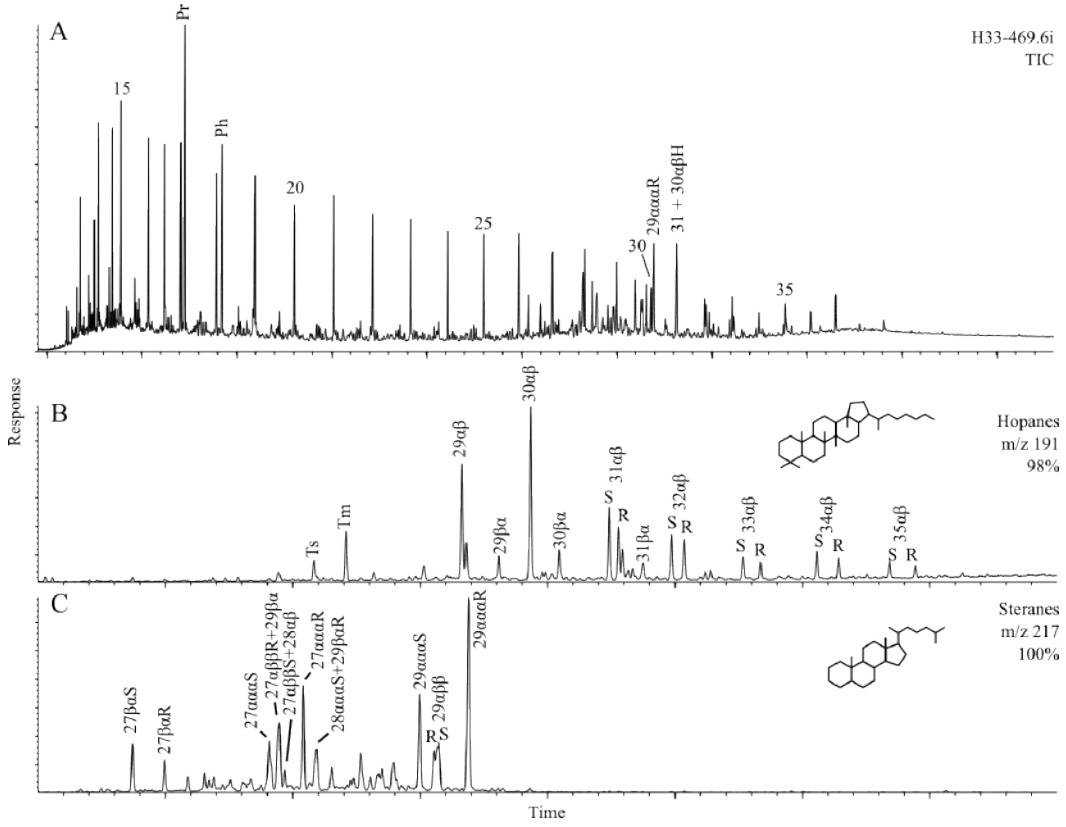

Figure 3.2: A. Total ion chromatograms (TIC) of saturated hydrocarbons and selected ion monitoring (SIM) chromatograms of B. hopanes (m/z 191), and C. steranes (m/z 217) detected in a rock bitumen from a sample (H33-469.6i) from the Elgin Member of the Maquoketa Formation.

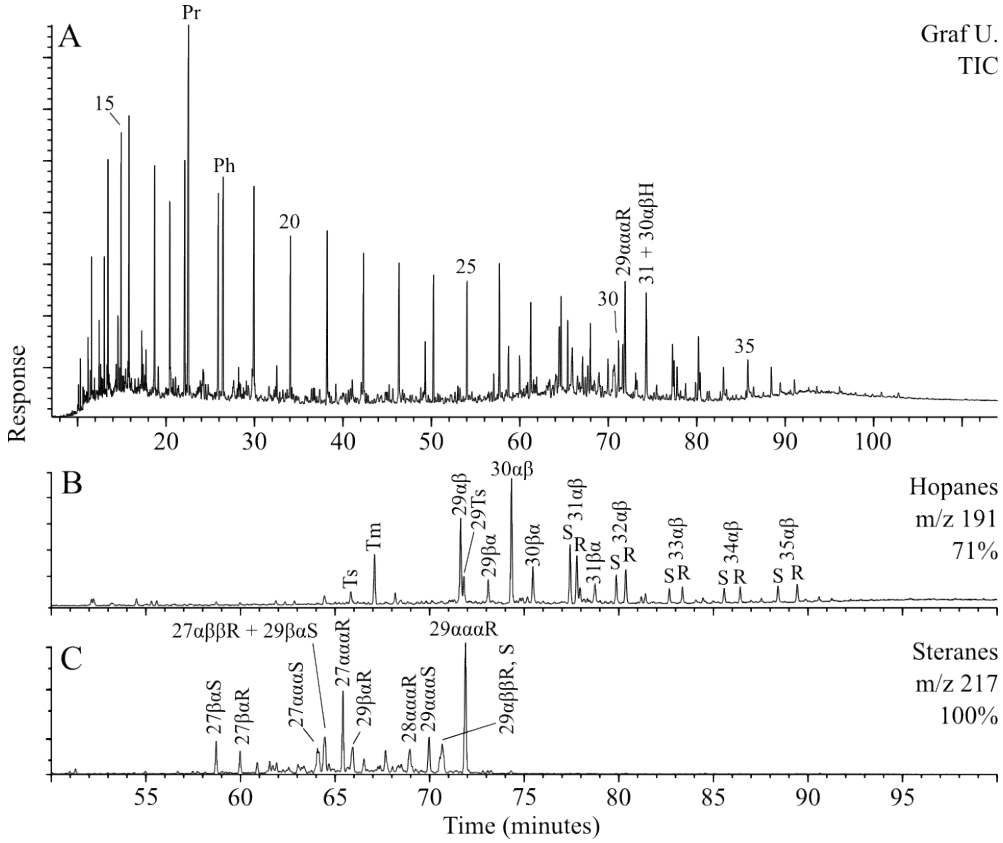

Figure 3.3: A. TIC of saturated hydrocarbons and SIM chromatograms of B. hopanes (m/z 191), and C. steranes (m/z 217) from the Elgin Member of the Maquoketa Formation at Graf, Iowa.

3.4 Results and Discussion

3.4.1 Lipid Biomarkers in Bitumen Extracted from the Winneshiek Lagerstatte

The sample of Winneshiek Lagerstatte (WS-10), on the other hand, yields an unusual maturity profile; for example the large amounts of C_{27} and C_{28} steranes are dominated by $\alpha\alpha\alpha$R and $\beta\alpha\alpha$R (C_{27} $\beta\alpha\alpha$R coelutes with C_{27} $\alpha\alpha\alpha$S, and C_{28} $\beta\alpha\alpha$R mostly co-elutes with C_{28} $\alpha\alpha\alpha$S) configurations, while the much less abundant C_{29} steranes have a more mature distribution, exhibiting and $\alpha\beta\beta$ as well as $\alpha\alpha\alpha$ configurations (Figure 1.3). The C_{27} and C_{28} sterane profiles have very different stereochemistry from the stratigraphically higher Graf sample presented above it (Figure 3.5). Although relatively immature C_{27}-dominated sterane isomer patterns have been described in a Devonian lagerstatte (Melendez et al., 2013) and based on the SIM (Figure 3.4) alone one might make a similar interpretation of the WS-10 sample, sensitive MRM-GC-MS analyses demonstrates the presence of smaller amounts of more mature C_{29} steranes. Analyses of the Maquoketa formation presented here suggest that the Winneshiek C29 isomer patterns are more consistent with the sample's Middle Ordovician stratigraphic position (see, e.g. Grantham and Wakefield, 1980) than the C_{27} and C_{28} pattern.

In the Devonian case, the C_{27} steranes are interpreted to derive from a crustacean exhibiting soft body preservation, preserved as a result of photic zone euxinic conditions (Melendez, et al., 2013). Organisms with soft body preservation have also been described in the Winneshiek Lagerstatte (Liu et al., 2006), however no macrofossils were observed in the analyzed sample. Even in the case of extensive natural vulcanization and early incorporation of steroids into kerogen as observed in Cenomanian-Turonian (Cre-

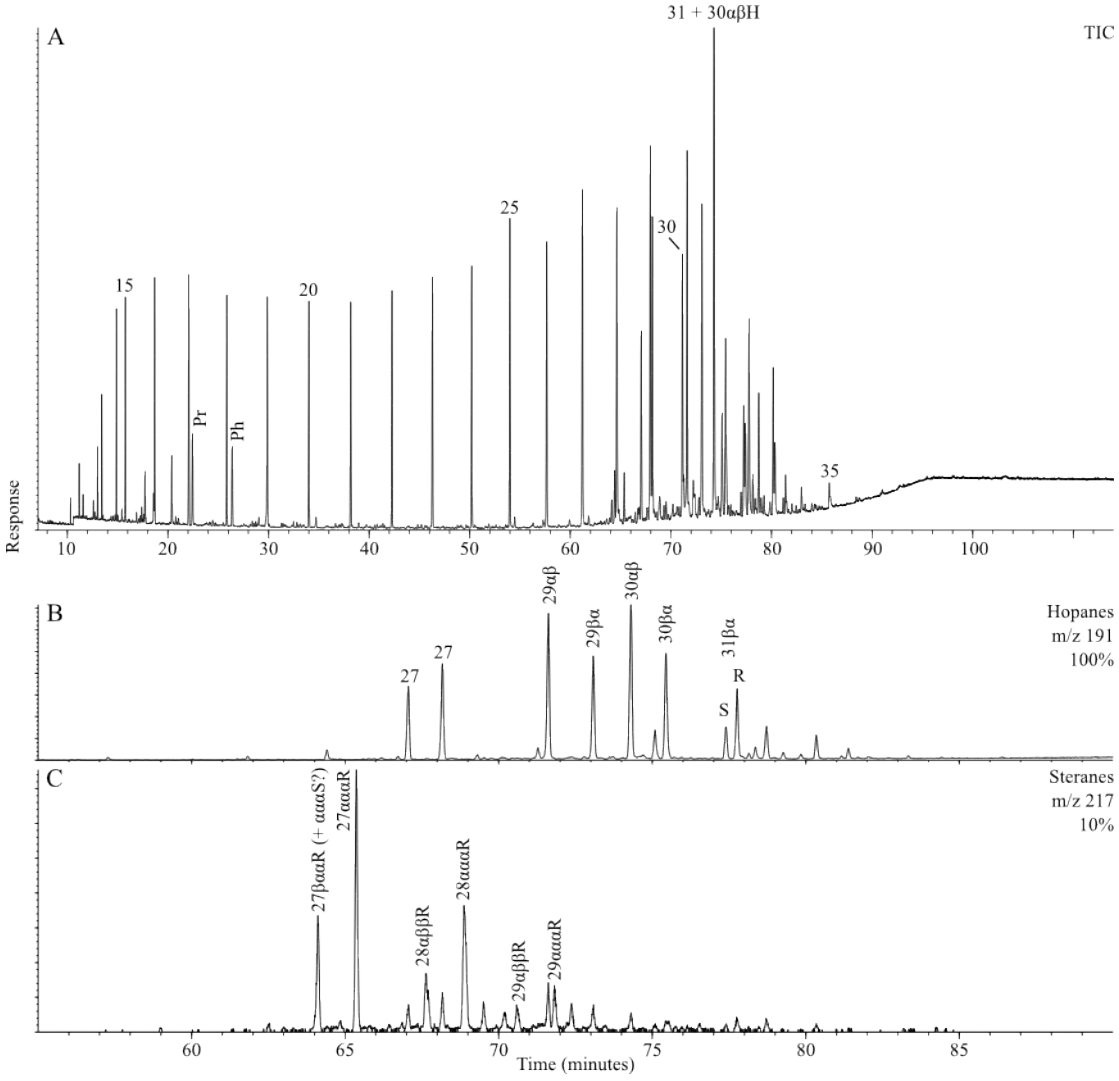

Figure 3.4: A. TIC of saturated hydrocarbons and SIM chromatograms of B. hopanes (m/z 191), and C. steranes (m/z 217) from the Winneshiek Lagerstatte, Middle Ordovician St. Peter Formation, eastern Iowa, USA.

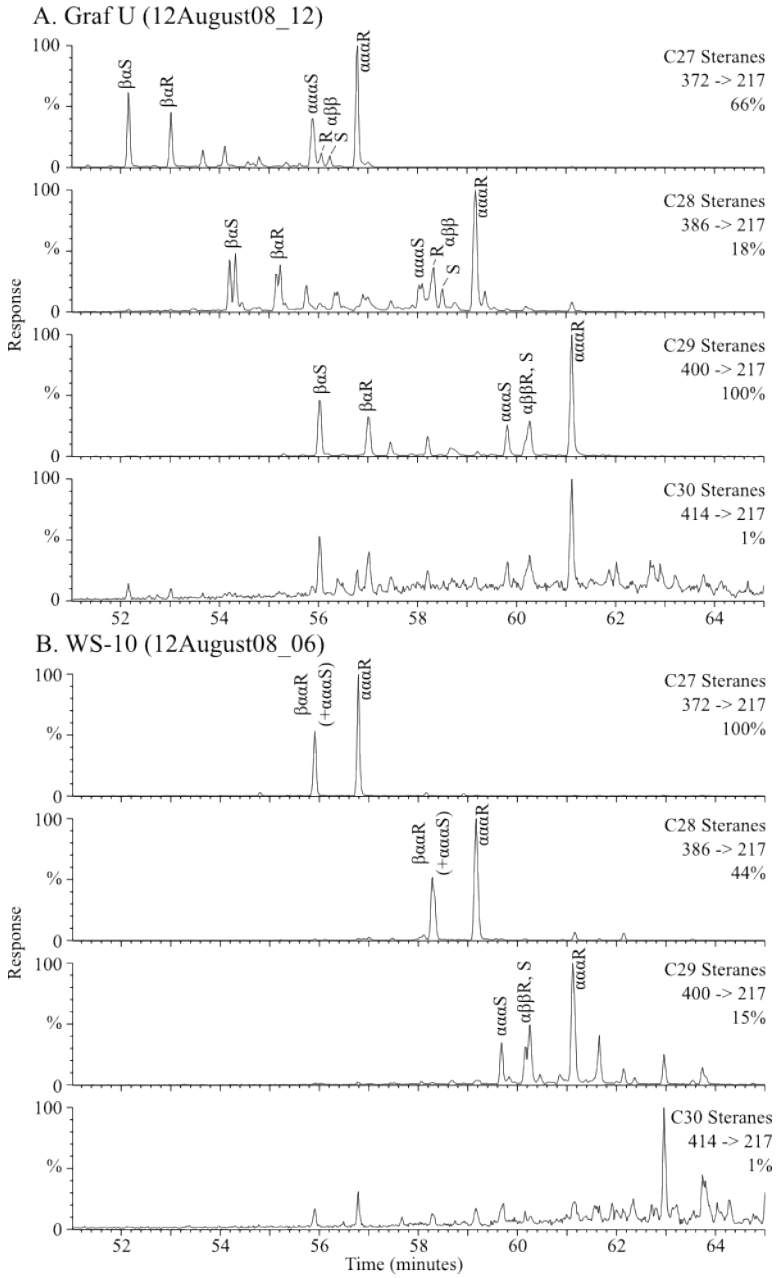

Figure 3.5: MRM-GC-MS chromatograms of steranes in saturated hydrocarbons from A. the Elgin Member at Graf, Iowa; and B. the Winneshiek Lagerstatte.

taceous) sediments from a permanently euxinic basin, there is no significant difference in sterane carbon number distribution between solvent extractable and kerogen-bound fractions despite substantially lower hopane/(sterane+sterene) ratios in the kerogen-bound organic matter (Owens et al., submitted; Rohrssen et al., in prep), thus it would indicate a substantially different algal community than so far reported from authentic Ordovician-age biomarkers. While a very different algal community is not difficult to imagine, it is difficult to envision a scenario in which the difference in thermal maturity between different sterane homologues would be so pronounced without a mixed origin for extractable biomarkers. Features of the WS-10 biomarker profile (particularly its high hopane/sterane ratio of 8.1, moderately high 3β-methylhopane index of 5.8 percent, apparent lack of C_{30} steranes, and very high proportion of moretanes Table 3.1) make the Winneshiek Lagerstatte an interesting topic for further study, yet this particular sample is likely overprinted by contamination (either with younger, immature material or with older, slightly more mature material) such that a purpose-collected sample for lipid biomarker analysis would be preferable. Alternatively, or in addition, application of catalytic hydropyrolysis (HyPy, Love et al., 1995) to selectively cleave biomarkers out of Winneshiek Lagerstatte kerogen would provide incontrovertibly indigenous biomarkers with which to test the bitumen biomarker profile. Either possible outcome will be interesting.

3.4.2 Influences of Lithology and Thermal Maturity on Lipid Biomarker Proxies

Biology produces only a few of the 2^n possible configurations for a given natural product molecule (where n = number of chiral, or asymmetric, centers) and often the biologically useful compounds are not the most thermodynamically stable. As a result,

rocks at any given thermal maturity preserve a mixture of geolipid stereochemistries according to processes that are increasingly well understood (Peters et al., 2003; Farrimond et al, 1998; Figures 1.3, 1.4) during progressive sub-surface burial maturation. For example, bacteria produce hopanes in the 17β,21β(H) configuration (H at both C-17 and C-21 are above the plane of the ring), a configuration which gives the molecule a moderately flat shape well-suited to modifying cell membrane properties (Figure 1.4). The 17β,21β biological configuration alters to 17β,21α (moretanes) and the thermodynamically most stable form, 17α,21β (H at C-17 is below the ring, H at C-21 is above) during diagenesis and catagenesis (Figure 1.4). Elongation of the side-chain in homohopanes creates another chiral center at C-22 such that the C_{31}-C_{35} homohopanes also may have S (H below the plane) or R (H above the plane) configuration at this carbon atom (Figure 1.4). A similar set of transformations takes place at different ranges of temperatures in steroids (Figure 1.3) and many other compound systems (summarized in Peters et al., 2003). This results in a suite of proxies based on ratios of mature products to the immature parents which can be used in conjunction to estimate the precise level of thermal maturity with respect to the oil window.

However, the straightforward transformation of biological stereochemistry to thermodynamically stable stereochemistry oversimplifies what actually happens in organic matter maturation in natural sedimentary systems with different basinal heat flows and lithofacies. Two factors generally complicate this model: differential generation and degradation of molecules with different stereochemistries from kerogen (Farrimond et al., 1998) and acid-catalysed rearrangements or stereo-specific adsorption on clay mineral surfaces (Peters et al., 2003; discussed in French et al., 2012).

Quantitative biomarker studies have demonstrated that different diastereoisomers reach maximum concentrations in bitumen at (slightly) different temperatures

(e.g. Farrimond et al., 1998). For example, Farrimond et al., (1998) quantified the total amount of 17β,21β, 17β,21α, and 17α,21β hopanes in bitumens extracted from Eocene-age claystones in the Berents Sea. Their results demonstrated that a) there were insufficient $\beta\beta$ hopanes in the starting bitumen to account for the amount of $\beta\alpha$ and $\alpha\beta$ hopanes in produced bitumen, and that b) the $\beta\alpha/(\beta\alpha + \alpha\beta)$ maturity index is driven by the fact that equilibrium between release from kerogen, conversion between isomers, and thermal degradation of $\beta\alpha$ isomers is achieved at slightly lower temperatures than $\alpha\beta$ isomers. In other words, both $\beta\alpha$ and $\alpha\beta$ isomers are produced at fairly low temperatures, but $\beta\alpha$ isomers reach maximum concentration in bitumen at lower temperatures than $\alpha\beta$ isomers, resulting in an overall decrease in the ratio $\beta\alpha/(\beta\alpha + \alpha\beta$ with increasing maturity. These two observations rule out straightforward transformation-based models and imply that it is possible to generate apparent stratigraphic trends in biomarker proxies that record maturity, rather than source organism change. For example, steranes reach their highest concentrations in bitumen at slightly lower thermal maturities than hopanes, potentially giving the false impression of an increase in hopane/sterane ratio with depth. Exceptions to this model have been observed (e.g. Cao et al., 2009) and attributed to difference in source organic matter or lithology.

A classic example of the influence of lithology on biomarker maturity proxies is that of acidic clays on the C_{27} hopanes 18α(H)-22,29,30-trisnorhopane II (Ts) and 17α(H)-22,29,30-trisnorhopane (Tm) (Seifert and Moldowan, 1978). Ts is the thermodynamically stable configuration whereas Tm degrades with increasing temperature such that the ratio Ts / (Ts+Tm) approaches 1 with increasing maturity (Seifert and Moldowan, 1978). In clay-rich rocks, however, this proxy tends to yield higher maturity estimates than, for example, vitrinite reflectance (Peters et al., 2003 and references

therein). Ts / (Ts+Tm), therefore, demonstrates that many biomarker proxies must be interpreted in context of both thermal maturity and lithology.

3.4.3 Maturity and Lithology Results for the Maquoketa Formation

Maquoketa Formation biomarkers exhibit complex interactions between thermal maturity, lithology, and source material (Figure 3.6) which may influence interpretation of biomarkers reflecting redox and source organisms (Figure 3.8). Figure 3.6 and 3.8 also include a cross-check for core contamination and laboratory procedures conducted by applying the full procedure to both outer (i.e. trimmed-off) and inner portions of the lowest sample in H33. Differences between the inner and outer portions of that sample are slight; where noticeable the line connects to the "inner" sample. Sterane stereochemistry for both cores is immature, with slightly higher maturity indicated for H-33 samples by higher hopane S / (S+R) and sterane $\alpha\alpha\alpha$ sterane, and largely isomature with depth. However, Ts / (Ts+Tm) and $\beta\alpha/(\beta\alpha + \alpha\beta)$ hopane indices suggest a substantial maturity change in H-33. As alluded to above, in a system controlled solely by temperature these two parameters are expected to demonstrate an inverse relationship, as observed (Farrimond et al., 1998). However, in H33 it is remarkable that this "difference in maturity" is reached over the space of less than ten meters and crosses a substantial change in lithology. Measuring yields of these compounds would be the easiest test for thermal maturity as an explanation and is in progress. Because the moretane ratio is effective at lower stages of thermal maturity than hopane and sterane S/(S+R), while Ts/(Ts+Tm) changes at slightly higher temperatures than sterane S/(S+R) (Farrimond et al., 1998), it is also unusual to have such dramatic changes in moretanes and Ts/(Ts+Tm) without a response from sterane S/(S+R), unless there is an influence from other factors than maturity. That is, if thermal maturity is invoked

to explain the moretane and Ts/(Ts+Tm) profiles, one would expect a similar response from hopane and sterane S/(S+R).

An alternative explanation arises from the observation of elevated moretane abundances in Late Permian shales (Cao et al., 2009; French et al., 2012). Elevated moretanes have been attributed to greater influxes of terrestrially-derived material, either from land plants or hopanoids from aerobic soils coupled with selective formation on and/or release from chlorite/illite clay minerals (French et al., 2012). Following the same reasoning as French et al., (2012), moretane inputs from higher plants would only be expected to impact C_{30} hopanes, however all homohopanes and methylhopanes demonstrate similar stereochemical profiles (Figure 3.7). Minimal organic matter derived from terrestrial vegetation is not surprising as vascular plants have not been observed to play a large role in the Late Ordovician terrestrial biosphere (e.g. Wellman and Gray, 2000; Gibling and Davies, 2012). Input of hopanes associated with clays, however, might be a possibility as the large increase in moretane abundance in H33 corresponds to a shift in lithology from brown shales and dolomitized limestones to green-gray shale and inferred shallower/better oxygenated water column conditions. This observation becomes important because a number of source and redox informative biomarker proxies co-vary with these two traditionally temperature-related proxies (moretanes and trisnorhopanes) in this interval; disentangling the drivers is essential to accurately interpreting the data.

It is interesting that, if increases in chlorite/illite impact hopane stereochemistry, diasteranes are not similarly affected (Figure 3.6). Instead of the monotonic increase exhibited by moretanes, the diasterane/regular sterane ratio peaks at the phosphatic transition between the Elgin and Clermont Members in H33 and is low on either side. A similar pattern for diasteranes exists in the Elgin member of BS-5, in which a

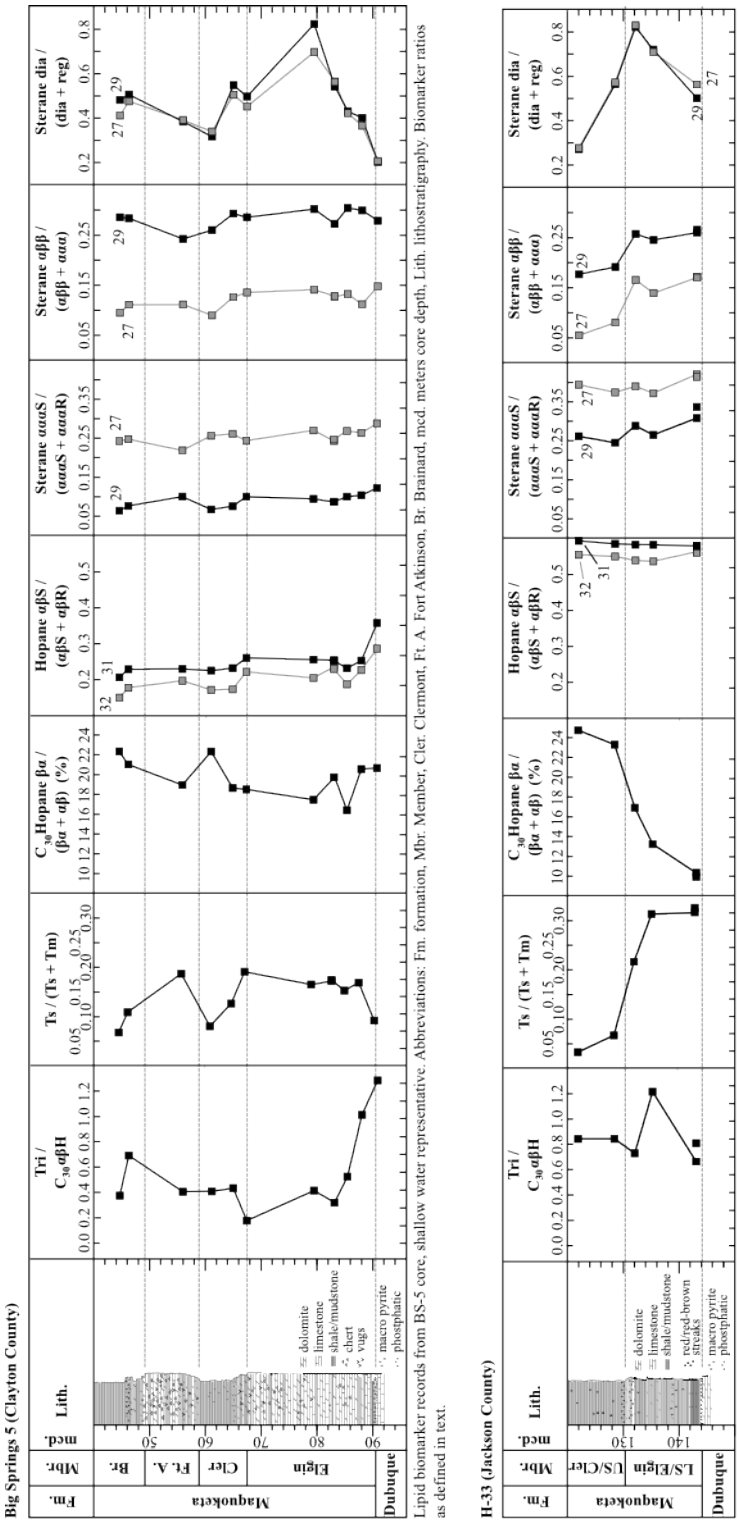

Lipid biomarker records from BS-5 core, shallow water representative. Abbreviations: Fm. formation, Mbr. Member, Cler. Clermont, Ft. A. Fort Atkinson, Br. Brainard, mcd. meters core depth, Lith. lithostratigraphy. Biomarker ratios as defined in text.

Lipid biomarker records from H-33 core, deeper water representative. Abbreviations: Fm. formation, Mbr. Member, US. Upper Scales Shale, Cler. Clermont, LS. Lower Scales Shale, mcd. meters core depth, Lith. lithostratigraphy. Biomarker ratios as defined in text.

Figure 3.6: Maquoketa Formation lipid biomarker ratios associated with thermal maturity and lithology.

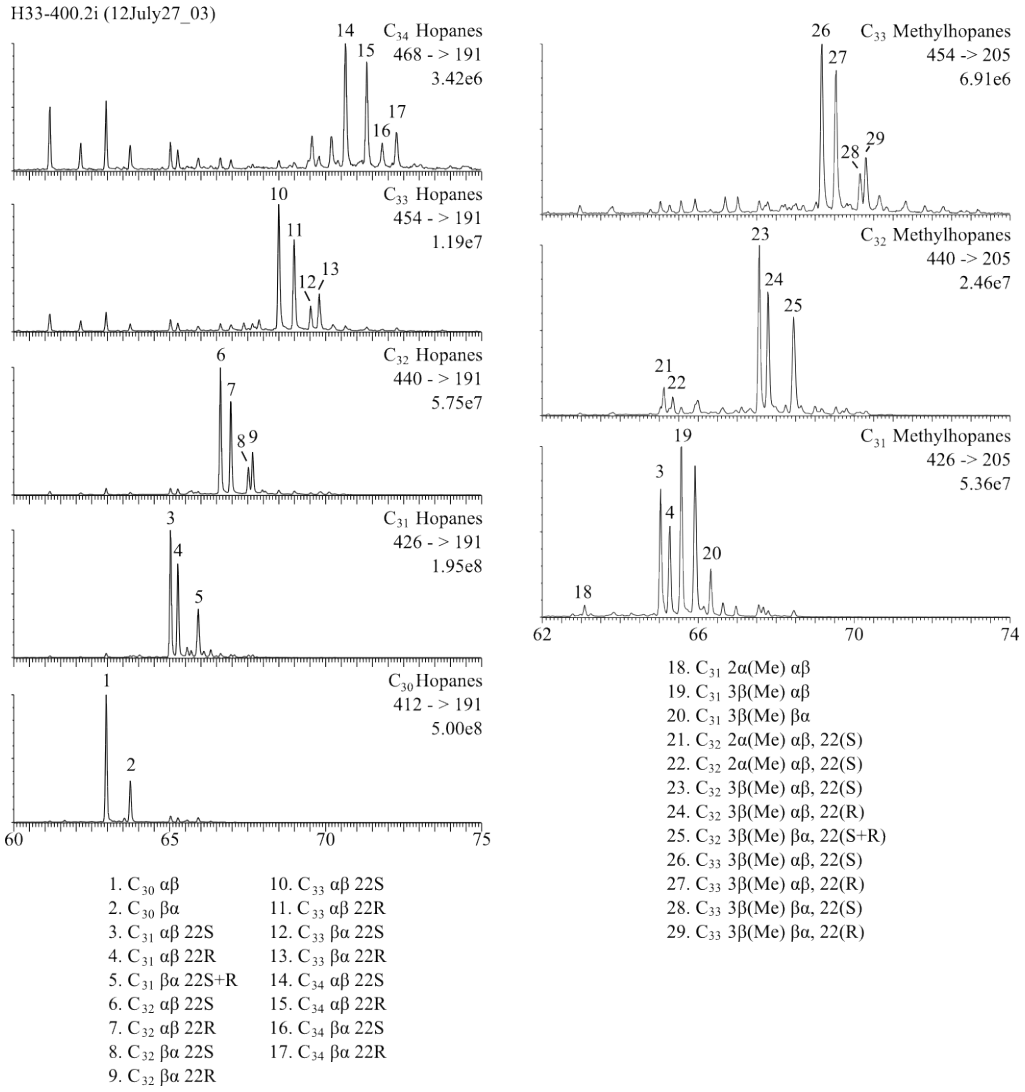

Figure 3.7: MRM-GC-MS chromatograms of hopanes (left) and methylhopanes (right), with isomers identified following French et al., 2012.

corresponding relationship with Ts/(Ts+Tm) or rearranged hopanes is also absent. Examination of stratigraphic and scatter plots reveals no relationship between diasteranes and any other measured biomarker parameter. Also interesting is that samples from Estonia, which have $\beta\beta$-hopanes do not have such elevated levels of moretanes (nor the very immature sterane profiles observed in WS-10).

Some clues may be derived from inspection of the two cores in relation to depositional environment. H33 is farther to the south, away from the transcontinental arch which is the most proximal source of terrigenous siliciclastics (Chetel et al., 2005). Chetel and coauthors found that sediment provenance in the underlying Galena, Platteville, and Ancell Formations strongly depends on sea level, with highstand systems (Galena Formation) characterized by widely disseminated sediment sources and lowstand (Platteville Formation, Glenwood Member of Ancell Formation) siliciclastics predominantly derived from more proximal sources (e.g. igneous rocks of the Superior Province and Midcontinent Rift). Thus, perhaps only the shallower facies at H33 reflect siliciclastics from the Transcontinental Arch (i.e. Superior Province and Midcontinent Rift), whereas BS-5 shows this influence at virtually all times as it is shallower and closer to the source.

3.4.4 Lipid Biomarkers Indicative of Source Organisms and Redox Conditions

Discussion of Ordovician organic geochemistry always includes reference to that extinct, enigmatic microorganism, *Gloeocapsamorpha prisca* Zalessky 1917. Findings presented here are consistent with the observation that although *G. prisca* debris are abundant in Galena Group samples (Fowler and Douglas, 1984; Guthrie, 1996; Pancost et al., 1998), material from the Maquoketa in Southeastern Iowa shows little contribution

from *G. prisca* (Guthrie, 1996). Traces of elevated n-C_{17} and n-C_{19}, alkylcyclohexanes, and methyl-alkylcyclohexanes associated with *G. prisca* are nowhere predominant (e.g. Figures 3.2 and 3.3). Indeed, *G. prisca* source inputs seem minor in Late Ordovician sedimentary organic matter in comparison to Middle and Early Ordovician rocks and oils.

The first features of the stratigraphic plots of source organism and redox informative biomarker proxies that jumps out on initial inspection is co-variation among pristane/phytane, C_{35} homohopane index, gammacerane/C_{30} $\alpha\beta$-hopane, and hopane/sterane with Ts / (Ts+Tm) and the $\beta\alpha/(\beta\alpha + \alpha\beta)$ hopanes (Figure 3.8). This tendency is evident in both cores but much more pronounced in H33, in which linear regressions in scatter plots for these relationships generally yield significant r^2 values.

Pristane/phytane (Pr/Ph) is a weakly reliable indicator of redox defined in the early days of organic geochemistry based on the diagenesis of chlorophyll a and bacteriochlorophylls a and b, the side-chains of which are the major contributors to pristane and phytane in sediments (Brooks et al., 1969; Powell and McKirdy, 1973). Under oxic conditions phtyol is preferentially converted to phytenic acid and ultimately converted to pristane (Pr), whereas in reducing environments the primary diagenetic pathway involves reduction of phytol ultimately to phytane (Ph) (Peters et al., 2003). In this framework, higher values of Pr/Ph roughly indicate oxic conditions. However, much subsequent work has demonstrated that Pr/Ph is influenced by contributions from other biomolecules than chlorophylls and is impacted by maturity (reviewed in Peters et al., 2003). Following a similar principle, higher values for the C_{35} homohopane index (HHI) reflect the greater preservation of the bacteriohopanepolyol side-chain under reducing conditions. No similar proxy exists for sterane carbon numbers because functional groups on the hopanoid side-chain makes them more susceptible to degradation

than side-chains of steroids which have double-bonds but are otherwise unfunctionalized. Pr/Ph and HHI follow generally similar trends in both cores, although correlation between them is weakly supported. Interestingly, in H33 correlation between HHI and Ts/(Ts+Tm) as well as $\beta\alpha/(\beta\alpha + \alpha\beta)$ hopanes is well-supported, while the relationship in BS-5 is less clear.

Gammacerane is thought to be the geolipid product of tetrahymanol, a lipid usually ascribed to a source from marine ciliates when their diet is devoid of sterols (Peters et al., 2003), though also produced by some *Rhizobiales* soil proteobacteria (Rashby et al., 2007). Such conditions tend to occur in stratified water columns with oxic surface waters in which the ciliates feed on bacteria living in the chemocline (Peters et al., 2003). High gammacerane/C_{30} $\alpha\beta$-hopane indices are therefor commonly taken to indicate deposition under strongly (redox-) stratified conditions (Peters et al., 2003) though the chemocline may exist in the water column or in shallow sediment pore waters. Gammacerane/C_{30} $\alpha\beta$-hopane decreases upsection from elevated levels in the lower portions of both cores, though most notably in H33, implying that the seaway became progressively less stratified with shallowing. Reports of ^{13}C-enriched aryl isoprenoids, indicative of *Chlorobiaceae* and therefor at least episodic periods of photic zone euxinia, in Maquoketa bitumens are consistent with evidence for strongly stratified conditions during deposition of the lower part of H33 (Guthrie, 1996). Finally, HHI decreases in parallel with gammacerane, consistent with oxygenation accompanying declining stratification.

The ratio of hopanes to steranes (H/St) reflects the relative contributions of bacteria and eukaryotes, respectively, to sedimentary organic matter (Peters et al., 2003). Maquoketa Formation biomarkers fall within the Phanerozoic average range of 0.5 to 2

Lipid biomarker records from BS-5 core, shallow water representative. Abbreviations: Fm. formation, Mbr. Member, Cler. Clermont, Ft. A. Fort Atkinson, Br. Brainard, mcd. meters core depth, Lith. lithostratigraphy. Biomarker ratios as defined in text. Lithology units as in Figure 3.6.

Lipid biomarker records from H-33 core, deeper water representative. Abbreviations: Fm. formation, Mbr. Member, US. Upper Scales Shale, Cler. Clermont, LS. Lower Scales Shale, mcd. meters core depth, Lith. lithostratigraphy. Biomarker ratios as defined in text. Lithology units as in Figure 3.6.

Figure 3.8: Maquoketa Formation lipid biomarker ratios associated with source organisms and depositional redox conditions.

(Cao et al., 2009). H/St increases markedly, although with a slight off-set, with Ts / (Ts+Tm) and the $\beta\alpha/(\beta\alpha + \alpha\beta)$hopanes in H33. Changes in H/St from less than 1 to greater than 1 are often taken to indicate a substantial change in microbial community structure, from algal-dominated to potentially more bacterially-dominated systems.

Nuance to interpretation of the H/St proxy arises from i) the aforemetioned potential impacts of thermal maturity, ii) some debate as to the impacts of microbially mediated diagenesis, and iii) potential contributions from transported contemporary, or re-worked ancient, sedimentary organic material.

With respect to point i): with careful consideration, it seems that one cannot interpret the observed change in H/St with Ts/(Ts+Tm) and the $\beta\alpha/(\beta\alpha + \alpha\beta)$ hopanes in terms of maturity because, as discussed above, thermal maturity would cause H/St to increase with depth and to be higher at lower $\beta\alpha/(\beta\alpha + \alpha\beta)$, neither of which is observed. With respect to point ii): very high H/St values (i.e. exceeding 2) have been attributed in some ancient rocks to enhanced bacterial degradation of sedimentary organic matter (e.g. Marynowski et al., 2000) using the line of reasoning that as bacteria degrade algal lipids they also produce their own lipids. On a small scale (e.g. within the range of 0.5 to 2.0) this may well be a factor but the overall balance of trophic webs, in which the biomass of each higher trophic level decreases by 90 percent, suggests that sedimentary organic matter is likely to always be dominated by primary producers, be they of whichever Domain. Thus, in instances where H/St exceeds the Phanerozoic average (e.g. shallow carbonate-rich faces of Hirnantian age, Rohrssen et al., 2013) or where independent evidence suggests a roughly constant depositional environment (e.g. continuously euxinic bottom waters, Owens et al., submitted), this ratio likely reflects changes in the balance of primary producers. Finally, with respect to point iii): transported sedimentary organic matter from soils or eroded rocks has been proposed as a

source of biomarkers in marine sedimentary rocks. Terrigenous biomarkers have been identified in modern marine sediments at substantial distances from shore so it seems possible that terrigenous material might influence the biomarker composition of ancient rocks as well, particularly in organic-lean, relatively near-shore deposits such as Anticosti Island. Re-depositing weathered organic matter from ancient sedimentary rocks has been observed, however deposition must take place close to the site of weathering as erosion and transport under oxygenated conditions would rapidly work to break down organic matter, even kerogen. The latter process might be identified through the presence of an enhanced unresolved complex mixture, elevated biomarker maturity ratios or age proxies (e.g. C_{28}/C_{29} sterane ratio) compared to the burial history of the rock or increases in maturity and/or age where deposition of weathered kerogen is suspected. In the Maquoketa Formation there is not a substantial difference in UCM, most maturity (with the exceptions of moretanes and Ts / (Ts+Tm) as discussed above) or age indicators between higher TOC and lower TOC samples, as one might expect if there was a background flux of weathered ancient kerogen superimposed on autocthonous production. The former process, input of syngenetic soils, is notable as there is little information about the Lower Paleozoic terrestrial biosphere.

In this case, the moderate H/St throughout BS5 indicates a stable flux of algal-dominated organic matter, with slightly elevated algal contributions during highstand as indicated by phosphatic sediments or hardground/starvation surfaces (basal Elgin, Clermont). Shallowing through the Ft. Atkinson and Brainard Members introduces slight secular increases in H/St, as well as increased oxygenation (HHI) and decreased stratification (Gamma/C_{30} $\alpha\beta$-hopane). In the deeper-water, H33 setting, H/St begins dominated by algae, consistent with its hypothesized position in a zone of upwelling above the paleo-shelfbreak. H/St remains low through deposition of the Elgin Member

then increases dramatically to bacterially-dominated sedimentary organic matter with the change to green-gray shales of the Clermont Member, coincident with a substantial increase in oxygenation (lower HHI) and reduced stratification (lower Gamma/C_{30} $\alpha\beta$-hopane), but slightly lagging the rise in moretane abundance. Reduction in upwelling during deposition of the Clermont Member may have driven local oligotrophication in H33 (and attendant oxygenation) that was not present, or perhaps compensated for by terrigenous nutrient supply in BS5.

As an increasingly notable characteristic of Late Ordovician lipid biomarker profiles, 3β-methylhopane abundances are very high, well above the Phanerozoic marine average of about 1 - 3 percent of C_{30} $\alpha\beta$-hopane (3β-methylhopane index, 3-MeHI) (Rohrssen et al., 2013). 3-MeHI are highest in shallower deposits: 3-MeHI is higher overall in BS-5 than in H33, and higher in the dolomitized carbonate intervals. The large swings in 3-MeHI in BS-5, from just over 18.6 percent in the uppermost Dubuque Formation to 5.1 percent in the highstand deposits of the lowermost Elgin Member phosphorite, back to 16.5 percent in the upper Elgin, down to 11.3 percent in the Clermont, and back to 14.2 percent through the Fort Atkinson and Brainard, may be attributable to changing local redox. For example, the phosphatic and pyritic dark brown shales in the basal Elgin likely record an anoxic depositional environment in which methanogenesis may have been less prolific than in other, lower oxidant inventory locations, or anaerobic methanotrophy might have outcompeted aerobic methanotrophs. The 3-MeH display the same moretane pattern as the homohopanes; while this may indicate a common, oxic soil source, it may also solely reflect the substantial influence of certain clays on hopane stereochemistry in ancient immature rocks (French et al.). Despite similar isomer patterns between desmethylhopanes and methylhopanes, 3-MeHI does not correlate well with moretane abundance or Ts / (Ts+Tm), suggesting that

any soil-derived hopanoid input (sensu French) includes, if anything, less 3-MeH than that associated with carbonate deposition. This lends support to the hypothesis that 3-MeH are produced in the marine realm and that that moretane production and/or preservation in this case, is largely driven by clay composition and abundance. H/St and 3-MeHI display a very weak positive correlation in BS-5 and to a lesser extent in H33.

Geographic considerations (Figure 3.1) and the initial emergence of plants into a canonically depauperate terrestrial biosphere make Late Ordovician epeiric seas an interesting context in which to consider the influence of soil-derived material on organic proxies. Middle to Late Ordovician-age spores and fungi (Redecker et al., 2000) indicate soil development sufficient to support early bryophytes (Wellman and Gray, 2000). Early terrestrial organisms and ecosystems in the Late Ordovician were likely comprised of microbial mats, bryophytes/bryophyte-like stem taxa, and fungi in intermittently to perennially damp settings (Wellman and Gray 2000). Expansion of ground-cover, changes in sediment binding properties between unrooted microbial mats and marginally rooted early embryophytes (land plants) may have substantially impacted Late Ordovician geomorphology, sediment transport (Gibling and Davies, 2012) and nutrient availability in the marine realm as well as on land (Lenton et al., 2012). As observed in the Late Permian (Cao et al., 2009), $\beta\alpha/(\beta\alpha + \alpha\beta)$ across all homologues and methylhopanes co-vary with Ts / (Ts+Tm), H/St, and HHI in a manner which is not explained by thermal maturity or input of hopanoids from higher plants (French et al., 2012). I suggest, as French et al. (2012), that the Maquoketa Formation documents the influence of elevated terrigenous flux in the north, though perhaps in the form of nutrients (Lenton et al., 2012) and clays (e.g. Gibling and Davies, 2012) rather than organic matter.

3.4.5 Integration of Lipid Biomarker Records with Broader Context

Lipid biomarker results from two shallowing up cycles (Elgin and Clermont Members) across a paleobathymetry gradient in the Maquoketa Formation of Eastern Iowa are consistent with a stratified quasiestuarine circulation model for this portion of the North American Midcontinent epeiric sea in Late Ordovician times. Different compositions and responses to shallowing between the BS-5 (northern) and H33 (southern) cores support the proposed facies belt model (Witzke, 1987; Raatz and Ludvigson, 1996). For example, hopane/sterane ratios are lowest in brown shales of the upwelling-influenced "southern facies" (Witzke, 1987), and somewhat higher in the "intermediate facies." Lipid biomarkers from an Elgin Member shale sample from the Graf roadcut support its assignment to low oxygen (anoxic or intermittently anoxic) depositional conditions, similar to the basal shales and phosphatic sediments in the Lower Elgin Member in cores H33 and BS-5 (Table 3.1). Interestingly, the elevated hopane/sterane ratios observed in the eastern part of the seaway – on Anticosti Island and on the other side of the Sebree trough in the Cincinnati region – are not observed in the Maquoketa despite a common Late Katian age for the Maquoketa, Vaureal (Anticosti Island), and Waynesville through Whitewater (Cincinnati region) Formations. Most likely, this reflects the position of the Maquoketa formation to the west of the Sebree trough, in which the quasiestuarine circulation coupled with bathymetrically-induced upwelling could supply elevated nutrients compared to Anticosti and the Cincinnati region, which may have had less pronounced connections to nutrient-rich deep waters.

Lipid biomarkers likely derived from methanotrophic bacteria (3β-methylhopane) correlate well with sea-level and circulation changes inferred from lithologies and paleobiology, with lower 3-MeHI in deeper water, less carbonate-rich facies ("southern facies").

This trend is born out in the relatively low 3-MeHI of the Vinini Formation in comparison to all other epeiric sites. The lower amounts of 3-MeH in phosphatic and pyritic brown shales may result from more effective anaerobic oxidation of methane at these sites (more similar to modern oceans), whereas in less eutrophic circumstances fewer oxidants are available to reduce methane production. Compounds associated with stratification (gammacerane) or anoxic conditions (HHI) outline a secular decrease in stratification and increase in oxygenation superimposed on the Elgin and Clermont Member shallowing up cycles, perhaps consistent with pre-Hirnantian cooling. Importantly, the relationship between facies and biomarker profiles in the Maquoketa Formation suggests that, as expected, circulation regime (with attendant oxicity and nutrient availability) plays a crucial role in determining the structure of microbial communities. This data supports strong coupling between circulation regime and the balance of bacterial versus eukaryotic primary producers, such that shallow carbonate facies are not always associated with elevated hopane/sterane ratios but require exceptional conditions to attain H/St ratios in excess of the Phanerozoic average of 0.5 to 2.0 (Cao et al., 2009). Thus, explaining the elevated baseline H/St of observed for Anticosti and the Cincinnati region by impacts of warm water temperatures and low nutrient availability on eukaryotes is probably correct, though it does appear to be an eastern Laurentia phenomenon. This strong connection between H/St and local nutrient availability requires that trends in H/St be observed in multiple locations, preferably in different basins, in order to construct any inferences about the broader ocean. The decrease in 3-MeHI during the Hirnantian glacial maximum and low-stand observed on Anticosti and in the Vinini, however, has the opposite sign to connections between sea-level and 3-MeHI in the Maquoketa. That is, the lowest 3-MeHI for the Maquoketa are found in the deepest, most organic-rich facies and shallowing leads to higher 3-MeHI. 3-MeHI are lower in the more organic-

rich, deeper water Vinini Formation than in organic-lean Anticosti carbonates, but in both settings 3-MeHI become lower with shallowing. So, decreased 3-MeHI on Anticosti, in which oligotrophic, oxygenated waters overlay poorly oxygenated sediments may be attributed to less methane production (and hence aerobic methane oxidation) due to increased oxidant supply. In the Maquoketa, decreased 3-MeHI are found under nutrient-replete, partially anoxic water columns and thus may instead result from more efficient anaerobic methane oxidation. It seems that the decrease in 3-MeHI on Anticosti and in the Vinini may well reflect overall decreases in methanogenesis during the Hirnantian.

3.5 Conclusions

Lipid biomarker assemblages obtained from two shallowing-upwards sequences in deeper water (H33) and shallower water (BS-5) facies of the Maquoketa formation are consistent with a stratified, quasiestuarine circulation system for the central Laurentian epeiric sea. Stratification and oxygen-poor conditions diminish up-slope as well as over the course of Maquoketa Formation deposition. Integration of these observations with previous work suggest that major changes in microbial community structure inferred from biomarker proxies during the Hirnantian observed elsewhere cannot be explained solely by shifting facies associated with eustatic sea level change but require other biogeochemical, oceanographic, and/or climatic perturbations to best explain the main temporal transitions. Hopane/sterane ratios further demonstrate the importance of local aquatic conditions; particularly supply and competition for fixed nitrogen species and other bioessential nutrients. Low hopane/sterane ratios for Late Ordovician rocks of less than 2.0 are often associated with productive marginal marine settings with en-

hanced upwelling while oligotrophic epeiric seaways have the highest hopane/sterane ratios. This disparity is particularly pronounced for the Late Ordovician compared with other intervals of the Phanerozoic eon and is likely exacerbated by the warm greenhouse conditions which prevailed at this time prior to and after the Hirnantian glaciations. The ubiquity of elevated 3β-methylhopane, most likely derived from methanotrophic bacteria, in terms of their relative and absolute abundances , continues to support the hypothesis of enhanced marine methane and increased methane flux through the marine water column in Late Ordovician epeiric seaways compared with younger Phanerozoic settings.

3.6 Acknowledgments

I would like to acknowledge Brian Witzke (Iowa Geological Survey) for access to cores, core descriptions and helpful discussion in the planning stages, Huaibao Liu for the sample of Winneshiek Lagerstatte, the Iowa Core Repository for generous access to samples, and the Geological Society of America and University of California, Riverside Dissertation Year Fellowship for funding.

3.7 References

1. Brooks., J.D., Gould, K., Smith, J.W., 1969, Isoprenoid hydrocarbons in coal and petroleum: Nature, v. 222, p. 257-259.

2. Chetel, L. Simo, T., Singer, B., Provinance of detrital K-feldspars, Ordovician, Upper Mississippi Valley, A 40Ar/39Ar geochronology perspective: in Ludvigson, G.A., and Bunker, B.J., eds., 2005, Facets of the Ordovician geology of the Upper Mississippi Valley region, Iowa Geological Survey Guidebook No. 24.

3. Farrimond, P., Talbot, H.M., Watson, D.F., Schulz, L.K., and Wilhelms, A., 2004, Methylhopanoids: Molecular indicators ofancient bacteria and a petroleum correlation tool: Geochimica et Cosmochimica Acta, v.68, p.38733882.

4. Fowler, M.G., and Douglas, A.G., 1984, Distribution and structure of hydrocarbons in four organic-rich Ordovician rocks: Organic Geochemistry, v. 6, p. 105-114.

5. Gibling, M.R., Davies, N.S., 2012, Palaeozoic landscapes shaped by plant evolution: Nature Geoscience, v. 5, p. 99-105.

6. Grantham, P.J., Wakefield, L.L., 1988, Variations in the sterane carbon number distributions of marine source rock derived crude oils through geological time: Organic Geochemistry, v. 12, p. 61-73.

7. Guthrie, J.M., and Pratt, L.M., 1995, Geochemical character and origin of oils in Ordovician reservoir rock, Illinois and Indiana, USA: American Association of Petroleum Geologists Bulletin, v. 79, p. 1631-1649.

8. Guthrie, J.M., 1996, Molecular and carbon isotopic analysis of individual biological markers: evidence for sources of organic matter and paleoenvironmental conditions in the Upper Ordovician Maquoketa Group, Illinois Basin, U.S.A.: Organic Geochemistry, v. 25, p. 439-460.

9. Holmden, C., Mitchell, C.E., LaPorte, D.F., Patterson, W.P., Melchin, M.J., Finney, S.C., 2013, Nd isotope records of late Ordovician sea-level change– Implications for glaciation frequency and global stratigraphic correlation: Palaeogeography, Palaeoclimatology, Palaeoecology, v. 386, p. 131-144.

10. Jacobson, S.R., Hatch, J.R., Teerman, S.C., Askin, R.A., 1988, Middle Ordovician organic matter assemblages and their effect on Ordovician-derived oils: American Association of Petroleum Geologists Bulletin, v. 72, p. 1090-1100.

11. Kolata, D.R., huff, W.D., Bergstrm, S.M., 2001, The Ordovician Sebree Trough: An oceanic passage to the Midcontinent United States: Geological Society of America Bulletin, v. 113, p. 1067-1078.

12. Lenton, T.M., Crouch, M., Johnson, M., Pires, N., Dolan, L., 2012, First plants cooled the Ordovician: Nature Geoscience, v. 5, p. 86-89.

13. Liu, H.P., McKay, R.M., Young, J.N., Witzke, B.J., McVey, K.J., Liu, X., 2006, A new lagerstatte from the Middle Ordovician St. Peter Formation in northeast Iowa, USA: Geology, v. 34, p. 969-972.

14. Love, G.D., Snape, C.E., Carr, A.D., Houghton, R.C., 1995, Release of covalently-bound alkane biomarkers in high yields from kerogen via catalytic hydropyrolysis: Organic Geochemistry, v. 23, p. 981-986.

15. Marynowski, L., Narkiewicz, M., Grelowski, C., 2000, Biomarkers as environmental indicators in a carbonate complex, example from the Middle to Upper Devonian, Holy Cross Mountains, Poland: Sedimentary Geology, v. 137, p. 187-212.

16. Melendez, I.M., Grice, K., Trinajstic, K., Ladjavardi, M., Greenwood, P., Thompson, K., 2013, Biomarkers reveal the role of photic zone euxinia in exceptional fossil preservation: An organic geochemical perspective: Geology, v. 41, p. 123-126. DOI: 10.1130/G33492.1.

17. Owens, J.D., Reinhard, C.T., Rohrssen, M., Love, G.D., Lyons, T.W., Marine trace-metal drawdown during the Cenomanian-Turonian boundary event (OAE2): Implications for global redox and biological perturbation. Submitted.

18. Pancost, R.D., Freeman, K.H., Patzkowsky, M.E., Wavrek, D.A., and Collister, J.W., 1998, Molecular indicators of redox and marine photoautotroph composition in the late Middle Ordovician of Iowa, U.S.A: Organic Geochemistry, v.29, p.16491662, doi:10.1016/S0146-6380(98)00185-5.

19. Peters, K.E., Walters, C.C., and Moldowan, J.M., 2003, The Biomarker Guide, 2nd edition: Cambridge, UK, Cambridge University Press, 1132 p.

20. Powell, T.G., McKirdy, D.M., 1973, Relationship between ratio of pristane to phytane, crude oil composition and geological environment in Australia: Nature: v. 243, p. 37-39.

21. Raatz, W.D., and Ludvigson, G.A., 1996, Depositional environments and sequence stratigraphy of Upper Ordovician epicontinental deep water deposits, eastern Iowa and southern Minnesota: Geological Society of America. Special Paper, v.306, p.143159.

22. Rashby, S.E., Sessions, A.L., Summons, R.E., Newman, D.K., 2007, Biosynthesis of 2-methylbacteriohopanepolyols by an anoxygenic phototroph: Proceedings of the National Academy of Sciences, v. 104, p. 15099-15104.

23. Redecker, D., Kodner, R., Graham, L.E., 2000, Glomalean fungi from the Ordovician: Science, v. 289, p. 1920-1921.

24. Rohrssen, M., Love, G., Fisher, W., Finnegan, S., Fike, D.A., 2013, Lipid biomarkers record fundamental changes in microbial community structure of tropical seas during the Late Ordovician Hirnantian Glaciation: Geology, 2013, v. 41, p. 127-130. DOI: 10.1130/G33671.1.

25. Rohrssen, M., Owens, J.D., Lyons, T.W., Love, G.D., Lipid biomarker investigation of marine microbial community structure through the Cenomanian-Turonian Oceanic Anoxic Event (OAE2) at a permanently euxinic, upwelling-influenced site (Demerara Rise, ODP Leg 209). in prep.

26. Saltzman, M.R., 2005, Phosphorus, nitrogen, and the redox evolution of the Paleozoic oceans: Geology, v. 33, p. 573-576.

27. Seifert, W.K., Moldowan, J.M., 1978, Applications of steranes, terpanes and monoaromatics to the mauration, migration and source of crude oils: Geochimica et Cosmochimica Acta, v. 42, p. 77-95.

28. Seifert, W.K., Moldowan, J.M., 1980, The effec of themal stress on source-rock quality as measured by hopane stereochemistry: Physics and Chemistry of the Earth, v. 12, p. 229-237.

29. Sheehan, P.M., 2001, The Late Ordovician mass extinction: Annual Reviews Earth and Planetary Sciences, v. 29, p. 331-364.

30. Summons, R.E., Powell, T.G., 1986, Chlorobiaceae in Palaeozoic seas revealed by biological markers, isotopes and geology: Nature, v. 319, p. 763-765.

31. Summons, R.E., and Jahnke, L.L., 1990, Identification of the methylhopanes in sediments and petroleum: Geochimica et Cosmochimica Acta, v.54, p.247251, doi:10.1016/0016-7037(90)90212-4.

32. Welander, P.V., Coleman, M.L., Sessions, A.L., Summons, R.E., Newmann, D.K., 2010, Identification of a methylase required for 2-methylhopanoid production and implicatons for the interpretation of sedimentary hopanes: Proceedings of the National Academy of Sciences, v. 107, p. 8537-8542.

33. Welander, P.V., and Summons, R.E., 2013, Discovery, taxonomic distribution, and phenotypic characterization of a gene required for 3-methylhopanoid production: Proceedings of the National Academy of Sciences, v. 109, p. 12905-12910.

34. Wellman, C.H., Gray, J., 2000, The microfossil record of early land plants: Philosophical Transactions: Biological Sciences, v. 355, p. 717-732.

35. Witzke, B.J., Anderson, R.R., Heathcote, R.C., 1997, Upper Ordovician Brainard Shale (Maquoketa Formation): Stop 4: Highway 20, Dubuque County, in Geology in the Dubuque Area: Geological Society of Iowa Guidebook 63, 58p.

36. Witzke, B.J., Bettis, E.A., Anderson, R.R., Heathcote, R.J., 1997, Geology in the Dubuque Area: Geological Society of Iowa Guidebook 63, 58p.

37. Witzke, B.J., 1987, Models for circulation patterns in epicontinental seas applied to Paleozoic facies of North American craton: Paleoceanography, v.2, p.229248, doi:10.1029/PA002i002p00229.

Well number	County	Name	Depth (ft)	Depth (m)	Member	Pr/Ph	Tri / $C_{30}H$	Ts / (Ts+Tm)	C_{29}Ts/ C29H	$C_{30}H$ βα/ (βα+αβ) (%)
30190	Clayton	BS5	146.4	44.6	Brainard/Fort Atkinson?	1.81	0.37	0.07	0.13	22.34
30190	Clayton	BS5	151.7	46.2	Fort Atkinson/Brainard?	1.78	0.69	0.11	0.22	21.03
30190	Clayton	BS5	183.5	55.9	Clermont/Fort Atkinson	1.50	0.41	0.19	0.28	18.96
30190	Clayton	BS5	200.5	61.1	Clermont	0.66	0.41	0.08	0.15	22.33
30190	Clayton	BS5	212.9	65.0	Elgin/Clermont?	0.59	0.43	0.13	0.28	18.66
30190	Clayton	BS5	221.1	67.4	Elgin	1.71	0.18	0.19	0.25	18.52
30190	Clayton	BS5	260.6	79.4	Elgin	0.54	0.41	0.16	0.29	17.47
30190	Clayton	BS5	272.7	83.1		0.82	0.32	0.17	0.26	19.73
30190	Clayton	BS5	280.3	85.4	Elgin	1.58	0.52	0.15	0.21	16.40
30190	Clayton	BS5	288.8	88.0	Elgin	1.09	1.01	0.17	0.22	20.56
30190	Clayton	BS5	298	90.8	Dubuque	2.10	1.28	0.09	0.14	20.67
27543	Des Moines	H33	400.2	122.0	Upper Scales (Clermont)	2.40	0.84	0.03	0.04	24.75
27543	Des Moines	H33	421.6	128.5	Upper Scales (Clermont)	2.49	0.84	0.06	0.10	23.30
27543	Des Moines	H33	433.5	132.1	Lower Scales (Elgin)	2.43	0.73	0.21	0.30	16.91
27543	Des Moines	H33	444	135.3	Lower Scales (Elgin)	0.35	1.22	0.31	0.33	13.24
27543	Des Moines	H33	469.6	143.1	Lower Scales (Elgin)	0.47	0.66	0.31	0.30	10.34
27543	Des Moines	H33	469.6o	143.1	Lower Scales (Elgin)		0.81	0.32	0.29	9.94
n.a.	Graf, Iowa	Graf U	outcrop	outcrop	Elgin	1.66	1.51	0.21	0.29	15.50
n.a.		WS-10	outcrop	outcrop	Winnesheik shale, St. Peter Formation		0.07	0.01	0.00	29.84

Abbreviations: Pr, pristane; Ph, phytane; Tri, tricyclic terpanes;

Table 3.1: Lipid biomarkers from the Maquoketa Formation, Iowa, USA

Name	Depth (ft)	C_{31} αβH S/(S+R)	C_{32} αβH S/(S+R)	28,30DNH / (28,30DNH+C_{30} αβH) (%)	C_{29} ααα St S/(S+R)	C_{27} ααα St S/(S+R)	C_{29} St αββ/(ααα+αββ)	C_{27} St αββ/(ααα+αββ)	C_{29} Dia/St	C_{27} Dia/St
BS5	146.4	0.21	0.15	3.00	0.06	0.24	0.29	0.10	0.48	0.41
BS5	151.7	0.23	0.18	4.87	0.08	0.25	0.28	0.11	0.51	0.48
BS5	183.5	0.23	0.20	4.22	0.10	0.22	0.24	0.11	0.39	0.39
BS5	200.5	0.23	0.17	4.84	0.07	0.26	0.26	0.09	0.32	0.34
BS5	212.9	0.23	0.17	4.34	0.08	0.26	0.29	0.13	0.55	0.51
BS5	221.1	0.26	0.22	15.37	0.10	0.24	0.29	0.14	0.50	0.45
BS5	260.6	0.26	0.21	4.75	0.09	0.27	0.30	0.14	0.83	0.70
BS5	272.7	0.25	0.23	6.63	0.09	0.25	0.27	0.13	0.55	0.57
BS5	280.3	0.23	0.19	6.45	0.10	0.27	0.30	0.13	0.43	0.42
BS5	288.8	0.25	0.23	6.78	0.10	0.26	0.30	0.11	0.40	0.37
BS5	298	0.36	0.29	6.13	0.12	0.29	0.28	0.15	0.20	0.21
H33	400.2	0.59	0.55	2.81	0.26	0.39	0.18	0.05	0.27	0.28
H33	421.6	0.58	0.55	2.92	0.24	0.37	0.19	0.08	0.56	0.57
H33	433.5	0.58	0.54	5.07	0.29	0.39	0.26	0.16	0.82	0.83
H33	444	0.58	0.54	7.21	0.26	0.37	0.24	0.14	0.72	0.71
H33	469.6	0.58	0.56	15.65	0.31	0.41	0.26	0.17	0.50	0.56
H33	469.6o	0.58	0.56	17.16	0.34	0.42	0.27	0.17	0.55	0.57
Graf U	outcrop	0.55	0.49	19.86	0.20	0.34	0.24	0.11	0.55	0.58
WS-10	outcrop	0.29	0.16	20.25	0.04	0.02	0.37	0.26	0.01	0.00

Abbreviations: DNH, dinorhopane; dia, diasterane; st, sterane.

Table 3.2: Lipid biomarkers from the Maquoketa Formation, Iowa, USA, continued.

Name	Depth (ft)	Olea / $C_{30}\alpha\beta H$	C_{28}/ C_{29} St	C_{27}-C_{35} Hopane / C_{27}-C_{29}Sterane	% C_{27} St (C_{27}-C_{29})	% C_{28} St (C_{27}-C_{29})	% C_{29} St (C_{27}-C_{29})	2α-MeHI (%)	3β-MeHI (%)	Gam / $C_{30}\alpha\beta H$
BS5	146.4	0.00	0.20	0.57	31.6	11.4	57.0	0.3	13.1	0.03
BS5	151.7	0.00	0.24	0.43	38.7	12.0	49.3	0.6	14.2	0.03
BS5	183.5	0.01	0.22	0.37	34.9	11.6	53.5	0.0	14.0	0.04
BS5	200.5	0.00	0.24	0.38	36.9	12.0	51.1	0.9	11.3	0.03
BS5	212.9	0.00	0.21	0.27	36.7	11.0	52.4	0.8	12.9	0.04
BS5	221.1	0.00	0.16	0.47	27.8	10.1	62.1	1.1	16.5	0.06
BS5	260.6	0.00	0.24	0.22	35.8	12.3	51.9	0.6	10.0	0.03
BS5	272.7	0.00	0.25	0.42	35.0	13.2	51.9	0.6	6.4	0.07
BS5	280.3	0.01	0.26	0.37	34.8	13.6	51.6	0.6	8.7	0.08
BS5	288.8	0.00	0.27	0.11	32.7	14.1	53.2	0.9	5.1	0.12
BS5	298	0.01	0.20	0.59	38.4	10.2	51.4	0.7	18.6	0.11
H33	400.2	0.00	0.08	1.83	29.5	9.2	61.3	0.8	10.7	0.02
H33	421.6	0.00	0.16	1.30	29.6	9.6	60.8	0.8	11.0	0.03
H33	433.5	0.00	0.21	0.42	32.7	11.6	55.8	0.9	12.0	0.02
H33	444	0.00	0.21	0.27	34.0	11.6	54.4	0.4	6.3	0.08
H33	469.6	0.00	0.18	0.28	28.6	11.0	60.4	0.4	8.7	0.16
H33	469.6o	0.00	0.18	0.27	29.9	10.9	59.2	0.5	8.4	0.14
Graf U	outcrop	0.01	0.24	0.26	33.4	12.7	53.9	0.3	5.4	0.12
WS-10	outcrop	0.00	2.75	8.14	49.8	36.8	13.4	0.4	5.8	0.02

Abbreviations: olea, oleanane; st, sterane; MeHI, methylhopane index; gam, gammacerane; HHI, homohopane index.

Table 3.3: Lipid biomarkers from the Maquoketa Formation, Iowa, USA, continued.

Chapter 4

Absence of the "marine biomarker" 24-*n*-propylcholestane in Lower Paleozoic marine paleoenvironments

Megan Rohrssen *1, Gordon D. Love 1, Benjamin Gill 2

1 Department of Earth Sciences, University of California, Riverside, CA 92521, USA.

2 Department of Geosciences, Virginia Polytechnic Institute and State University, Blacksburg, VA, 24061, USA.

4.1 Abstract

24-*n*-propylcholestane (24-*n*pc), a C_{30} sterane compound derived from sterol precursors which are the major sterol constituents of modern pelagophyte microalgae,

occurs in certain Neoproterozic rocks and oils and throughout the Phanerozoic rock record. This broad distribution leads 24-*n*pc to be widely considered as a reliable indicator of an open or partially restricted marine depositional setting for source rocks and oils. The sub-detection limit concentration of 24-*n*pc in definitively marine rocks of the Late Ordovician has lead to identification of other Lower Paleozoic marine rocks in which 24-*n*pc is also undetected. Strong temporal and lithofacies influences on the abundance of 24-*n*pc yield insight into the evolutionary history and environmental tolerances of early Pelagophytes and reinforce that caution be applied when interpreting the depositional environments of source rocks in certain intervals of Early Paleozoic time

4.2 Introduction

The C_{30} sterane, 24-*n*-propylcholestane (24-*n*pc), is commonly used as an indicator of marine origins for sedimentary organic matter (Moldowan, 1984; 1990). 24-*n*-propylidene-cholesterol and 24-*n*-propylcholesterol, the precursor molecules to 24-*n*pc, have at present only been detected in pelagophyte microalgae, including the "brown tide" algae *Aureoumbra* and *Aureococcus* (Giner et al., 2009; Volkman, 2003), and was recently found in a culture of the heterotrophic foraminifer *Allogromia laticollaris* (Grabenstatter et al., 2013). Pelagophytes synthesize 24-*n*pc through an unusual pathway involving a cyclopropyl intermediate (Giner and Djerassi, 1991; Hong et al., 2013). Pelagophyceae is a small class of marine chromophyte algae which feature 24(E)-24-propylidenecholesterol as their dominant sterol and are widespread in modern marine environments, reflecting the physiological versatility of this clade (Worden et al., 2012; Gobler and Sanudo-Wilhelmy, 2001; Doblin et al., 2004; DeYoe et al., 1997; Lomas et al., 2001; Berg et al., 2008). Pelagophytes are present in open marine, coastal marine,

estuarine, and superlittoral modern settings, but most well-known for their tendency to form harmful algal blooms in both the warm eutrophic waters and saline lagoons of the Gulf of Mexico, and the cooler, less nutrient-replete waters of the North Atlantic. *Aureococcus*, at least, is able to grow on both organic and inorganic nitrogen species, though they are out-competed by other algae under nitrate-replete conditions, able to uptake organic phosphorous, and able to supplement photosynthetic carbon fixation with assimilation of glucose (Gobler et al., 2001, Lomas et al., 2001; Berg et al., 2008). *Aureoumbra*, the genus responsible for Texas brown tides, forms bloom at temperatures as high as 25 - 30°C (e.g. Rhudy et al 1999), while *Aureococcus* grows well in the cooler waters of the North Atlantic. Less is known about the metabolic versatility of their open ocean counterparts.

The C_{30} sterane, 24-*n*pc, is commonly used as an indicator of marine origins for sedimentary organic matter (Moldowan, 1984), to such an extent that the absence of 24-*n*pc has sometime been considered sufficient to classify an oil or source rock as non-marine. The absence of 24-*n*pc in Lower Palaeozoic source rocks and oils independently constrained to marine depositional conditions (e.g. in the Middle Ordovician Trenton-Black River Formation of the Michigan Basin, Peters et al., 2003) was initially used to infer that pelagophyte microalgae appeared in Early Ordovician to Devonian times (Moldowan et al., 1990). Subsequently, 24-*n*pc has been described in rocks as old as Neoproterozoic in age (e.g. McCaffrey et al., 1994; Logan et al., 1997; Grosjean, 2009; Pratt et al., 1991; Love et al., 2009), most likely indicating an earlier appearance of the Pelagophytes, a result broadly consistent with molecular clock analyses (e.g. Brown and Sorhannus, 2010).

This note identifies two extended intervals within the Early Paleozoic, for which demonstrably marine-deposited rocks lack significant quantities of 24-*n*pc at the detec-

tion limits of highly sensitive Metastable Reaction Monitoring-Gas Chromatography-Mass Spectrometry (MRM-GC-MS) relative to other sterane compounds (less than 0.5 percent of total C_{27} - C_{30} steranes).

4.3 Materials and Methods

4.3.1 Materials

Lipid biomarker data from two distinct sets of rocks samples of different ages are presented in this study. The first set comprises a suite of Cambrian-age samples collected from drill core (Gill et al., 2011). The second consists of suite of Late Ordovician age carbonate and siliciclastic marine rocks spanning a wide range of total organic carbon (TOC) contents from less than 0.1 - 18.4 weight percent, obtained both from outcrop and drill core as described previously (Rohrssen et al., 2013; Gill et al., 2011).

4.3.2 Late Cambrian, Mt. Whelan Formation, Queensland, Australia

The first suite of samples derives from Cambrian (Steptoean) rocks of the Mt. Whelan Formation, Queensland, Australia. The Mount Whelan number 1 core was drilled in the Eastern Georgina Basin in Queensland, Australia. The sampled portion of the core consists of limestone assigned to the Georgina Limestone (Green and Balfe, 1980). The Georgina Limestone at this location (approximately 90 percent) consists almost entirely of argillaceous micrite, which is laminated on the millimeter-scale (Green and Balfe, 1980). Carbonate contents range from 30 to 75 weight percent (Gill et al., 2011). Occasional decimeter scale upward-fining units with peloidal, intraclastic and oolitic packstones or grainstones as bases likely represent turbidite deposits. Calcite and pyrite nodules are also abundant throughout the core. Disseminated pyrite contents

range from 0.5 to 5.7 weight percent (Gill et al., 2011). Due to the presence of the fine lamination and a general lack of current structures the depositional environment of the Georgina has been interpreted as below storm wave base (Green and Balfe, 1980).

Although the core is largely unfossiliferous, the key biostratigraphic fossils *Oidalagnostus personatus*, *Glyptagnostus reticulatus*, and *Irvingella tropica* have been identified at 359.0 195.0 and 22.9 meters, respectively (Green and Balfe 1980). The *G. reticulatus* and *I. tropica* occurrences place the upper portion of the core within the Australia Idamean Stage, which correlates to the International Paibian Series (Peng et al. 2004). This stratigraphic placement is confirmed by the carbon isotope stratigraphy, which has identified the Steptoean Positive Carbon Isotope Excursion or SPICE in the Georgina in this core (Saltzman et al., 2000). Additionally, the positive excursion in carbonate-associated sulfate and pyrite sulfur that is coeval with the SPICE has also been identified (Gill et al., 2011).

4.3.3 Late Ordovician, Anticosti Island, Canada

The second suite of rocks comes from the Late Ordovician succession of Anticosti Island, Quebec, Canada. Anticosti Island preserves mixed carbonate-siliciclastic rocks deposited in a paleo-tropical, storm-influenced ramp to shelf environment (e.g. Long and Copper, 1994). Samples were collected from outcrops of the Vaureal, Ellis Bay, Becscie and Merrimack Formations and drill core material (D3) from the Macasty Formation.

High subsidence rates coupled with high eustatic sea level are thought to have kept the Anticosti basin in contact with the open ocean and Laurentian epeiric seaway through much of the Late Ordovician (Long, 2007). Decreased subsidence, as well as sea level fall during the Hirnantian glacioeustatic regression, may have reduced the con-

nection from the Anticosti basin to both the open ocean and epeiric seaway during the latest Ordovician. Shallower intervals during deposition of the Vaureal and upper Ellis Bay Formation are indicated by development of coral-algal and coral-stromatoporoid patch reefs and bioherms, often accompanied by oncoidal limestones (Copper, 2001). Other paleontological support for the Paleozoic normal marine nature of Anticosti rocks are crinoid, trilobite and other marine fossils present in even the shallowest water settings. The absence of sedimentological evidence for development of hyper- or hypo-saline conditions (e.g. no evaporite deposits, minimal evidence for freshwater alteration of carbonates) suggests that Western Anticosti rocks remained marine throughout the Late Ordovician to Early Silurian (approximately 488 to 428 Ma) (Long, 2007; Copper, 2001; Desrochers et al., 2010). The only interval of possible emergence occurs in the uppermost Ellis Bay Formation (Laframboise Member), more than 1,000 meters (approx. 6 myr) above the last observed occurrence of 24-*n*-propylcholestane.

4.3.4 Late Ordovician, Vinini Formation, Nevada, USA

A third suite of rocks was collected from the Vinini Formation at Vinini Creek in the Roberts Mountains of Nevada, USA (Finney et al., 1999). The Vinini Formation comprises interbedded graptolitic brown shales with sandstones and siltstones, which during the Hirnantian lowstand are replaced with organic carbon-rich carbonates (Finney et al., 1997) Phosphatic intervals within the brown shale rich middle of the section (*Normalograptus pacificus* zone) are interpreted as recording deep water deposition under an oxygen minimum zone (Finney et al., 1999; 2007). Shallowing in the upper N. pacificus zone continues through the Hirnantian-age *Metabolograptus extraordinarious* and *M. persculptus* graptolite biozones but did not result in exposure of this deep water section (Finney et al., 1997). A low-angle thrust fault cross-cuts the upper portion of the

Vinini Creek section resulting in anomalous biomarker maturity indicators proximal to the fault due to frictional heating (c.f. Polissar et al., 2011) but does not appear to have caused much duplication or loss of section (Finney et al., 1997), or to have introduced allocthnonous bitumen.

4.3.5 Methods

Outcrop and core samples (Table 4.1) for biomarker analysis were trimmed using solvent washed saw blades to remove outer weathered surfaces and to expose a solid inner portion. and Large pieces were crushed with a hammer and the resulting chips were solvent-rinsed prior to powdering. Lipid biomarkers were extracted in 9:1 vol/vol dichloromethane/methanol using a Microwave Accelerated Reaction System (CEM Corp.) and separated into aliphatic, aromatic, and polar fractions by silica column chromatography prior to Metastable Reaction Monitoring-Gas Chromatography-Mass Spectrometry (MRM-GC-MS). MRM-GC-MS was conducted with a Waters Autospec Premier mass spectrometer equipped with an Agilent 7890A gas chromatograph and DB-1MS coated capillary column (60m x 0.25 mm, 0.25 um film) using He for carrier gas. The GC temperature program used for compound separation consisted of an initial hold at 60°C for 2 min, heating to 150°C at 10°C/min followed by heating to 315°C at 3°C/min, and a final hold at 320°C for 22 min. 24-*n*pc isomers were unambiguously identified when present in MRM-GC-MS by comparison of retention time difference between C_{29} steranes and authentic 24-*n*pc diastereoisomer determined in a known oil standard. Procedural blanks yielded less than 0.5 ng/g of powder of individual hopane isomers and less than 0.3 ng/g powder for the most abundant sterane. Cross-talk from the C_{30} and C_{31} hopane and C_{29} sterane channels dominates the 414 - 217 signal in low C_{30} sterane samples (less than 0.5 percent of C_{27} - C_{30} steranes). Cross-talk in 414 - 217

from C_{30} and C_{31} hopanes is less than 0.2 percent of 412 - 191 hopane signal and less than 1 percent of the 426 - 191 signal, respectively. In low 24-*n*pc samples, the most conservative metric for detection (i.e. combining any real 24-*n*pc signal plus background noise at the appropriate retention times) yields 24-*n*pc abundances of 0.1 - 0.5 percent of C_{27} - C_{30} steranes.

4.4 Results and Discussion

In the Middle Cambrian-age Whelan Formation, 24-*n*pc is absent throughout sampled core coverage despite these being independently constrained marine rocks (Fig. 4.1C, Table 4.1). The absence of detectable 24-*n*pc in the Whelan Formation continues through a proposed reduction in widespread euxinia and contraction of oxygen minimum zones (Gill et al., 2011).

In Anticosti rock extracts (Fig. 4.1A), 24-*n*pc steranes are present in trace amounts, not detectable via bench-top GC-MS but just around Autospec MRM detection limits, only in drill core from the Late Caradoc-age (approx. 449-453 Ma) Macasty Formation. 24-*n*pc then falls below the detection limit in both younger (the Rawtheyan through Rhuddanian-age; Vaureal, Ellis Bay, Becscie and Merrimack Formations) and older (the Caradoc-age Trenton-Black River Formation) strata (Table 4.1). The disappearance of 24-*n*pc substantially precedes environmental perturbations associated with the Hirnantian Stage glacial maximum and does not detectably increase again even during an interval hypothesized to have had higher overall algal contribution to sedimentary organic matter (Rohrssen et al., 2013). The lithofacies difference between the brown shale of the Macasty Formation and the laminated argillaceous limestones of the Vaural Formation is substantial and potentially relevant to the decrease in 24-*n*pc.

However, organic carbon content and lithofacies do not appear to be the only controls; despite higher total organic carbon and overall greater proportions of steranes in samples of the Vinini Formation at Vinini Creek (Fig. 4.1B), 24-*n*pc remains below GC-MS detection in our samples and near detection limits of Autospec MRM-GC-MS. Hydrous pyrolysis products also evidently lack SIR-GC-MS-detectable amounts of C30 steranes (Wei et al., 2007). Thus, whether in the oligotrophic, warm, bacterially-dominated conditions of Late Ordovician Anticosti Island or the nutrient-replete, algal-dominated conditions that prevailed during deposition of the Vinini Formation, algae which produced precursors to 24-*n*pc were not abundant in the ocean in Late Ordovician times. Upper Ordovician rocks from the US midcontinent and Estonia also lack 24-*n*pc in GC-MS detectable levels and, where present in MRM-GC-MS remain near to detection limits (Rohrssen et al., unpublished), reflecting the ubiquity of low 24-*n*pc in Late Ordovician-age rocks.

4.5 Conclusions

Although widely identified in most Neoproterozoic-Cenozoic marine source rocks and oils, 24-*n*-propylcholestane is not always present in detectable concentrations in Lower Paleozoic marine rocks even using highly sensitive MRM-GC-MS methods of detection for C_{30} steranes. Indeed this biomarker seems very rare in occurrence and abundance in Upper Ordovician-age sedimentary deposits and trace amounts of C_{30} steranes (both 24-*n*pc and 24-*iso*-propylcholestane), along with elevated 3β-methylhopane indices (Rohrssen et al., 2013), appear to be characteristic of Upper Ordovician marine rocks. Source organisms that synthesized 24-*n*pc steroids, most likely marine pelagophyte algae, were easily detectable in Neoproterozoic and other portions of the Lower

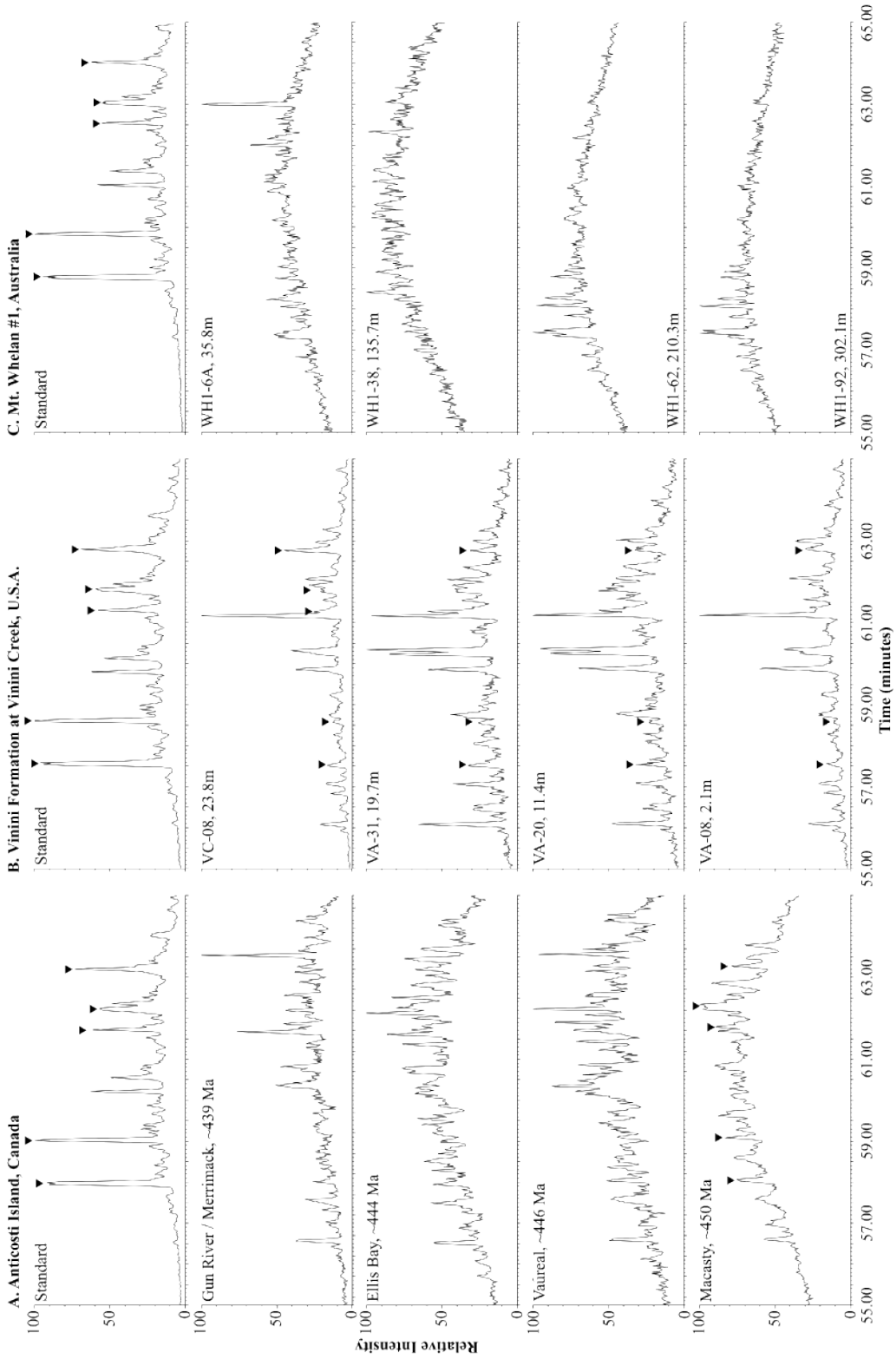

Figure 4.1: MRM-GC-MS m/z 414 - 217 chromatograms scaled to response of largest peak in each trace for samples from A. Anticosti Island (approximate ages from Long, 2007), B. Vinini Formation at Vinini Creek, and C. Mt. Whelan Formation. Triangles indicate 24-*n*-propylcholestane isomers. Chromatograms are scaled to the most abundant peak in each trace.

Paleozoic but do not appear to have flourished in Late Ordovician seas. Higher relative algal versus bacterial contribution to sedimentary organic matter, as evidenced by lower values of hopane/sterane ratio, does not result in detectable quantities of 24-*n*pc in these same intervals.

4.6 Acknowledgments

Funding for this project was provided by an Agouron Institute grant to G.D.L. and Dissertation Year Fellowship awarded to MR. The authors wish to thank D. Boulet and the Societe des etablissements de plein air du Qubec for assistance with work in Anticosti National Park, as well as D. Jones (Amherst College), D. Fike (Washington University, St. Louis), S. Finnegan (Stanford) and W. Fisher (Caltech) for assistance in the field and collecting core at the Geological Survey of Canada's geological core and sample repository.

4.7 References

1. Berg, G.M., Shrager, J., Glckner, G., Arrigo, K.R., Grossman, A., 2008, Understanding nitrogen limitation in *Aureococcus anophagefferens* (Pelagophyceae) through cDNA and qRT-PCR analysis: Journal of Phycology, v. 44, p. 1235-1249.

2. Copper, P., 2001, Reefs during the multiple crises towards the Ordovician-Silurian boundary: Anticosti Island, eastern Canada, and worldwide: Canadian Journal of Earth Sciences, v. 38, p. 153-171.

3. Desrochers, A., Farley, C., Achab, A., Asselin, E., Riva, J.F., 2010, A far-field record of the end Ordovician glaciation: The Ellis Bay formation, Anticosti, Island, Eastern Canada: Palaeoceanography, Palaeoclimatology, Palaeoecology, v. 296, p.248-263.

4. DeYoe, H.R., Stockwell, D.A., Bidigare, R.R., Latasa, M., Johnson, P.W., Hargraves, P.E., Suttle, C.A., 1997, Description and characterization of the algal species *Aureoumbra lagunensis* gen. et sp. nov. and referral of *Aureoumbra* and *Aureococcus* to the Pelagophyceae: Journal of Phycology, v. 33, p. 1042-1048.

5. Doblin, M.A., Popels. L.C., Coyne, K.J., Hutchins, D.A., Cary, S.C., Dobbs, F.C., 2004, Transport of the harmful bloom alga *Aureococcus anophagefferens* by

oceangoing ships and coastal boats: Applied and Environmental Microbiology, v. 70, p. 6495-6500.

6. Finney, S.C., Berry, W.B.N., Cooper, J.D., Ripperdan, R.L., Sweet, W.C., Jacobson, S.R., Soufiane, A., Achab, A., Noble, P.J., 1999. Late Ordovician mass extinction: A new perspective from stratigraphic sections in central Nevada. Geology 27, 215-218.

7. Finney, S.C., Cooper, J.D., Berry, W.B.N., 1997, Late Ordocician mass extinction: Sedimentologic, cyclostratigraphic, and biostratigraphic records from platform and basin successions, Central Nevada: BYU Geology Studies, v. 42, p. 79-103.

8. Finney, S.C., Berry, W.B.N., and Cooper, J.D., 2007, The influence of denitrifying seawater on graptolite extinction and diversification during the Hirnantian (latest Ordovician) mass extinction event: Lethaia, v. 40, p. 281291.

9. Gill, B.C., Lyons, T.W., Young, S.A., Knoll, A.H., Kump, L.R., Saltzman, M.R., 2011, Geochemical evidence for widespread euxinia in the Later Cambrian ocean: Nature, v. 469, p. 80-83.

10. Giner, J.-L., and Djerassi, C., 1991, Biosynthetic studies of marine lipids: 31. Evidence for a protonated cyclopropyl intermediate in the biosynthesis of 24-propylidenecholesterol: Journal of the American Chemical Society, v. 113, p. 1386-1393.

11. Giner, J.-L., Li, X., Boyer, G.L., 2001, Sterol composition of *Aureoumbra lagunensis*, the Texas brown tide alga: Phytochemistry, v. 57, p. 787-789.

12. Giner, J.-L., Zhao, H., Boyer, G.L., Satchwell, M.F., Andersen, R.A., 2009, Sterol chemotaxonomy of marine Pelagophyte algae: Chemistry and Biodiversity, v. 6, p. 1111-1130.

13. Gobler, C.J., and Sanudo-Wilhelmy, S.A., 2001, Effects of organic carbon, organic nitrogen, inorganic nutrients, and iron additions on the growth of phytoplankton and bacteria during a brown tide bloom: Marine Ecology Progress Series, v. 209, p. 19-34.

14. Grabenstatter, J., Mhay, S., McIntyre-Wressnig, A., Giner, J.-L., Edgcomb, V. P., Beaudoin, D. J., Bernhard, J. M., Summons, R. E., 2013, Identification of 24-n-propylidenecholesterol in a member of the Foraminifera: Organic Geochemistry, v. 63, p. 145-151.

15. Green, P. M., Balfe, P. E., 1980, Stratigraphic drilling report-GSQ Mt Whelan 1 and 2: Queenland Goverment Mining Journal, v. 81, p. 162-178.

16. Grosjean, E., Love, G.D., Stalvies, C., Fike, D.A., Summons, R.E., 2009, Origin of petroleum in the Neoproterozoic-Cambrian South Oman Salt Basin: Organic Geochemistry, v. 40, p. 87-110.

17. Hong, Y.J., Giner, G.-L., Tantillo, D.J., 2013, Triple shifts and thioether assistance in rearrangements associated with an unusual biomethylation of the sterol side chain: Journal of Organic Chemistry, v. 78, p. 935-941.

18. LaPorte, D.F., Holmden, C., Patterson, W.P., Loxton, J.D., Melchin, M.J., Mitchell, C.E., Finney, S.C., Sheets, H.D., 2009, Local and global perspectives on carbon and nitrogen cycling during the Hirnantian glaciation: Palaeogeography, Palaeoclimatology, Palaeoecology, v. 276, p. 182-195.

19. Logan, G.A., Summons, R.E., Hayes, J.M., 1997, An isotopic biogeochemical study of Neoproterozoic and Early Cambrian sediments from the Centralian Superbasin, Australia: Geochimica et Cosmochimica Acta, v. 61, p. 5391-5409.

20. Lomas, M.W., GIlbert, P.M., Clougherty, D.A., Huber, D.R., Jones, J., Alexander, J., Haramoto, E., 2001, Elevated organic nutrient ratios associated with brown tide algal blooms of *Aureococcus anophagefferens* (Pelagophyceae): Journal of Plankton Research, v. 23, p. 1339-1344.

21. Long, D.G.F., Copper, P., 1987, Stratigraphy of the Upper Ordovician upper Vaureal and Ellis Bay formations, eastern Anticosti Island, Quebec: Canadian Journal of Earth Sciences, v. 24, p. 1807-1820.

22. Long, D.G.F., 2007, Tempestite frequency curves: a key to Late Ordovician and Early Silurian subsidence, seal-level change, and orbital forcing in the Anticosti foreland basin, Quebec, Canada: Canadian Journal of Earth Sciences, v. 44, p. 413-431.

23. Love, G.D., Grosjean, E., Stalvies, C., Fike, D.A., Grotzinger, J.P., Bradley, A.S., Kelly, A.E., Bhatia, M., Meredith, W., Snape, C.E., Bowring, S.A., Condon, D.J., Summons, R.E., 2009, Fossil steroids record the appearance of Demospongiae during the Cryogenian period: Nature, v. 457, p. 721-722.

24. McCaffrey, M.A., Moldowan, J.M., Lipton, P.A., Summons, R.E., Peters, K.E., Jeganathan, A., Watt, D.S., 1994, Paleoenvironmental implications of novel C_{30} steranes in Precambrian to Cenozoic age petroleum and bitumen: Geochimica et Cosmochimica Acta, v. 58, p. 529-532.

25. Moldowan, J.M., 1984, C_{30}-steranes, novel markers for marine petroleums and sedimentary rocks: Geochimica et Cosmochimica Acta, v. 48, p. 2767-2768.

26. Peng, S., Babcock, L.E., Robison, R.A., Lin, H., Rees, M.N., Saltzman, M.R., 2004, Global Standard Stratotype-section and Point of the Furongian Series and Paibian Stage Cambrian: Lethaia, v. 37, p. 365-379.

27. Peters, K.E., Walters, C.C., Moldowan, J.M., 2003, The Biomarker Guide, 2nd edition: Cambridge University Press, Cambridge. p. 785.

28. Polissar, P.J., Savage, H.M., Brodsky, E.E., 2011, Extractable organic material in fault zones as a tool to investigate frictional stress: Earth and Planetary Science Letters, v. 311, p. 439-447.

29. Pratt, L.M., Summons, R.E., Hieshima, G.B., 1991, Sterane and triterpane biomarkers in the Precambrian Nonesuch Formation, North American Midcontinent Rift: Geochimica et Cosmochimica Acta, v. 55, p. 911-916.

30. Rhudy, K.B., Sharma, V.K., Lehman, R.L., McKee, D.A., 1999, Seasonal variability of the Texas "brown tide" (*Aureoumbra lagunensis*) in relation to environmental parameters: Estuarine, Coastal, and Shelf Science, v. 48, p. 565-574.

31. Rohrssen, M., Love, G.D., Fisher, W., Finnegan, S., Fike, D.A., 2013, Lipid biomarkers record fundamental changes in the microbial community structure of tropical seas during the Late Ordovician Hirnantian glaciation: Geology, v. 47, p. 127-30.

32. Saltzman, M.R., Ripperdan, R.L., Brasier, M.D., Lohmann, K.C., Robison, R.A., Chang, W.T., Peng, S., Ergaliev, E.K., Runnegar, B., 2000, A global carbon isotope excursion (SPICE) during the Late Cambrian: relation to trilobite extinctions, organic-matter burial and sea level: Palaeogeography, Palaeoclimatology, Palaeoecology, v. 162, p. 211-223.

33. Volkman, J.K., 2003, Sterols in microorganisms: Applied Microbiology and Biotechnology, v. 60, p. 495-506.

34. Wei, Z., Moldowan, J.M., Zhang, S., Hill, R., Jarvie, D.M., Wang, H., Song, F., Fago, F., 2007, Diamondoid hydrocarbons as a molecular proxy for thermal maturity and oil cracking: Geochemical models fom hydrous pyrolysis: Organic Geochemistry, v. 38, p. 227-249.

35. Worden, A.Z., Janouskovec, J., McRose, D., Engman, A., Welsh, R.M., Malfatti, S., Tringe, S.G., Keeling, P.J., 2012, Global distribution of a wild alga revealed by targeted metagenomics: Current Biology, v. 22, p. R675-R677.

Table 5.1. Lipid biomarker ratios for Late Ordovician and Cambrian-age rock extracts

Sample	Formation	Sample Type	Stage[1]	TOC (wt%)	TIC (wt%)
916-29.1	Gun River/Merrimack	Outcrop	Rhuddanian	<0.1	10.8
901-3.5	Ellis Bay	Outcrop	Hirnantian	0.29	8.7
906-44	Vaureal	Outcrop	Katian	0.37	9.4
D3-3927	Macasty	Core	Katian	4.9	1.6
VC-08	Vinini	Outcrop	Hirnantian	0.46	11.2
VA-31	Vinini	Outcrop	Hirnantian/Katian	n.m.	n.m.
VA-23	Vinini	Outcrop	Katian	0.0	18.4
VA-20	Vinini	Outcrop	Katian	2.10	10.3
VA-08	Vinini	Outcrop	Katian	0.52	9.6
WHI-6A	Whelan	Core	Steptoean	n.m.	n.m.
WHI-38	Whelan	Core	Steptoean	n.m.	n.m.
WHI-62	Whelan	Core	Steptoean	n.m.	n.m.
WHI-92	Whelan	Core	Steptoean	n.m.	n.m.

[1]Stage assigned using Sadler et al., 2009 with Long, (2007) and Finney et al. (2009) for Anticosti and the Vinini Formation, respectively.

Table 4.1: Selected organic geochemical data for Late Ordovician and Cambrian-age rock extracts.

Table 5.1. Lipid biomarker ratios for Late Ordovician and Cambrian-age rock extracts cont.

Sample	Ts/ (Ts+Tm)	Tricyclics / C_{30} αβH	C_{31}H S/ (S+R)	C_{32}H S/ (S+R)	H/St	C_{29} ααα S/(S+R)	C_{27} ααα S/(S+R)	C_{29} St dia/reg	C_{27} St dia/reg	C_{27} St (%)	C_{28} St (%)	C_{29}St (%)	C_{30} St (%)	C_{28}/C_{29} Sterane
916-29.1	0.07	0.37	0.60	0.49	5.91	0.44	0.49	0.44	0.59	26.6	11.5	61.5	0.4	0.19
901-3.5	0.15	0.45	0.58	0.59	5.48	0.45	0.47	0.52	0.69	27.1	10.2	62.2	0.5	0.16
906-44	0.18	0.43	0.57	0.52	4.26	0.44	0.44	0.53	0.90	32.1	14.7	52.8	0.3	0.28
D3-3927	4.20	0.87	0.55	0.54	0.34	0.54	0.58	0.66	0.83	29.7	16.6	52.5	1.2	0.32
VC-08	0.80	0.32	0.57	0.55	0.48	0.27	0.15	0.21	0.28	19.1	11.0	69.5	0.4	0.16
VA-31	1.26	0.30	0.61	0.59	0.64	0.58	0.55	0.37	0.48	22.0	10.8	67.0	0.3	0.16
VA-23	3.87	0.20	0.60	0.60	0.79	0.47	0.54	0.22	0.30	27.2	11.4	61.3	0.1	0.19
VA-20	0.73	0.24	0.59	0.61	0.79	0.54	0.52	0.28	0.35	18.3	10.1	71.2	0.4	0.14
VA-08	0.56	0.28	0.60	0.58	0.99	0.26	0.12	0.22	0.32	20.6	12.4	66.8	0.2	0.19
WHI-6A	5.63	0.93	0.52	0.56	0.69	0.59	0.56	3.20	1.89	28.6	24.4	47.0	0.0	0.52
WHI-38														
WHI-62														
WHI-92														

Abbreviations: H, hopane; St, sterane; dia, diasterane.

Table 4.2: Selected organic geochemical data for Late Ordovician and Cambrian-age rock extracts, continued.

Chapter 5

Lower Paleozoic biosphere and climate: Modes of marine primary production and methane cycling feedbacks

with Chris Reinhard, Woodward Fischer, Tim Lyons

5.1 Abstract

As a way of characterizing ancient marine microbial communities and their co-evolution with surface environmental conditions, much interest lies in obtaining robust lipid records for Palaeozoic rocks. Major environmental and climatic perturbations, such as cooling and ventilation during the Hirnantian glaciation in the Late Ordovician, have been shown to significantly influence marine microbial community structure in fundamental ways that are coherently recorded in ancient biomarker lipid patterns (Rohrssen

et al., 2013).

We have compiled detailed lipid biomarker stratigraphic records of marine microbial community structure through greenhouse intervals of the Paleozoic Era from thermally well preserved rocks of Late Ordovician and early Silurian age. Ocean redox chemistry, sea surface temperature variations, and upwelling supply of nutrients/fixed nitrogen species all strongly control the balance of bacterial versus eukaryotic primary production, reflected in measured hopane/sterane ratios and other more detailed biomarker proxies. Our biomarker records suggest that intervals of Palaeozoic time were associated not only with elevated atmospheric pCO_2 (approximately 5 - 16x preindustrial atmospheric levels, PAL) (e.g. Berner and Kothavala, 2001; Pancost et al., 2013), but also with a higher average marine methane flux than in Recent oceans, emanating from sediments and only partially oxidized in the water column. Because the destruction rate of atmospheric methane scales inversely with atmospheric methane abundance (e.g., Schmidt and Shindell, 2003), increased fluxes to the atmosphere will often translate into higher steady-state atmospheric concentrations.

Recent models suggest that "chemistry-climate feedbacks," particularly methane cycling, were more important in driving Mesozoic and younger greenhouse conditions than previously realized, such that a modest increase of 4 - 5x PAL of methane can provide 2-3^{o}C of warming (Beerling et al., 2011). Methane cycling feedbacks on climate must have been of similar or greater importance in the Palaeozoic, with greenhouse conditions promoting higher oxygen demands and greater fermentative recycling of sedimentary organic matter (Stanley, 2010; Finnegan et al., 2012), and an enhanced methane cycle in the marine realm (Luo et al., 2010; Rohrssen et al., 2013). Reduced oxidant availability has two mutually reinforcing effects first, a larger proportion of remineralized organic matter is passed through microbial methanogenesis; second, the

efficacy of combined anaerobic methane oxidation processes as a throttle for methane fluxes to the atmosphere is attenuated.

3β-methylhopane s (3-MeH) are lipid biomarkers known to be produced mainly by Type I microaerophilic methanotrophic proteobacteria, as well as acetic acid bacteria which are not ecologically prominent in oceans. The Phanerozoic marine average of C_{31} 3β-methylhopane for oils and source rocks relative to C_{30} $\alpha\beta$-hopane, as expressed by a 3-MeHI typically only in the range of 1 - 3 percent, is substantially exceeded in Late Ordovician and Silurian age rock extracts, often by an order of magnitude. Although other bacterial sources are possible for 3-methylhopanoids (Welander et al., 2012), we hypothesize that the high 3-MeH abundances observed in many Lower Palaeozoic rocks and oils were largely derived from microaerophilic methanotrophic bacteria and were at times interrelated with greenhouse climates through positive feedbacks between marine temperature and enhanced diagenetic recycling of methane from sedimentary organic matter.

5.2 Introduction

Much debate has arisen around the relationship between atmospheric pCO_2 and Late Ordovician glaciation (reviewed in Melchin et al., 2013). The controversy lies firstly in whether pCO_2 was really as high as 8-16x pre-industrial atmospheric levels (PAL, Berner and Kothavala, 2001), and secondly in whether decline in pCO_2 is necessary to instigate glaciation, as suggested by models (e.g. Herrmann et al., 2004). Finally, if pCO_2 decline did transpire, whether this was due to organic matter burial or silicate weathering. It is now well demonstrated that there were smaller glaciations prior to, and after, the Hirnantian Stage (e.g. Page et al., 2007), which might make a glacial

maximum in Hirnantian times somewhat less anomalous. The presence of a globally documented, approximately 4 permilpositive carbon isotope excursion (Hirnantian Isotopic Carbon Excursion, HICE) in both carbonate and organic matter coincident with the (glacioeustatic) regression has added both insight and confusion to the debate.

The HICE is one of a series of positive carbon isotope excursions in Middle Ordovician to Silurian carbonates and organic matter (see, e.g. Saltzman et al., 2005; Bergstrom, 2010), some though not all of which are associated with lithological evidence for high-latitude glaciation or incursions of cold-favoring taxa into tropical waters. These carbon isotope excursions, including the GICE (Guttenberg Isotopic Carbon Excursion) and Ireviken Event, have been attributed to regional or global perturbations to the carbon cycle through enhanced organic matter production and/or preservation (e.g. Brenchley et al., 1994; Finnegan et al. 2012; Jones and Fike, 2013), or on more local scales to migration of ^{13}C-enriched dissolved inorganic carbon in seawater, either as shifting water masses with different isotopic compositions or changes in sea level relocating vertical isotopic gradients (Holmden et al., 1998; Fanton and Holmden, 2007; Melchin and Holmden, 2006) among several other possibilities (summarized in Kaljo et al., 2004). Despite many attempts, coherent differentiation between competing - often non-exclusive - models for the glaciations and carbon isotope excursions remains elusive.

Although debate around glaciation in Late Ordovician times has centered on $p\mathrm{CO}_2$, lipid biomarker records indicate that a different greenhouse gas, methane, may also have played a role in Lower Palaeozoic climate. As shown previously (Rohrssen et al., 2013; this dissertation) elevated levels of 3-MeH, compounds typically associated with Type I microaerophilic methane oxidizing proteobacteria, have been detected in tropical Late Ordovician age rocks from oligotrophic (Anticosti, Cincinnati Arch) and nutrient-replete (Maquoketa Formation) regions of shallow epicontinental seas, con-

tinental shelves (Kukruse through Juuru Stages, Viki Borehole, Estonia, Figure 6.6), and deep waters (Vinini Formation). Elevated levels of 3-MeH persist into the Silurian (Lower and Upper Visby Formations, Gotland, Sweden, Figure 6.8). These elevated levels decline during the Hirnantian glacial maximum (Figure 2.7), suggesting that cooling climate and oxygenation diminished methanogenesis, and hence, methane supply to aerobic methanotrophs. Here we discuss the distribution of 3β-methylhopane in Lower Palaeozoic-age rock extracts and attempt to rationalize the elevated abundances of 3-MeH in Lower Paleozoic-age rocks through a marine organic matter remineralization regime that offers a positive feedback on climate through enhanced diagenetic methane cycling. This "chemistry-climate feedback" mechanism may not explain initiation of Lower Paleozoic ice house (e.g. Page et al., 2007) cooling, but would contribute to establishment of a dynamic feedback system which promoted perturbations to climate and carbon cycling through portions of Lower Palaeozoic time.

5.3 Materials and Methods

5.3.1 Sample Collection and Database

For this analysis we utilize a database of lipid biomarker ratios obtained from rock extracts of 90 Late Ordovician through early Silurian carbonates, marls, and shales from paleotropical North America, Sweden, and Estonia. From this suite of bitumens, samples for compound-specific carbon isotope analysis (CSIA) were selected on the basis of optimal compromise between yield of saturated hydrocarbons and elevated 3-MeHI (Table 5.2). Initial results have proven promising and an additional set of samples is presently in progress.

5.3.2 Sample Preparation and Analytical Methods

Outcrop and core samples of carbonates, marls, and carbonaceous shales were trimmed and the inner portions cut into pieces. The inner pieces were then ultrasonically washed with ultrapure water, methanol, dichloromethane, hexane, and dichloromethane again, prior to powdering in a ceramic or zirconia puck mill (SPEX 8510 Shatterbox). The puck mill was cleaned between samples by powdering two batches of fired sand (850°C, overnight) followed by rinses with the same sequence of solvents described above. Samples were powdered in two aliquots, with the first discarded and the second collected for extraction. Fired sand procedural blanks were crushed with each batch of samples and processed identically to sample powders to monitor background levels of biomarker analytes. In addition to the powder reserved for lipid biomarker analyses, a split was collected for inorganic geochemical analyses.

Lipid biomarkers were extracted from 10-40 g of rock powder in a Microwave Accelerated Reaction System (CEM corp.) with dichloromethane and methanol (9:1 v/v) at 100°C for 15 minutes. Elemental sulfur was removed from the total extract with HCl-activated, solvent washed copper pellets prior to silica gel column chromatography. Total extracts were fractionated with hexane, hexane:dichloromethane (1:1 v/v), and dichloromethane:methanol (3:1 v/v) to elute saturated hydrocarbons, aromatic hydrocarbons, and polar (N, S, and O-containing) compounds, respectively.

Gas chromatography-mass spectrometry (GC-MS) analyses of saturated (Figure 2.3) and aromatic hydrocarbons was conducted with an Agilent 7890A, equipped with a DB-1MS capillary column (60 m x 0.32 mm, 0.25 um film) and run with He as carrier gas. The temperature program for GC-MS full scan and selected ion monitoring was 60°C (2 min), ramp to 250°C at 20°C/min, to 325°C at 2°C/min, and hold at 325°C

for 20 min.

Multiple reaction monitoring (MRM) GC-MS of saturated hydrocarbons (Figures 1.2, 1.3) was carried out with a Waters AutoSpec Premier mass spectrometer equipped with an Agilent 7890A gas chromatograph and DB-1MS coated capillary column (60m x 0.25 mm, 0.25 um film) using He for carrier gas. MRM GC-MS measurements were conducted with a temperature program of 60°C for 2 min, heating to 150°C at 10°C/min followed by heating to 315°C at 3°C/min with a final hold at 315°C for 22 min. Biomarker compounds were identified based on retention time and published mass spectra and quantified in MRM GC-MS by comparison with a deuterated C29 sterane internal standard (d_4-$\alpha\alpha\alpha$-24-ethylcholestane (20R), Chiron Laboratories, AS), assuming equal response factors between sample compounds and the internal standard. Individual yields of hopane and sterane diastereoisomers found in laboratory procedural blanks were typically less than 0.1 ng of individual compounds and polycyclic alkane biomarker MRM GC-MS signal (hopanes, steranes, methylsteranes, methylhopanes, tricyclic terpanes, Table 2) from rock samples was typically at least 2-3 orders of magnitude higher in total than those detected in blanks (i.e. less than or equal to 0.03 ng C_{29} $\alpha\alpha\alpha$ R sterane/g extracted sand blank vs greater than or equal to10 ng C_{29} $\alpha\alpha\alpha$ R sterane/g TOC in samples) (Table 2.3).

Saturated hydrocarbons from samples selected for CSIA were subjected to silicalite separation of branched and cyclic alkanes from n-alkanes (Figure 5.1). Silicalite separations were conducted by transferring a saturate fraction in minimal pentane onto a pipette packed with approximately 10 mm of finely powdered, anhydrous silicalite on top of approximately 2 mm of pre-combusted 60 mesh silica gel. Branched and cyclic alkanes were obtained through elution of 1 mL of pentane and screened for yields *via*

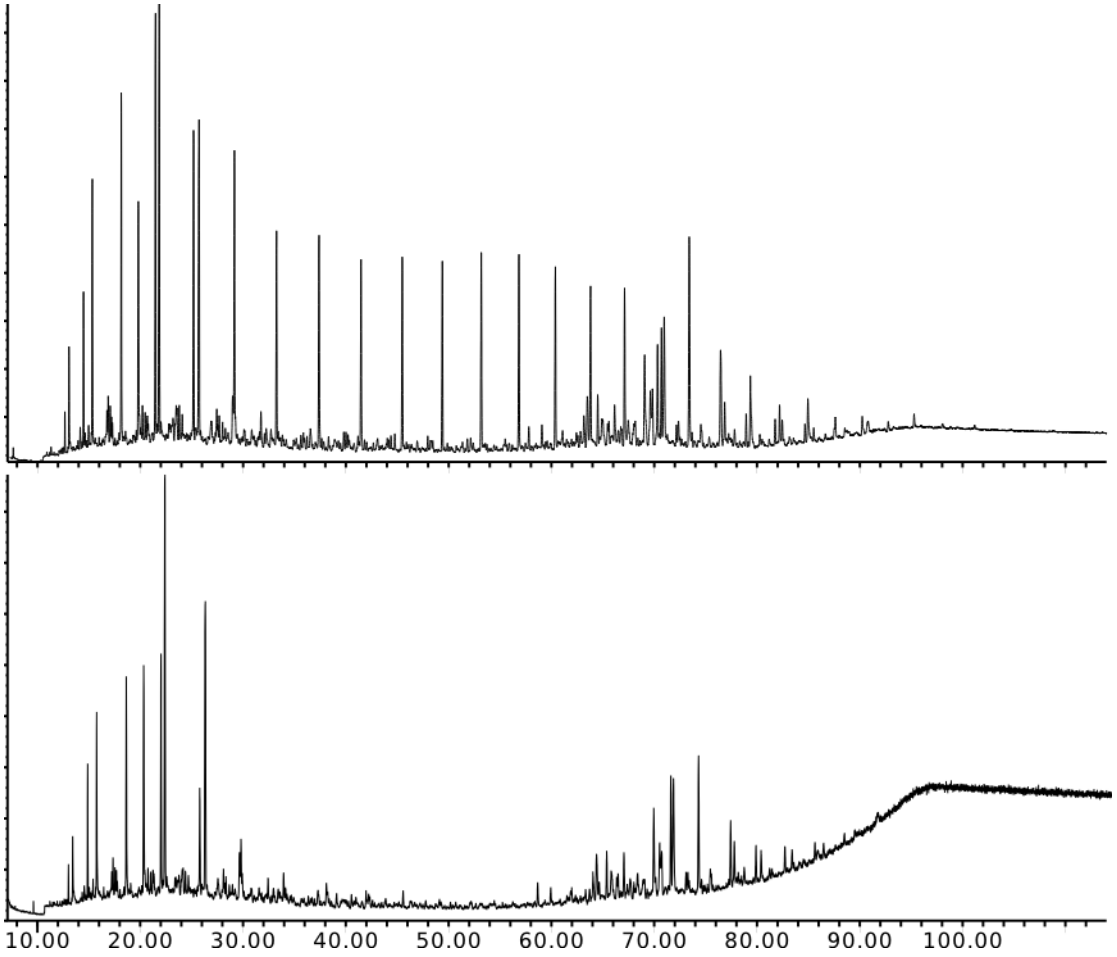

Figure 5.1: Total ion chromatograms of saturated hydrocarbon from the rock bitumen of sample VA-08 from the Vinini Formation shown before (above) and after (below) silicalite seiving of *n*-alkanes. Note that a proportion of the shorter chain *n*-alkanes (up to C_{19}) are found in the branched/cyclic alkane fraction (below). Baseline rise in the bottom trace is due to a dilute solution being injected.

GC-MS before shipment to GB Analytics for analysis (GB Analytics, Tahoe, CA, USA).

5.4 Results and Discussion

5.4.1 Temporal and Lithological Patterns in Lipid Biomarker Evidence for Enhanced Diagenetic Methane Cycling

Evidence for enhanced diagenetic methane cycling derives from elevated abundances of 3β-methylhopane s in rocks of Late Ordovician and Silurian age worldwide (Rohrssen et al., 2013; this dissertation). These compounds are usually attributed to Type I methanotrophic microaerophilic proteobacteria (Peters et al., 2003) due to the abundance of their precursor compounds in these organisms (Neunlist and Rohmer, 1985) and reports of ^{13}C-depletion in hopanes when 3β-methylhopane s are abundant (e.g. Farrimond et al., 2004; Ruble et al., 1994; Birgle et al., 2008), although other sources are possible (Welander et al., 2013). These compounds are traditionally presented as a percentage of the C_{30} $\alpha\beta$-desmethylhopane (3β-methylhopane index, 3-MeHI) in MRM GC-MS (Summons and Jahnke, 1990; Peters et al., 2003): as [(peak area of 3β-MeH in 426-¿205 transition) /(peak area of C_{30} $\alpha\beta$-desmethylhopane in 412-191 + peak area of 3-MeH in 426-205)]*100. In addition, samples are screened for, and ratios calculated using, the full homologous series of A-ring methylated extended hopanes (C_{32}-C_{36} methylhopanes), which should display the same stereochemistry (usually 17α,21β(H)- with both 22 and 22R epimers present) as the extended desmethylhopanes (C_{31}-C_{35} hopanes, e.g. Figure 3.8).

Ordovician and Silurian rock extracts examined to date display high 3-MeHI (average 9.0 +/- 4.9, n = 90, Table 6.3, Chapters 2, 3, 6), typically far in excess of the Phanerozoic marine average range of 1-3 percent of C_{30} $\alpha\beta$-hopane (Cao et al., 2009).

3-MeHI does not tend to correlate with other biomarker proxies (Figures 2.5, 2.6, 3.8, 6.6, 6.8). However, where evidence from the same samples for contemporaneous temperature change and 3-MeHI is available (Rohrssen et al., 2013, figure 2.4, 2.6), they display positive correlation: higher temperatures are associated with higher 3-MeHI. Under a temperature-dependant scenario, the lower 3-MeHI observed in the Vinini Formation and their earlier decline (with the first peak in the $\delta^{13}C_{carb}$ excursion) may reflect oceanographic differences between the western margin and eastern, semi-restricted shelf of Laurentia, however the timeframe is long, perhaps more than half a million years. 3-MeHI are high in oligotrophic, carbonate-dominated locations (Anticosti, Cincinnati Arch, Gotland) but also in mixed carbonates, marls, and phosphatic siliciclastic rocks of the North American midcontinent (Maquoketa Formation). Lower 3-MeHI in Ordovician rocks are only observed i). during cooling intervals (Hirnantian and Wenlock Stages), and in ii). in some organic-rich, phosphatic facies (Vinini Formation, lower Elgin Member of the Maquoketa Formation). Further examination of the relationship between lithofacies and 3-MeHI is ongoing.

It is important to note that, although attempts have been made to locate them in GC-MS, isoprenoidal lipids derived from archaea (methanogens and/or methanotrophs, biphytane and 2,6,10,14,18-pentamethylicosane, Table 1.1) have yet to be conclusively identified. Crocetane has been detected in samples as old as the 1.64 Ga Barney Creek Formation (Greenwood and Summons, 2003) and is present along with a series of low molecular weight isoprenoids in a number of Ordovician-age crude oils from Australia, although none are particularly depleted in ^{13}C (Barber et al., 2001). The relative abundance of phytane in the samples investigated here, which may include a contribution from degradation of archaeal lipids and coelutes with crocetane on DB-1MS columns, does not apparently scale with 3β-methylhopane abundance. Given that

redox and maturity may impact phytane abundance this is not necessarily surprising. Quantitative measurements and analysis of these samples on a stationary phase capable of separating crocetane and phytane remain to be done to test this more robustly. It is possible, particularly in the least mature samples, that archaeal lipids are present in the polar fraction of total lipid extracts not investigated here.

5.4.2 Preliminary Compound-Specific Carbon Isotope Analyses to Assess Contributions from Aerobic Methanotrophic Bacteria

Despite these relationships and the typical attribution of 3-MeH to methanotrophic bacteria, the most robust support for this assignment would come from compound specific carbon isotope analyses of hopanes. Even at 20 percent of C_{30} $\alpha\beta$-hopane, low methylhopane absolute abundance prevents measurement through typical GC-C-IRMS. Fortunately, methanotrophic bacteria also contribute to desmethylhopanes, which are analysable. Although extremely ^{13}C-depleted values have been reported for hopanes in Cretaceous methane seeps (e.g. Birgle et al., 2008) and inferred to represent periods of enhanced methane cycling in Lake Uinta (Ruble et al., 1994), we do not expect to see such exceptionally depleted compositions. For example, taking an average carbon isotope composition for hopanes of -30 permil, and methanotroph-derived hopanes of -80 permil, a 10 percent contribution from methanotrophs would result in a hopane carbon isotope composition of -35 permil (Table 5.1). At lower 3-MeHI, the hopane ^{13}C depletions become even more muted (Table 5.1). Further, only minor ^{13}C-depletions are anticipated because we envision diffuse, slow, diagenetic methane cycling on a broad scale rather than the rapid, localized methane flux typical of seeps. An additional complication is that at very high rates of aerobic methane oxidation, incorporation of ^{13}C-depleted CO2 by photoautotrophs could damp the difference in carbon

isotope composition between hopanes and bulk organic matter or algal-derived lipids while potentially driving bulk δ^{13}C lighter (Ruble et al., 1994), changing the difference in δ^{13}C between bactivorous infauna and phytoplankton/zooplankton, or even impacting higher trophic levels (reviewed in Jones and Grey, 2011).

Compound specific carbon isotope analyses were attempted to address contributions from methanotrophic bacteria as well as possible differences in the carbon isotope composition of steranes which might then be correlated back to $p\mathrm{CO}_2$ (Table 5.2). Hopane carbon isotope compositions were not inconsistent with a contribution from aerobic methanotrophic bacteria, 0.7 to 4.7 permil lighter than short chain n-alkanes, pristane, and phytane, however substantial scatter in the data - including one sample in which hopanes are heavier than the short-chain compounds likely due to low signal strength and coelution or integration issues - make this inconclusive at present (Table 5.2). The expected positive relationship between 3-MeHI and either carbon isotope composition of hopanes or difference in carbon isotope composition between hopanes and compounds derived from phototrophic organisms (pristane and phytane) or many sources (short chain *n*-alkanes) is also largely masked by the scatter. It is important to consider the carbon isotope composition of hopanes relative to other lipids and bulk organic matter as well as the absolute δ^{13}C value because the of the well-recognized Hirnantian and Wenlock-Llandovery carbon isotope excursions and possibly changing $p\mathrm{CO}_2$ during the Hirnantian glacial maximum, as proposed to accompany the Guttenberg isotope excursion (Pancost et al., 2013). Unfortunately, coelution and low abundance of steranes prevented measurement of sterane carbon isotope composition in most of the samples. Additional analysis is being undertaken to clarify this issue.

5.4.3 Implications for Lower Palaeozoic Climate

In present-day marine sediments, much of export production is remineralized via respiration, nitrogen cycling, and sulfate reduction in broad redox zones, with some proportion of that organic matter ultimately being remineralized through methanogenesis (Figure 5.2B, D). Of the methane which is produced, the vast majority is consumed through anaerobic oxidation of methane (AOM) by consortia of sulfate reducing bacteria an anaerobic methane oxidizing ANME archaea, leaving only a smaller amount to be oxidized aerobically or to enter the atmosphere (Figure 5.2B, D). Lower marine dissolved sulfate concentrations in the early Paleozoic (approximately 6-12 mM as opposed to 28 mM today, Gill et al., 2007), in which nitrate and other inorganic oxidants are also likely low for energetic reasons, coupled with estuarine circulation in some regions of shallow Late Ordovician seas likely meant dissolved inorganic oxidant availability for long-term organic matter diagenesis was low. Given the very high microbial metabolic rates, and high sensitivity of these rates to temperature change, estimated for the Late Ordovician (Finnegan et al., 2012; Stanley, 2010) microbial methane cycling warrants further investigation as a positive feedback on Lower Paleozoic climate. We explore the possible implications of this for Paleozoic biogeochemical cycles and climate with a series of simple mass balance calculations given a range of carbon flux and anaerobic remineralization scenarios.

When inorganic oxidant availability is low for anaerobic respiration, as in some lacustrine environments in the modern, methanogenesis linked to other degradation pathways may account for a more significant proportion of organic matter diagenesis in the shallow subsurface (Figure 5.2A, C) or even in the deep ocean. Under this scenario, not only does methanogenesis account for a greater proportion of organic matter

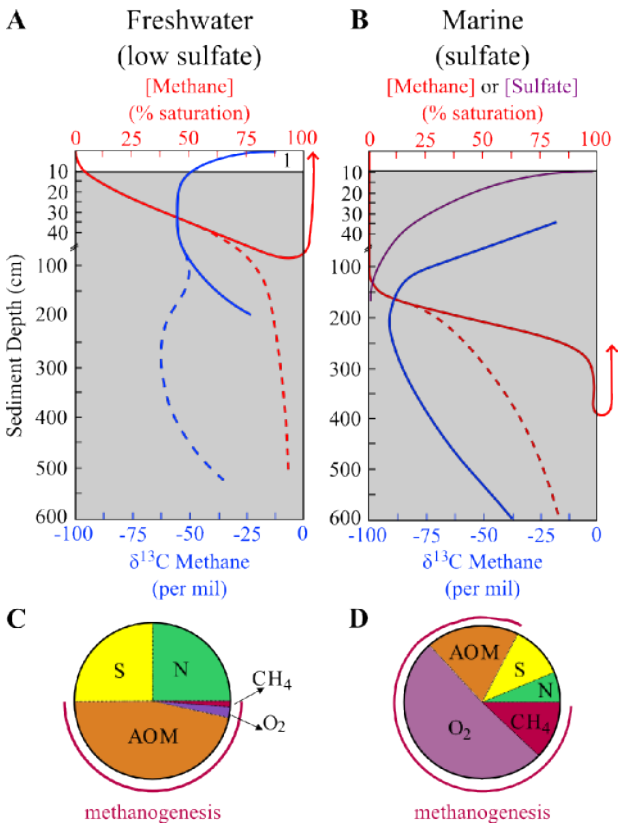

Figure 5.2: Hypothetical porewater geochemical profiles for sulfate-replete (A) and low sulfate (B) environments modified from Whiticar, 1999. Schematic pie charts reflect the proportion of organic matter remineralized through different inorganic oxidant pathways under high sulfate (C) and low sulfate (D) conditions. When oxidants are abundant, sulfate is present deep into sediments (A), less organic matter is remineralized through methanogenesis, and more methane is oxidized through AOM (C). When sulfate is low, geochemical gradients are compressed (B), more methane may be produced, and less oxidized through AOM (D).

remineralization, but less of the produced methane flux would be oxidized via sulfate, nitrate, or metal reduction (Figure 5.2C). More methane, therefore, may have been available to aerobic methanotrophs in the ocean around the chemocline and more may have reached the atmosphere (Figure 5.2C) since methane solubility is low in aqueous media and Type I methanotrophic proteobacteria have only a limited time window to capture this substrate. As a result, diagenetic methane cycling may have been an important process in Late Ordovician epeiric seaways, both in terms of the proportion of labile organic matter reaching the methanogenic zone and in the proportion of methane escaping AOM to be oxidized aerobically. Pyrite-lined burrows in Anticosti rocks, for example, indicate the presence of a chemocline at shallow sediment depths below, or possibly above, the sediment-water interface, consistent with compression of geochemical gradients and onset of methanogenesis at shallow depths in the sediments.

5.5 Conclusions

Enhanced abundances of 3β-methylhopanes relative to desmethylhopanes relative to the Phanerozoic have been identified in rocks from tropical Late Ordovician and Early Silurian rocks world-wide. The relative abundance of these compounds decreases during glacial intervals. Compound specific carbon isotope analyses of hopanes yield values of -35 to -48 permil, which indicates a ^{13}C-depleted source contribution amongst bacterial inputs to the hopane pool most likely from methanotrophic bacteria. In light of this organic geochemical evidence for enhanced marine aerobic methane oxidation most likely in the water column, we propose that the elevated methanotrophy during warm intervals reflects enhanced diffuse, slow, diagenetic methane production in underlying sediment during warm intervals of the Lower Palaeozoic. Another important

implication of this is the likelihood of an enhanced flux of methane to the atmosphere from the oceans during this interval. We suggest that relatively low levels of inorganic oxidants (sulfate, nitrate) promoted both methanogenesis and diminished the efficacy of anaerobic methane oxidation. Cooling climate during glacial intervals would slow methanogenesis and increase the oxidant inventory available for aerobic remineralization of organic matter. Geochemical box models indicate that elevated methane fluxes from the water column increase Lower Palaeozoic pCH_4 and cause warming. Further models suggest that low pO_2 in the Lower Palaeozoic atmosphere would favor anaerobic conditions in the water column, a first step in assessing the possibility of an enhanced methane cycle in the Lower Palaeozoic. Since sulfate availability in sediment porewaters and the deep ocean imposes such a strong control on both methanogenesis and anaerobic methane oxidation (AOM) in modern oceans, further microbiology work is needed to assess whether a diminished marine sulfate concentration of seawater of even 5 mM sulfate in the Late Ordovician ocean would significantly influence the efficiency of methane flux captures by AOM processes.

5.6 Acknowledgments

The authors would like to acknowledge Geoff Bott of GB Analytics for CSIA analysis, as well as funding to GDL from NASA Astrobiology Institute and Shell, and a University of California, Riverside dissertation year fellowship to MR.

5.7 References

1. Barber, C.J., Grice, K., Bastow, T.P., Alexander, R., Kagi, R.I., 2001, The identification of crocetane in Australian crude oils: Organic Geochemistry, v. 32, p. 943-947.

2. Beerling, D.J., Fox, A., Stevenson, D.S., Valdes, P.J., 2011. Enhanced chemistry-

climate feedbacks in past greenhouse worlds: Proceedings of the National Academy of Sciences, v. 108, p. 9770-75.

3. Bergstrom, S.M., Young, S., Schmitz, B., 2010, Katian (Upper Ordovician) $\delta^{13}C$ chemostratigraphy and sequence stratigraphy in the United States and Baltoscandia: A regional comparison: Palaeogeography, Palaeoclimatology, Palaeoecology, v. 296, p. 217-234.

4. Berner, R.A., and Kothavala, Z., 2001, GEOCARB III: A revised model of atmospheric CO_2 over Phanerozoic time: American Journal of Science, v.301, p.182204, doi:10.2475/ajs.301.2.182.

5. Birgel, D., Himmler, T., Freiwald, A., Peckmann, J., 2008, A new constraint on the antiquity of anaerobic oxidation of methane: Late Pennsylvanian seep limestones from southern Namibia: Geology, v. 36, p. 543-546.

6. Brenchley, P.J., Marshall, J.D., Carden, G.A.F., Robertson, D.B.R., Long, D.G.F., Meidla, T., Hints, L., and Anderson, T.F., 1994, Bathymetric and isotopic evidence for a short-lived Late Ordovician glaciation in a greenhouse period: Geology, v.22, p.295298.

7. Fanton, K.C., Holmden, C., 2007, Sea-level forcing of carbon isotope excursions in epeiric seas: implications for chemostratigraphy: Canadian Journal of Earth Sciences, v. 44, p. 807-818.

8. Farrimond, P, Talbot, H.M., Watson, D.F., Schulz, L.K., Wilhelms, A., 2004, Methylhopanoids: Molecular indicators of ancient bacteria and a petroleum correlation tool: Geochimica et Cosmochimica Acta, v. 68, p. 3873-3882.

9. Finnegan, S., Fike, D.A., Jones, D.S., Fischer, W.W., 2012, A temperature-dependant positive feedbacl on the magnitude of carbon isotope excursions: Geosciences Canada, v. 139. p. 122-131.

10. Gill, B.C., Lyons, T.W., Saltzman, M.R., 2007, Parallel, high-resolution carbon and sulfur isotope records of the evolving Paleozoic marine sulfur reservoir: Palaeogeography, Palaeoclimatology, Palaeoecology, v. 256, p. 156-173.

11. Gill, B.C., Lyons, T.W., Saltzman, M.R., 2005, Parallel, high-resolution carbon and sulfur isotope records of the Late Ordovician and Late Carboniferous records of two different glacial episodes: American Geophysics Union Annual Meeting, San Francisco.

12. Greenwood, P.F., Summons, R.E., 2003, GC-MS detection and significance of crocetane and pentamethylicosane in sediments and crude oils: Organic Geochemistry, v. 42, p. 1211-1222.

13. Guthrie, J.M., and Pratt, L.M., 1995, Geochemical character and origin of oils in Ordovician reservoir rock, Illinois and Indiana, USA: American Association of Petroleum Geologists Bulletin, v. 79, p. 1631-1649.

14. Hammarlund, E.U., Dahl, T.W., Harper, D.A.T., Bond, D.O.G., Nielsen, A.T., Bjerrum, C.J., Schovsbo, N.H., Schnlaub, H.O., Zalasiewicz, J., Canfield, D.E., 2012, A sulfidic driver for the end-Ordovician mass extinction: Earth and Planetary Science Letters, v. 331-332, p. 128-129.

15. Herrmann, A.D., Patzkowsky, M.E., Pollard, D., 2004, The impact of paleogeography, pCO_2, poleward ocean heat transport and sea level change on global cooling during the Late Ordovician: Palaeogeography, Palaeoclimatology, Palaeoecology, v. 206, p. 59-74.

16. Holmden, C., Creaser, R.A., Muehlenbachs, K., Leslie, S.A., Bergstrom, S.M., 1998, Isotopic evidence for geochemical decoupling between ancient epeiric seas and bordering oceans: implications for secular curves: Geology, v. 26, p. 567-570.

17. Jones, D.S., Fike, D.A., 2013, Dynamic sulfur and carbon cycling through the end-Ordovicianextinction revealed through paired sulfate-pyrite $\delta^{34}S$: Earth and Planetary Science Letters, v. 363, p. 144-155.

18. Jones, R.I., and Grey, J., 2011, Biogenic methane in freshwater food webs: Freshwater Biology, v. 56, p. 213-229.

19. Kaljo, D., Hints, L., Martma, T., Nlvak, J., Oraspld, A., 2004, Late Ordovician carbon isotope trend in Estonia, its significance in stratigraphy and environemental analysis: Palaeogeography, Palaeoclimatology, Palaeoecology, v. 2010, p. 165-185.

20. LaPorte, D.F., Holmden, C., Patterson, W.P., Loxton, J.D., Melchin, M.J., Mitchell, C.E., Finney, S.C., and Sheets, H.D., 2009, Local and global perspectives on carbon and nitrogen cycling during the Hirnantian glaciation: Palaeogeography, Palaeoclimatology, Palaeoecology, v.276, p.182195, doi:10.1016/j.palaeo.2009.03.009.

21. Luo, G., Kump, L.R., Wang, Y., Tong, J., Arthur, M.A., Yang, H., Huang, J., Yin, H., and Xie, S., 2010. Isotopic evidence for an anomalously low oceanic sulfate concentration following end-Permian mass extinction: Earth and Planetary Science Letters, v. 300, p.10111.

22. Melchin, M.J., Holmden, C., 2006, Carbon isotope chemostratigraphy in Arctic Canada: Sea-level forcing of carbonae platform weatherin and implications for Hirnantian global correlation: Palaeoceanography, Palaeoclimatology, Palaeoecology, v. 234, p. 186-200.

23. Melchin, M.,J., Mitchell, C.E., Holmden, C., Storch, P., 2013. Environmental changes in the Late Ordovician-Early Silurian: Review and new insights from black shales and nitrogen isotopes. Geological Society of America Bulletin, v. 125, p. 1635-1670.

24. Neunlist, S., and Rohmer, M., 1985, Novel hopanoids from the methylotrophic bacteria *Methylococcus capsulatus* and *Methylomonas methanica*: Biochemical Journal, v. 231, p. 635-639.

25. Page, A.A., Zalasiewicz, J.A., Williams, M., Popov, L.E., 2007, in Williams, M., Haywood, A.M., Gregory, F.J., and Schmidt, D.N. (eds.), Were transgressive black shales a negative feedback modulating glacioeustasy in the Early Palaeozoic Icehouse?: Deep Time Perspectives on Climate Change: Marrying the Signal from Computer Models and Biological Proxies. The Micropalaeontological Socity, Special Publications. The Geological Society, London, p. 123-156.

26. Pancost , R.D., Pagani, M., 2006, Controls on the carbon isotope compositions of lipids in marine environments: Handbook of Environmental Chemistry, vol. 2, Springer-Verlag, Heidelberg, p. 209-249.

27. Pancost, R.D., Freeman, K.H., Herrmann, A.D., Patzkowsky, M.E., Ainsaar, L., Martma, T., 2013, Reconstructing Late Ordovician carbon cycle variations: Geochemica et Cosmochimica Acta, v. 105, p. 433-454.

28. Pancost, R.D., Freeman, K.H., Patzkowsky M.E., 1999, Organic-matter source variation and the expression of a late Middle Ordovician carbon isotope excursion: Geology, v. 27, p. 1015-1018.

29. Peters, K.E., Walters, C.C., and Moldowan, J.M., 2003, The Biomarker Guide, 2nd edition: Cambridge, UK, Cambridge University Press, 1132 p.

30. Rohrssen, M., Love, G.D., Fisher, W., Finnegan, S., Fike, D.A., 2013. Lipid biomarkers record fundamental changes in the microbial community structure of tropical seas during the Late Ordovician Hirnantian glaciation: Geology, v. 47, p. 127-30.

31. Ruble, T.E., Bakel, A.J., and Philp, R.P., 1994, Compound specific isotopic variability in Uinta Basin native bitumens: Paleoenvironmental implications: Organic Geochemistry, v.21, p.661671.

32. Schmidt, G.A., Shindell, D.T., 2003. Atmospheric composition, radiative forcing, and climate change as a consequence of a massive methane release from gas hydrates: Paleoceanography, v. 18.

33. Stanley, S.M., 2010, Relation of Phanerozoic stable isotope excursions to climate, bacterial metabolism, and major extinctions: Proceedings of the National Academy of Sciences, v. 107, p. 19185-19189.

34. Summons, R.E., and Jahnke, L.L., 1990, Identification of the methylhopanes in sediments and petroleum: Geochimica et Cosmochimica Acta, v.54, p.247251.

35. Welander, P.V., Summons, R.E., 2012. Discovery, taxonomic distribution, and phenotypic characterization of a gene required for 3-methylhopanoid production: Proceedings of the National Academy of Sciences, v. 109, p. 12905-10.

36. Yan, D., Chen, D., Wang, Q., Wang, J., Wang, Z., 2009, Carbon and sulfur isotopic anomalies across the Ordovician-Silurian boundary, Yangtze Platform, South China: Palaeogeography, Palaeoclimatology, Palaeoecology, v. 274, p. 32-39.

	$\delta^{13}C_{org}$ (permil)		
3-MeHI (%)	**-25 permil**	**-30 permil**	**-35 permil**
20	-11.0	-10.0	-9.0
10	-5.5	-5.0	-4.5
5	-2.8	-2.5	-2.3

Table 5.1: Predicted hopane carbon isotope depletions for a range of mixing scenarios between methanotroph-derived hopanes (assumed to be -80 permil) and non-methanotroph derived hopanes. For example, at a 3-MeHI of 10 percent and average carbon isotope composition of -30 per mil, including the methanotroph-derived hopanes would result in a 7.0 permil ^{13}C depletion. At 3-MeHI less than 5 - 10 percent, it becomes difficult to identify a contribution from methanotrophic bacteria.

Source	Sample	3-MeHI	H/St	n-C_{17}	Pr	n-C_{18}	Ph	avg[1]	stdev
Vinini Creek, Vinini Formation	VA-08	5.7	0.6	-33.7	-34.5	-33.7	-34.6	-34.1	0.5
Iowa, Maquoketa Formation	H33-444	6.3	0.3	-32.2	-33.8	-33.2	-34.3	-33.4	0.9
Anticosti, Merrimack Formation	916-29.1	6.7	5.9						
Anticosti, Vaureal Formation	902-7.5	6.8	4.8	-42.9		-33.6		-38.3	6.6
Anticosti, Ellis Bay Formation	901-5.0	7.8	3.8	-33.2	-34.4	-32.4		-33.3	1.0
Anticosti, Ellis Bay Formation	901-3.5	8.9	5.5	-31.6	-32.4	-32.3	-31.5	-31.9	0.5
Viki Borehole, Nabala Stage	OM9-5b	10.6	5.7	-33.3	-34.1	-33.5	-33.4	-33.6	0.4

Source	$C_{29}\alpha\beta$	$C_{30}\alpha\beta$	$C_{31}\alpha\beta S$	$C_{31}\alpha\beta R$	$C_{32}\alpha\beta S$	$C_{32}\alpha\beta R$	$C_{33}\alpha\beta S$	$C_{33}\alpha\beta R$	avg[2]	stdev	avg[1] – avg[2]
Vinini Creek, Vinini Formation	-32.4	-34.5	-39.1	-35.6	-35.6	-35.7	-34.9	-34.8	-35.3	1.9	1.2
Iowa, Maquoketa Formation		-33.0	-34.1	-37.4		-47.7			-38.1	6.7	4.7
Anticosti, Merrimack Formation	-30.7	-34.8	-35.5	-34.3	-36.1	-35.6	-35.6	-33.5	-34.5	1.8	
Anticosti, Vaureal Formation	-28.6	-32.2	-32.6	-32.5	-33.0	-32.2	-34.0	-31.4	-32.1	1.6	-6.2
Anticosti, Ellis Bay Formation	-34.4	-32.8	-32.7	-32.4	-32.2	-36.9	-33.4	-31.1	-33.2	1.8	-0.1
Anticosti, Ellis Bay Formation	-29.8	-32.0	-32.9	-32.4	-32.0	-33.8	-34.4	-33.7	-32.6	1.5	0.7
Viki Borehole, Nabala Stage		-34.7		-34.8		-34.7			-34.7	0.0	1.2

[1]Average of non-hopanes: n-C_{17}, Pristane, n-C_{18}, Phytane, steranes. [2]Average of hopanes

Table 5.2: Carbon isotope compositions of selected compounds.

Chapter 6

Today Baltica, tomorrow the world: synthesis and conclusions

In collaboration with Woodward Fischer, Renata Cummins, Thijs Vandenbroucke, and Olle Hints

6.1 Abstract

The Late Ordovician through Silurian was long considered a climatically warm, ecologically stable period, interrupted only by the Hirnantian glacial maximum and mass extinction. Recent carbon isotope chemostratigraphies and improved biostratigraphic correlations have demonstrated that this period was, instead, one of substantial volatility. Here we assess global similarities and variability in reconstructed Late Ordovician microbial community structure and response to Late Ordovician environmental change as recorded by lipid biomarkers. Rock bitumens extracted from samples of the Viki drill core (OM9, Saaremaa Island, Estonia) of Middle Ordovician to Early Silurian age exhibit exceptionally immature biomarker distributions, including a large proportion of poly-

cyclic biomarker compounds that retain their biological configurations, consistent with the known thermal maturities assessed from conodont alteration indices. Results from the Viki drill core indicate that microbial community structures reconstructed for Laurentia extended throughout the paleotropics, particularly elevated levels of compounds derived from aerobic methanotrophic bacteria, and that microbial community structure in Baltican seas exhibited a similar response to Late Ordovician climate change.

We also present data from the Silurian age Ireviken Event (Llandovery-Wenlock Stages approx. 427 Ma) exposed in outcrop on the island of Gotland (Sweden), a period recognized for its carbon isotope excursion and extinction interval. Results from the Ireviken Event analyses demonstrate continuation - or recurrence - of typical Ordovician marine microbial community structure as baseline ecology in Early Silurian times. Further, we identify parallels between the Hirnantian glacial maximum and Ireviken Event - particularly an increase in algal contributions to sedimentary organic matter and decrease in methane cycling related compounds.

This new data is used in conjunction with biomarker data from North America (Chapters 2 and 3) to refine a suite of biomarker features characteristic of Late Ordovician and early Silurian age source rocks.

6.2 Introduction

Since recognition of the Late Ordovician mass extinction, with its contemporaneous evidence for glaciation and carbon isotope excursions, the Late Ordovician has seen extensive study (reviewed in Sheehan, 2001; Melchin et al., 2013). Questions of particular interest have included characterizing the extinction, deconvoluting the implications of the common cause hypothesis, and constraining the cause(s), duration, and

consequences of Late Ordovician environmental change. Although microbial communities form the basis for marine nutrient cycles and food webs that would be impacted by, and in turn have impacts on, Late Ordovician extinction and environmental change, they are seldom studied in the Paleozoic due to low fossilization potential. Fortunately, analysis of lipid biomarkers, the recalcitrant constituents of cell membranes and pigments, provide a tool for studying these otherwise invisible portions of ancient ecosystems and the geochemical environment in which they lived. Lipid biomarker analyses have proven capacity to identify MCS in ancient environments (e.g. Pancost et al., 1998) and the response of MCS to environmental changes surrounding mass extinctions (e.g. Cao et al., 2009) or other environmental perturbations such as the Cretaceous ocean anoxic events (e.g. Kuypers et al., 2004). However, few stratigraphic studies of Late Ordovician biomarkers exist (Pancost et al., 1998; 1999; Armstrong et al., 2009). Following the identification of coherent patterns in microbial community structure within epicontinental seas, the next task was to establish whether these patterns extended to other paleocontinents and to periods of Lower Palaeozoic environmental change.

To assess the global extent of the microbial community structures reconstructed for Laurentia (Rohrssen et al., 2013) we investigated thermally well-preserved Late Ordovician rocks present in the subsurface of Estonia on a paleodepth gradient from shallow water facies in the north to deeper, epeiric basin in the south (Kaljo et al., 2004). These deposits record several carbon isotope excursions correlated through graptolite and chitinozoan biostratigraphy to sections in North America (e.g. Brenchley et al., 2003; Young et al., 2010; Bergstrom et al., 2010). Extensive literature on the Late Ordovician in Estonia provides excellent paleobiological and geochemical context for this study. Lipid biomarker analyses from a drill core through shallow water facies to the north in Estonia will likely prove an excellent comparison to samples from Anticosti

Island, Canada, the Cinncinnati region USA and northeastern Iowa, USA. Analysis of a core through shallow water facies from northwestern Estonia may be comparable to samples from Anticosti Island, Canada, or the US midcontinent.

In order to constrain the temporal extent of the reconstructed microbial community structures and explore possiblity that subsequent glaciations had similar effects on microbial community structure, we extend the examined sections to a younger interval of climatic change and extinction, the Llandovery-Wenlock Ireviken Event as preserved on the island of Gotland, Sweden (e.g, Jeppsson, 1997; Calner, 2008).

6.3 Materials and Methods

6.3.1 Geological Context and Sample Collection

The Baltic Ordovician-Silurian sample set comprises Late Ordovician material from the Viki drill core in Estonia and from a pyritic black shale sample exposed in outcrop in Sweden, and Early Silurian samples from outcrops on Gotland.

The Viki drill core (OM9) penetrates 363 m of Late Ordovician through Early Silurian strata, of which the Kukruse through Juuru Baltic Stages were sampled in this study. Considerable information regarding the Viki drill core is available through the Estonian geological survey and Tallinn University of Technology (Viki drill core database). These rocks were deposited on the Estonian carbonate platform shelf, in Late Ordovician-early Silurian times bounded to the northeast by the Fennoscandian Shield, to the southwest by the Livonian and Scandinavian Basins, and separated from Laurentia by the closing Iapetus Ocean and on-going Taconic Orogeny (Figure 6.1). In Late Ordovician times the Estonian shelf lay in the subtropics to tropics (Cocks and Torsvik, 2002). Extensive literature documents the lithostratigraphy and facies rela-

tionships, isotope chemostratigraphy, and biostratigraphy of Ordovician-Silurian rocks in the Estonian subsurface, including the Viki drill core (e.g. Hints et al., 2013; Harris et al., 2004; Poldvere, 2010), although precise correlation among Baltic and Laurentian sections remains somewhat hampered by the well-recognized challenges of endemism and the strong facies affinities of conodonts and graptolites. Overlying Silurian samples have low thermal maturities, with conodont alteration indices (CAI) of 1 (Lehnert et al., 2010).

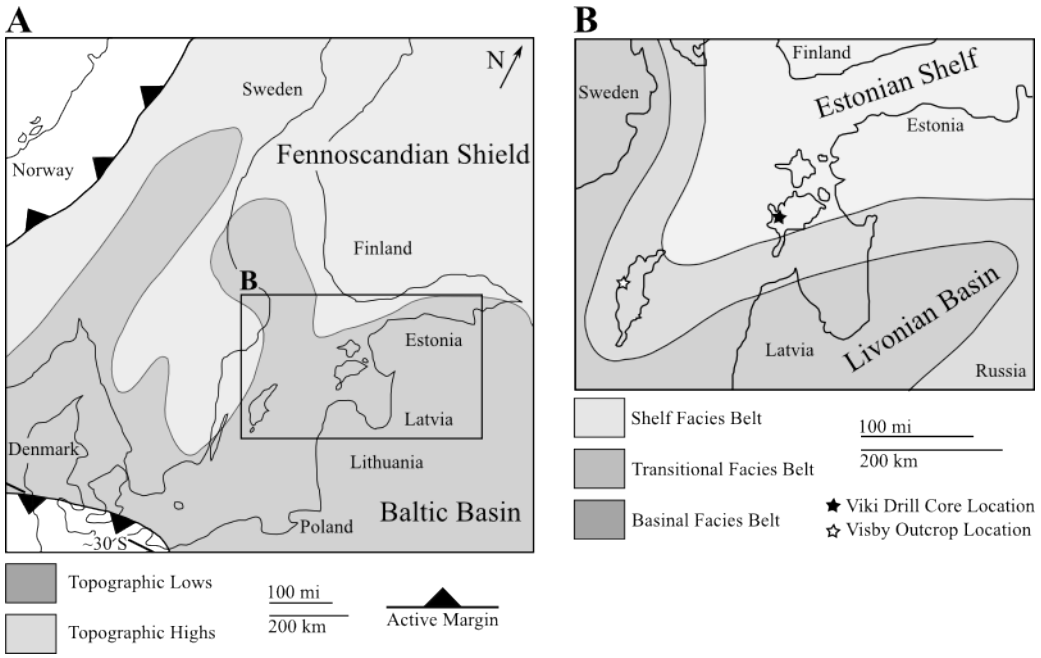

Figure 6.1: A Baltica in Wenlock-Llandovery times (modified from Calner, 2008 and Cocks and Torsvik, 2002), and B. location map indicating location of Viki Drill Core relative to Katian age lithofacies belts (modified from Harris et al., 2004), as well as outcrop sampling location for the Upper and Lower Visby Formations along the northwest coast (after Munnecke, 2003).

Rocks from the Late Ordovician Estonian shelf analysed in this study include carbonates, argillaceous carbonates, and marls, deposited below fair weather wave base in progradational wedges on the outer margin of the shelf (e.g. Harris et al., 2004; Poldvere, 2010). The Nabala Stage sample was comprised predominantly of tan micrite

with the notable exception of concentrated intervals of fine, brown laminations (Figure 6.2). To assess the origin of these organic carbon-rich laminae (i.e. whether their higher organic carbon content was simply a function of concentration of material from the same source as the dispersed organic matter, or had a different origin), two subsamples were taken from this approximately 10 cm interval. The portion of this sample with a greater concentration of fine brown laminations is denoted by gray symbols at 316 m in Figures 6.4 and 6.5,while the tan "background" portion data points are black.

Samples spanning the Llandovery-Wenlock Stage boundary in the paleotropical Baltic basin were collected from the Upper and Lower Visby Formations near the northwest coast of Gotland, Sweden (Figure 6.1A, B). The Lower Visby Formation consists of alternating limestones and marls which record below storm wave base, distal shelf deposition shallowing into the bioherm-bearing, limestone-dominated higher energy deposits of the Upper Visby (Calner et al., 2004). Distinction between the Upper and Lower Visby Formations is made on the basis of an interval with high abundances of the solitary rugose coral *Phaulactis angusta* (Lonsdale), det. Keith Mitchell 1990 (Calner et al., 2004), which also corresponds approximately to the initiation of the "Ireviken Event" positive carbon isotope excursion. This bed is taken as the 0 m datum for consistency with other studies; sample nomenclature and meterage are identical to Cummins et al., (submitted). Lower and Upper Visby Formation rocks also have very low thermal maturities, identified both on the basis of CAI 1 (Jeppsson, 1983) and clumped isotope paleothermometry measurements which identify a maximum of approximately 60°C during burial (Cummins et al. submitted). Following a similar motivation to the texture-specific sampling described for the Viki drill core sample, portions of the 0 m sample were prepared separately. One portion of the sample was laminated (G1-0.0lam) while the other contained abundant shell material (G1-0.0sb); these are presented as

replicates at 0.0 m with the filled point (black or gray) indicating the laminated sample and the open (white) symbol denoting the shell-bearing portion.

6.3.2 Sample Preparation and Analytical Methods

Outcrop and core samples of carbonates, marls, and carbonaceous shales were trimmed and the inner portions cut into pieces. The inner pieces were then ultrasonically washed with ultrapure water, methanol, dichloromethane, hexane, and dichloromethane again, prior to powdering in a ceramic or zirconia puck mill (SPEX 8510 Shatterbox). The puck mill was cleaned between samples by powdering two batches of fired sand (850°C, overnight) followed by rinses with the same sequence of solvents described above. Samples were powdered in two aliquots, with the first discarded and the second collected for extraction. Fired sand procedural blanks were crushed with each batch of samples and processed identically to sample powders to monitor background levels of biomarker analytes. In addition to the powder reserved for lipid biomarker analyses, a split was collected for inorganic geochemical analyses.

Lipid biomarkers were extracted from 10 - 40 g of rock powder, depending on TOC, in a Microwave Accelerated Reaction System (CEM corp.) with dichloromethane and methanol (9:1 v/v) at 100°C for 15 minutes. Elemental sulfur was removed from the total extract with HCl-activated, solvent washed copper pellets prior to silica gel column chromatography. Total extracts were fractionated with hexane, hexane:dichloromethane (1:1 v/v), and dichloromethane:methanol (3:1 v/v) to elute saturated hydrocarbons, aromatic hydrocarbons, and polar (N, S, and O-containing) compounds, respectively.

Gas chromatography-mass spectrometry (GC-MS) analyses of saturated (Figure 6.3) and aromatic hydrocarbons was conducted with an Agilent 7890A, equipped

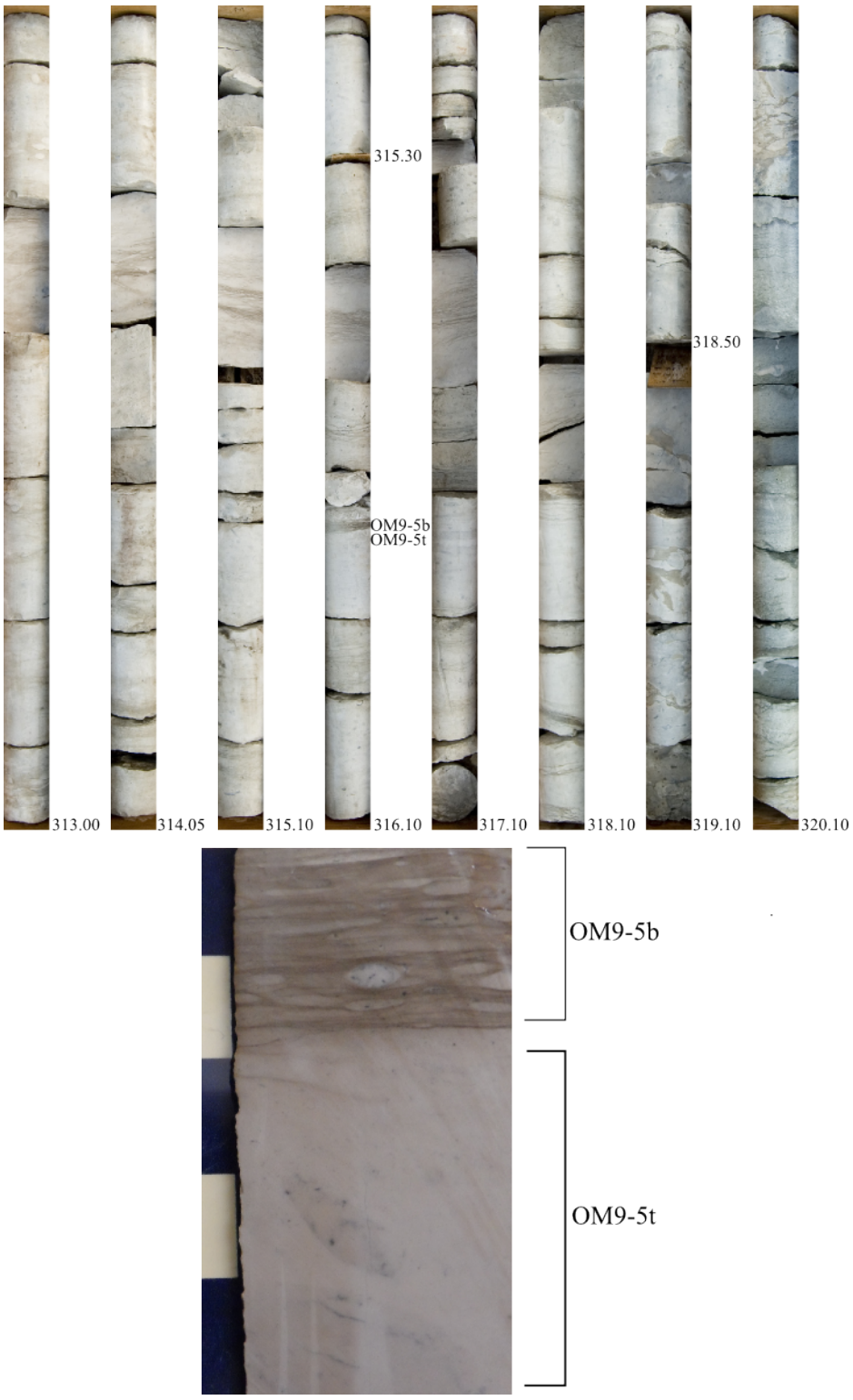

Figure 6.2: Above, photographic log of a portion of the Viki Drill Core (modified from Poldvere, 2010), numbers indicate meters core depth; and Left, slab showing brown laminations and tan micritic with 1 cm scale bar intervals.

with a DB-1MS capillary column (60 m x 0.32 mm, 0.25 um film) interfaced to an Agilent 5975C MSD mass spectrometer and utilizing He as carrier gas. The temperature program for GC-MS full scan and selected ion monitoring was 60°C (2 min), ramp to 250°C at 20°C/min, to 325°C at 2°C/min, and hold at 325°C for 20 min.

Multiple reaction monitoring (MRM) GC-MS of saturated hydrocarbons (Figure 6.4, 6.5) was carried out with a Waters AutoSpec Premier mass spectrometer equipped with an Agilent 7890A gas chromatograph and DB-1MS coated capillary column (60m x 0.25 mm, 0.25 um film) using He for carrier gas. MRM-GC-MS measurements were conducted with a temperature program with an initial hold at 60°C for 2 min, heating to 150°C at 10°C/min followed by heating to 315°C at 3°C/min, and a final hold at 320°C for 22 min. Biomarker compounds were identified based on retention time and published mass spectra and quantified in MRM GC-MS by comparison with a deuterated C_{29} sterane internal standard (d4-$\alpha\alpha\alpha$-24-ethylcholestane (20R), Chiron Laboratories, AS), assuming equal response factors between sample compounds and the internal standard. Individual yields of hopane and sterane diastereoisomers found in laboratory procedural blanks were typically less than 0.1 ng of individual compounds and polycyclic alkane biomarker MRM-GC-MS signal (hopanes, steranes, methylsteranes, methylhopanes, tricyclic terpanes) from rock samples was typically at least 2-3 orders of magnitude higher in total than those detected in blanks (i.e. less than 0.03 ng C29 $\alpha\alpha\alpha$ R sterane/g extracted sand blank vs greater than 10 ng C_{29} $\alpha\alpha\alpha$ R sterane/g TOC in samples).

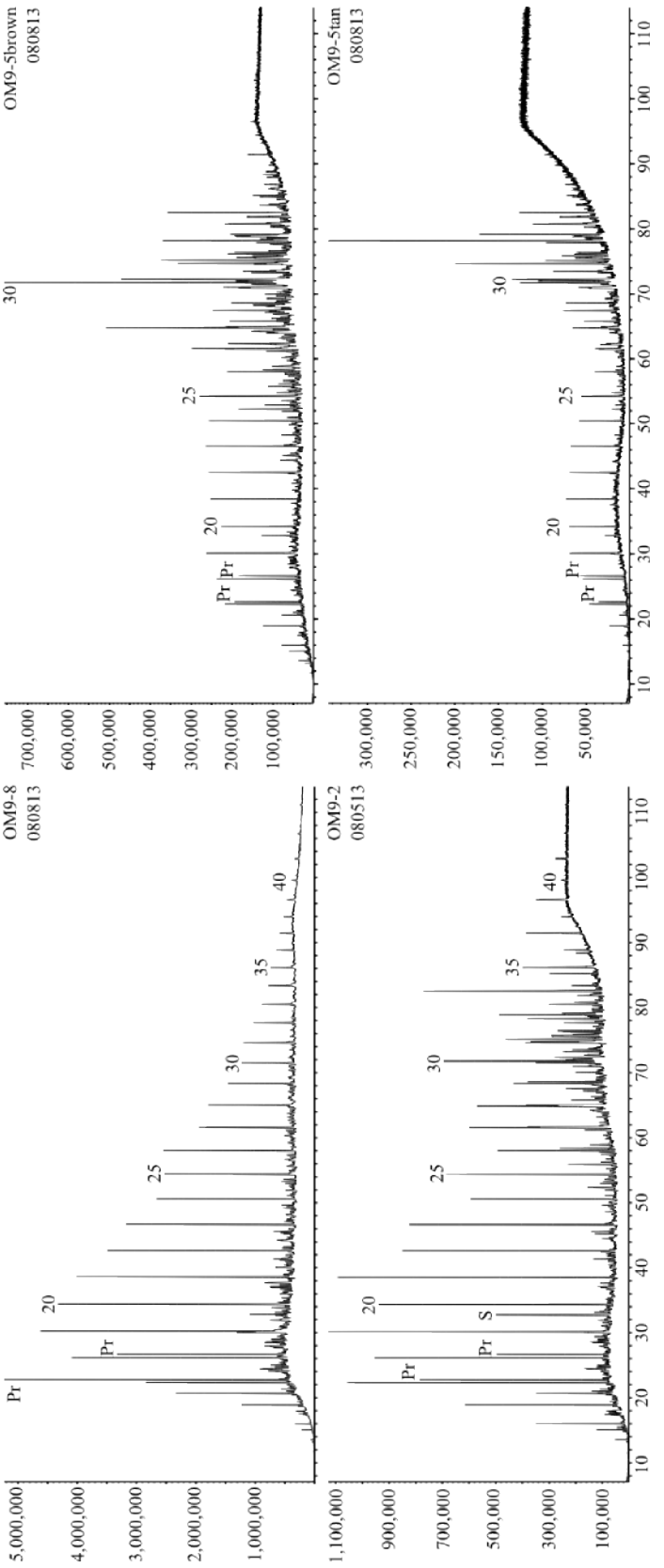

Figure 6.3: Total ion chromatograms for Viki drill core samples. Abbreviations: Pr, pristane; Ph, phytane; Numbers correspond to n-alkane chain length.

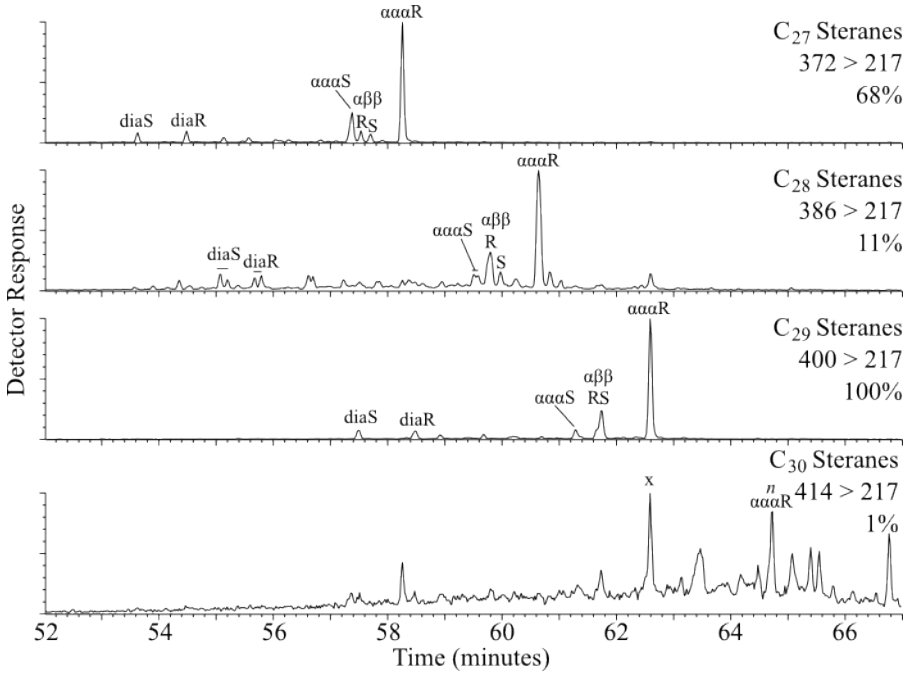

Figure 6.4: MRM-GC-MS chromatograms of OM9-01 free steranes. Percentages quoted represent a measure of relative signal intensity given relative to C_{29} sterane peak height.

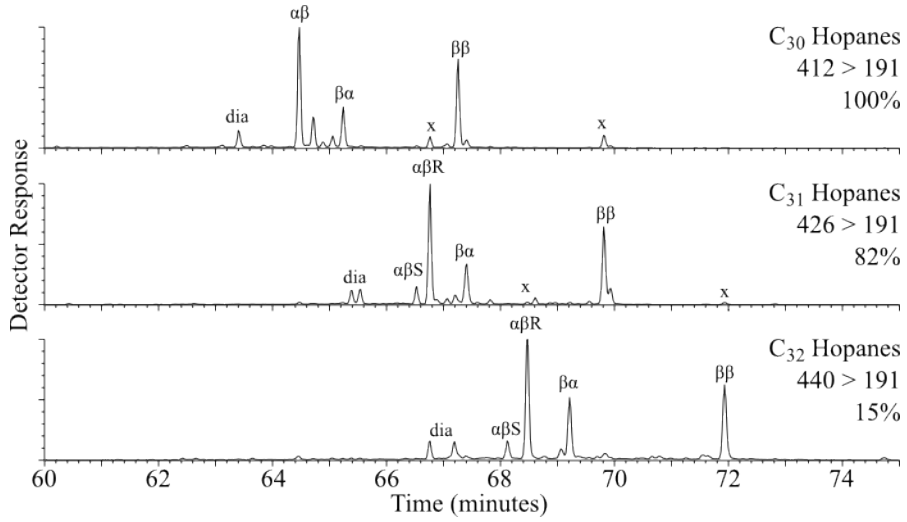

Figure 6.5: MRM-GC-MS chromatograms of OM9-01 free hopanes. Percentages quoted represent a measure of relative signal intensity given relative to C_{30} hopane peak height.

6.4 Results and Discussion

6.4.1 Middle to Late Ordovician Baltica - Viki Drill Core (OM9), Saaremaa Island, Estonia

Lipid biomarkers extracted from Viki drill core rocks exhibit exceptionally immature biomarker distributions, including 17β,21β(H) and 17α,21β(H)-R hopanes, moretanes, hopenes, diasterenes, and $\alpha\alpha\alpha$ R steranes indicating a very low degree of diagenetic and burial alteration, consistent with low thermal maturity assigned on the basis of conodont color alteration (CAI 1) in overlying Silurian rocks (Lehnert et al., 2010).

Viki drill core biomarkers exhibit similar features and overall stratigraphic patterns to those derived from Anticosti Island, although Hirnantian (Porkuni) Stage strata were not sampled in this study. Hopane/sterane ratio, reflecting the relative contributions of bacteria and eukaryotes, respectively, indicates bacterially-dominated primary producer communities for the Katian-age Kukruse through Nabala Stages (H/St of 1.6 to 5.7, Figure 6.6,Table 6.1), consistent with oligotrophic, warm conditions for this tropical carbonate shelf. The Vormsi and Pirgu Stage samples present a transient shift to algal-dominance (H/St 0.8 and 0.4, respectively), although the Pirgu Stage sample must be treated with skepticism because of possible contamination. This interval of algal primary production is followed by a dramatic rise in H/St in the Juuru Stage (Rhuddanian) to 17.2 (Table 6.1). The paucity of datapoints makes for uncertain interpretation, however this pattern is reminiscent of the Hirnantian on Anticosti, in which large excursions in H/St in the Lousy Cove Member precede the Laframboise Member maximum carbon isotope excursion (Chapter 2).

Compounds most likely derived from aerobic methanotrophic proteobacteria

(3β-methylhopanes) are present in very elevated relative amounts as a percentage of C_{30} $\alpha\beta$-desmethylhopane (3β-methylhopane index, 3-MeHI) in comparison to the Phanerozoic average range of 1.0 - 3.0 percent. Very high 3-MeHI of 14.3 - 16.2 percent in the Kukruse through Keila Stages descend to 5.4 - 10.6 percent in the Rakvere through Juuru Stages (Figure 6.6). If reproduced in HyPy products, this would suggest that the decrease in 3-MeHI in the Viki borehole begins in the lower Katian and therefore precedes the decline in 3-MeHI observed on Anticosti, which takes place in the upper Hirnantian (Chapter 2). This may also precede the decline in 3-MeHI observed in the Vinini Formation, although it is possible that 3-MeHI had already begun to decline at the base of the Vinini Creek section, given recent stratigraphic correlation schemes (Holmden et al., 2013; Melchin et al., 2013). In any case, elevated 3-MeHI in all samples of the Estonian Viki drill core confirm that enhanced methane cycling was a widespread feature of Late Ordovician tropical seas world wide, and that methane release was curtailed approaching the Hirnantian glacial maximum. This offers further support for our hypothesis that methane cycling could serve as a positive feedback on Lower Palaeozoic climate.

The tan "background" and brown lamination-rich portions of the 316 m (OM9-5) sample yielded interestingly different features (Figures 6.3; Figures 6.6, 6.7 wherein the brown laminated portion is indicated by a gray symbol, tan by black). The brown laminations are enriched in C_{27} steranes, hopanes, 3-MeH and a presently un-identified diunsaturated C_{29} hopane, and have less 2-MeH relative to the tan material. The brown lamination-rich sample exhibits higher sterane $\alpha\alpha\alpha$ S/($\alpha\alpha\alpha$ S+ $\alpha\alpha\alpha$ R) and tricyclics, but also yield higher $\beta\beta$ hopanes and moretanes and lower hopane 22S/(S+R); the higher sterane $\alpha\alpha\alpha$ S/($\alpha\alpha\alpha$ S+ $\alpha\alpha\alpha$ R) may therefore result from coelution of $\beta\alpha\alpha$R with $\alpha\alpha\alpha$ S in these very immature rocks. Given these differences in lipid biomarker

profile it seems safe to say that the organic-rich laminations are not due to concentration of "background" organic matter, be it through enhanced preservation or production of the same microbial community, or lessened carbonate dilution. One scenario that could result in milimetric organic carbon-rich laminations with elevated hopanes and C_{27} steranes in otherwise bioturbated micrite is the formation of microbial mats. Blooms of C_{27} sterane-producing algae and, perhaps, hopane-producing bacteria fueling anoxia and enhanced organic matter preservation and lessened bioturbation is another possibility, although biomarker proxies weakly associated with redox (pristane/phytane, figure 5.3, homohopane index figure 5.6) make it less favorable. These laminated intervals appear intermittently from about 318 to 310 m core depth (Figure 5.2); tracking their occurrence and assessing whether their biomarker composition changes through the Nabala Stage may provide insight into environmental conditions during deposition.

More mature *n*-alkane and biomarker profiles are found in upper intervals of the core that most likely represent migrated of petroleum fluids, likely also of Palaeozoic origin. The most extreme example of this is evidenced by comparison between OM9-5brown (Figure 6.3 and indicated by gray symbols in Figures 6.6 and 6.7) and OM9-8 (Figure 6.3, and indicated by white symbols in Figures 6.6 and 6.7). The immature end member in this mixing scenario is too thermally immature to migrate readily, whereas the oil window maturity of the other end member allows that hydrocarbons may well have migrated into upper portions of the core. In most cases, migrated petroleum contaminants would dilute the unusual features of Late Ordovician bitumens, such that 3-MeHI, in particular, may be suppressed. Mesozoic contaminants, for example, are likely to also have a substantial impact on sterane distributions (higher C_{28}/C_{29} steranes, abundant dinosteranes, often higher C27 steranes, and 24-*n*-propylcholestanes.

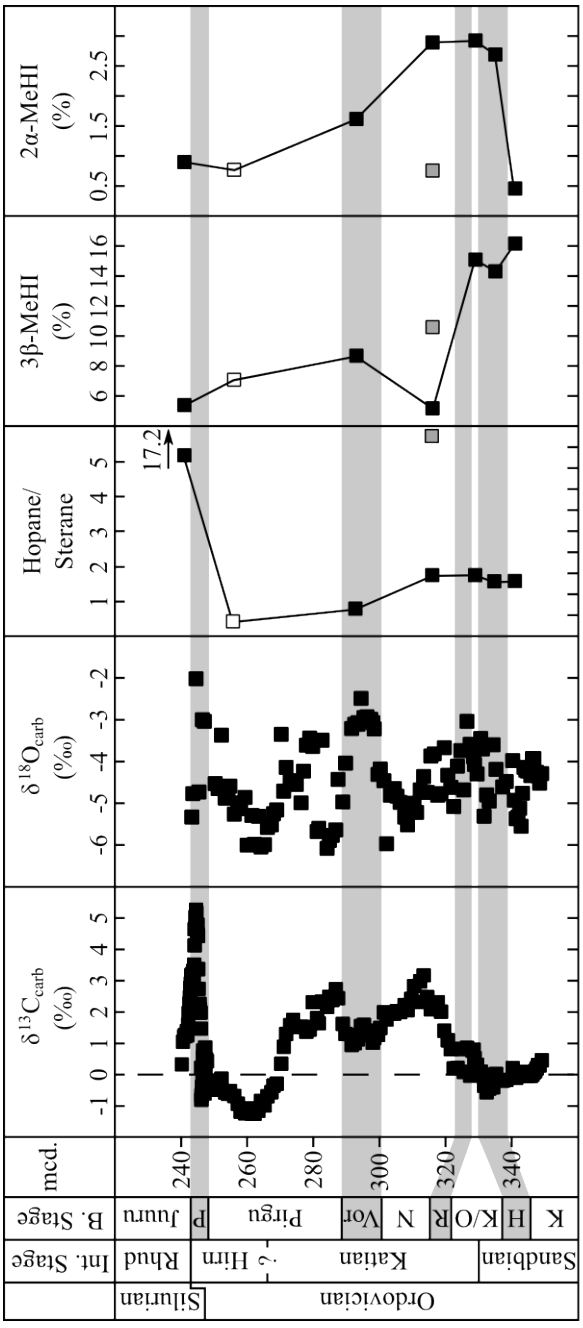

Stratigraphic lipid biomarker profiles for Viki Borehole, Estonia with carbon and oxygen isotope data. Carbon and oxygen isotope analyses and Baltic Stage assignments, on the basis of biostratigraphy, conducted by workers at the Geological Survey of Estonia and Talinn University of Technology, and by comparison with Holmden et al., 2013. Gray symbols: OM9-5 brown horizon. Open symbol: suspicious datapoint (OM9-8). Abbreviations: Int., International; B. Baltic; mcd., meters core depth; MeHI, methylhopane index; Rhud, Rhuddanian; Hirn, Hirnantian; P, Porkuni; Vor, Vormsi; N, Nabala; K/O, Keila/Oandu; R, Rakvere; H, Haljala; Kuk, Kukruse.

Figure 6.6: Selected lipid biomarker profiles for Viki Drill Core rock extracts, Saaremaa, Estonia.

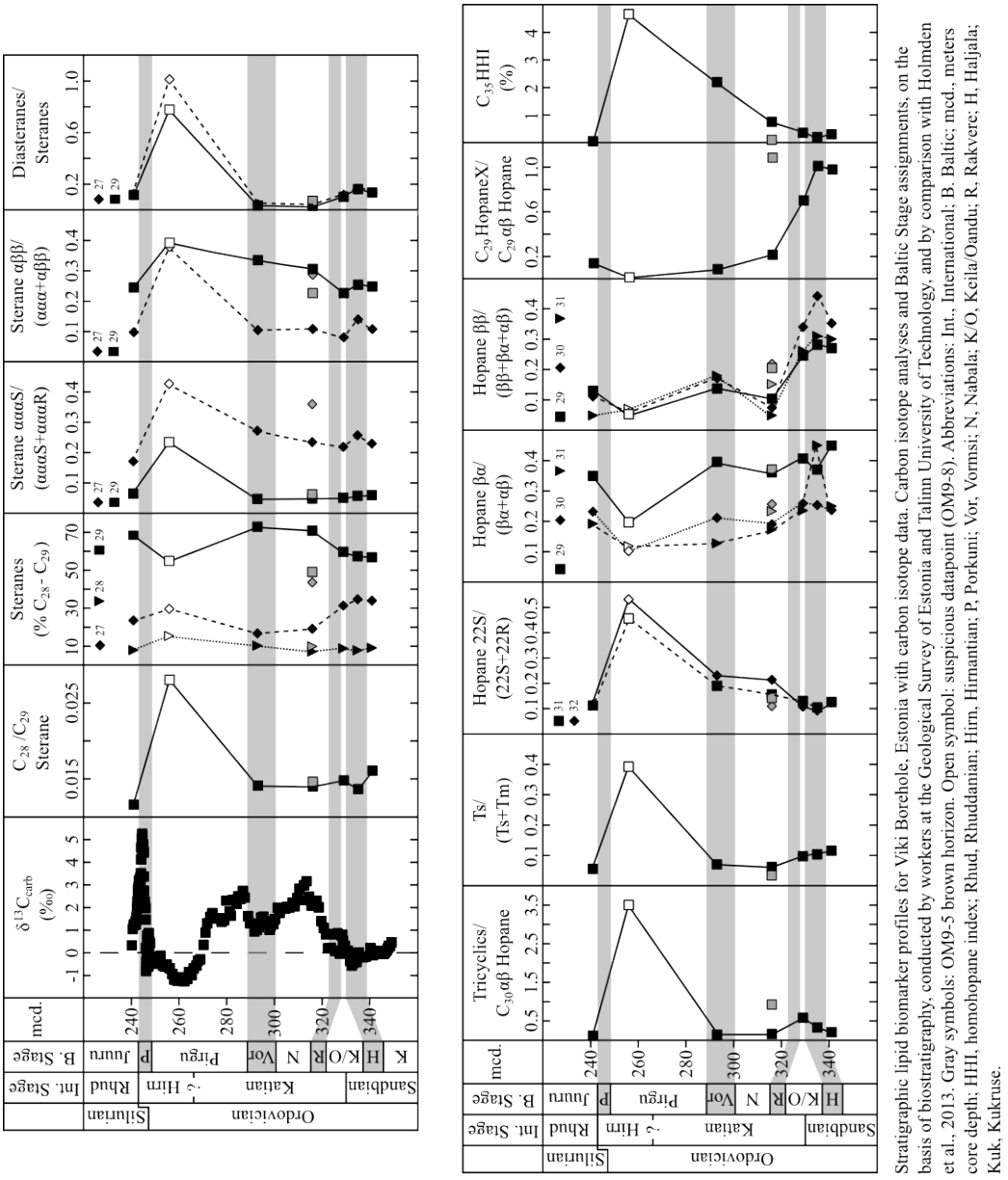

Stratigraphic lipid biomarker profiles for Viki Borehole, Estonia with carbon isotope data. Carbon isotope analyses and Baltic Stage assignments, on the basis of biostratigraphy, conducted by workers at the Geological Survey of Estonia and Tallinn University of Technology, and by comparison with Holmden et al., 2013. Gray symbols: OM9-5 brown horizon. Open symbol: suspicious datapoint (OM9-8). Abbreviations: Int., International; B. Baltic; mcd., meters core depth; HHI, homohopane index; Rhud, Rhuddanian; Hirn, Hirnantian; P, Porkuni; Vor, Vormsi; N, Nabala; K/O, Keila/Oandu; R, Rakvere; H, Haljala; Kuk, Kukruse.

Figure 6.7: Lipid biomarker profiles for Viki Drill Core rock extracts, Saaremaa, Estonia, continued.

Interestingly, OM9-8 retains a high 3-MeHI compared to Phanerozoic average, and the 3-MeH in OM9-8 also presents a somewhat more mature profile than the over- and underlying samples, suggesting that the contaminant likely also has a somewhat high 3-MeHI. On the basis of elevated rearranged and $\alpha\beta\beta$steranes, a C_{28}/C_{29} sterane ratio of 0.28, the absence of 24-*n*-propylcholestane, high 3-MeH (despite swamping of the biomarker signature) and absence of oleanane, I suggest this migrated hydrocarbon contaminant derives from a lower Paleozoic shale, perhaps even the nearby Ordovician basinal Fjaka shale. Alkylcyclohexanes associated with *G. prisca* may be present in trace levels but are not abundant.

The very low maturity of Viki drill core material is promising for further paleoclimate and paleoecology investigations, for example, samples from a core closer to the Fennoscandian shield might prove suitable for screening for compounds derived from early land plants. Catalytic hydropyrolysis on the pre-extracted kerogen phases (insoluble organic matter) will be performed in the future on a subset of our samples to distinguish the genuine syngenetic biomarker signals from those contributions from migrated petroleum. In the meantime, the maturity parameters in Figure 6.7 provide an indication of the degree of interference from more mature contaminants.

6.4.2 Ireviken Event - Lower Visby, Upper Visby, and Silte Formations, Gotland, Sweden

Parallels have been drawn between the positive carbon isotope excursion and faunal extinction episodes of the Ireviken Event (Wenlock-Llandovery Stage boundary) and those of the Hirnantian glacial maximum and mass extinction (Azmy et al, 1998; Munnecke et al., 2003), partly on the basis of South American diamictites which have subsequently been reassigned to the Llandovery (Diaz-Martinez and Grahn, 2007). More

recently, the Ireviken Event has been interpreted to represent elevated organic matter burial in marginal settings during post-glacial transgression (Cramer and Saltzman, 2005; 2007; Page et al., 2007). Both interpretation schemes have been developed in light of, and integrated with Jeppson's (1990) model of alternating climatic states, in which the Ireviken Event constitutes an intermediary between the Snipklint Primo (cool/dry) and Vattenfallet Secundo (warm/wet) Episodes (Jeppsson, 1990; 1997; Munnecke et al., 2003; Bickert et al., 1997). Complex interplay between temperature and humidity could be disentangled through clumped isotope measurements, unfortunately the first attempt has been unable to resolve a change in paleotropical water temperatures or isotopic composition during deposition of the Llandovery to Wenlock-age rocks used in this study (Cummins et al. *submitted*).

The organic geochemical record of the Ireviken Event on Gotland (Figure 6.8) indicates substantial variations in microbial community structure through the Event (Figure 6.8, Table 6.2) as predicted by the alternating climate states models. Following the conodont extinction datum numbering system summarized in Munnecke et al. (2003; Figure 6.7), we place our zero datum at the *Phaulactis* bed. Our sample set therefore begins around datum 2, an interval within the Ireviken Event and upper Telychian H-period, during which extinctions of trilobite and graptolite taxa take place. This sample yields a higher than Phanerozoic average (0.5 to 2, Cao et al., 2009) H/St ratio of 3.8 (Figure 6.8, Table 6.2). Bacterial contributions to sedimentary organic matter decline through the Ireviken Event, reaching a minnimum of 0.92 at 3 meters above the *Phaulactis* bed. In sum, pre-Ireviken H/St (meters -3 to -1) average 2.7, H/St during the Ireviken Event (meters 0 to +6) average 1.0, while the post-Event sample (G8-1.5) has a H/St of 2.7.

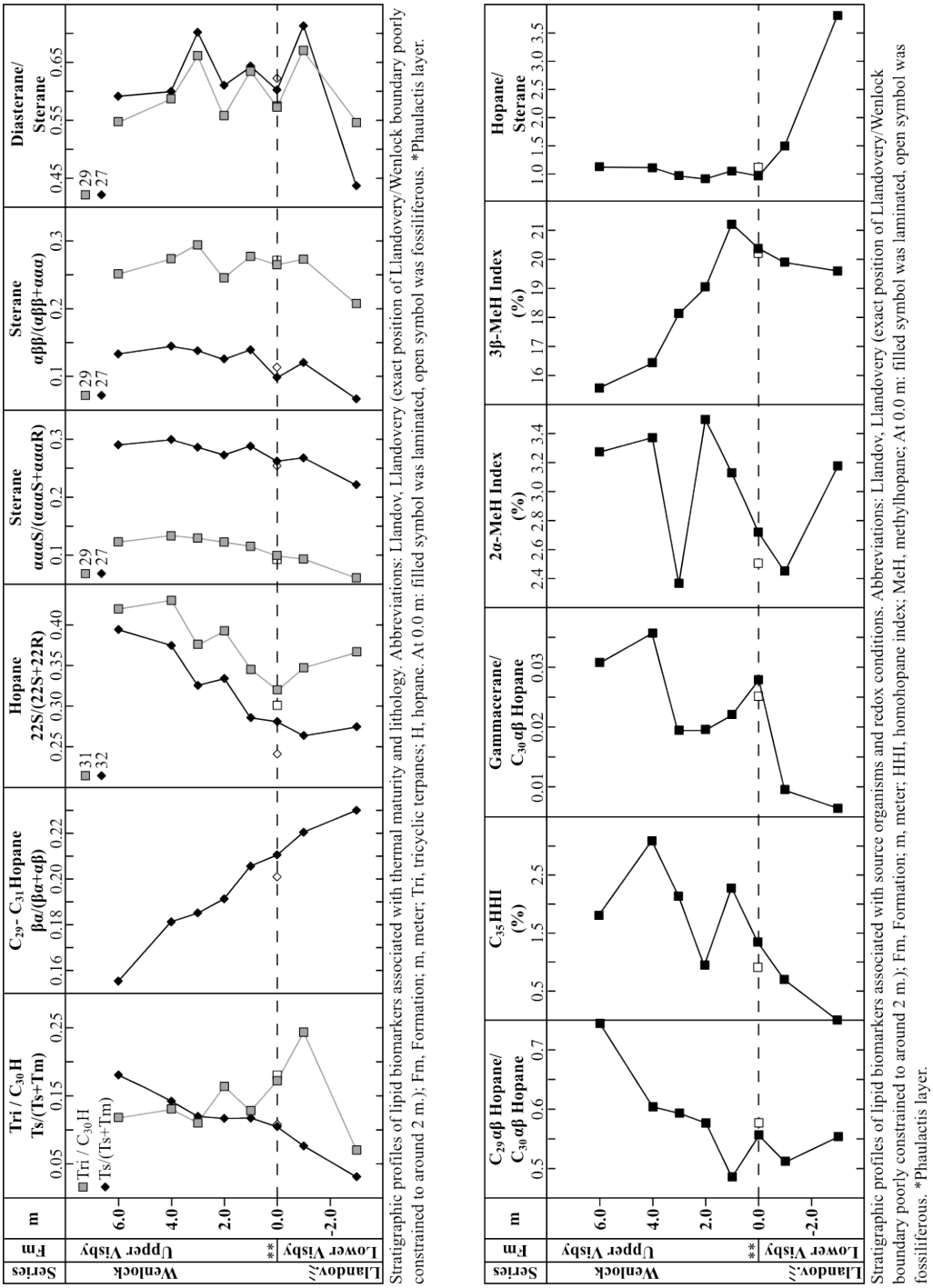

Stratigraphic profiles of lipid biomarkers associated with thermal maturity and lithology. Abbreviations: Llandov, Llandovery (exact position of Llandovery/Wenlock boundary poorly constrained to around 2 m.); Fm, Formation; m, meter; Tri, tricyclic terpanes; H, hopane. At 0.0 m: filled symbol was laminated, open symbol was fossiliferous. *Phaulactis layer.

Stratigraphic profiles of lipid biomarkers associated with source organisms and redox conditions. Abbreviations: Llandov, Llandovery (exact position of Llandovery/Wenlock boundary poorly constrained to around 2 m.); Fm, Formation; m, meter; HHI, homohopane index; MeH, methylhopane; At 0.0 m: filled symbol was laminated, open symbol was fossiliferous. *Phaulactis layer.

Figure 6.8: Lipid biomarker profiles for the Lower and Upper Visby Formations, Gotland, Sweden

The increase in the proportion of algal organic matter over this interval, similar to that observed in the Hirnantian (see Chapter 2), is the opposite of what one might expect from a decrease in riverine nutrient supply or weakened upwelling associated with estuarine circulation. Both of these tend to promote deposition of algae-rich organic matter in the ancient (this dissertation) as well as in today's oceans. Minor increases in hopane side-chain preservation (homohopane index), 2α-methylhopane likely derived from marine cyanobacteria, and gammacerane may indicate increasing stratification through the studied interval (Figure 6.8), perhaps reflecting development of antiestuarine circulation as proposed (Jeppsson, 1990; Munnecke et al., 2003), however the absolute values for both are low and not particularly indicative of substantial stratification or anoxic/sulfidic conditions.

Instead, following the model presented for Anticosti Island (Chapter 2) and that based on the temperature-dependance of microbial metabolism (Stanley, 2010; Laws et al., 2000; Finnegan et al., 2012), the decline in hopane/sterane ratios from bacterially-dominated organic matter to organic matter bearing a greater contribution from eukaryotes is consistent with cooling from a warm state as early models for the Ireviken Event suggested. Primary production in the modern ocean on a global scale largely does not correlate with temperature, and the net driver of organic matter export appears to be strongly temperature dependent microbial remineralization (Laws et al., 2000; Finnegan et al., 2012), thus at warmer temperatures hopane/sterane is expected to be higher. However, it is difficult to ascribe all changes in hopane/sterane ratio on a local basis solely to temperature-dependent remineralization rates, even in tandem with positive feedback from oxygen solubility. Oxidant abundance, the composition of primary producers, and local changes in depositional environment are other potential factors at play (see Chapter 3). Thus, although consistent with cooling, the decrease in

h/st from more bacterial than the Phanerozoic average to within the Phanerozoic average range, needs to be reproduced in other locations to assess its relevance to climate.

3β-methylhopanes likely derived from methanotrophic bacteria also hint at an interesting parallel between the Ireviken Event and Hirnantian glacial maximum. 3-MeHI are exceptionally high throughout the section: averaging 18.6 percent, well above the Phanerozoic average range of 1 - 3 percent (Cao et al., 2009) and among the highest ever reported. 3-MeHI increase slightly at the base of the section, from 19.6 percent at -3 m to 21.2 percent at +1 m, then exhibit a monotonic decline through the rest of the sampled interval, reaching the "lowest" values of 15.6 percent at +6 m, and 15.3 percent in the post-Ireviken Event Silte Formation sample (Figure 6.7, Table 6.2), very much in parallel to the timing of the Ireviken Event carbon and oxygen isotope excursion. The timing and pattern of hopane/sterane and 3-MeHI are not parallel, as one might predict under the remineralization regime, again emphasizing the importance of local factors in organic geochemical proxies. Thus, while decreasing 3-MeHI may reflect lessened remineralization rates due to global cooling, unless in a strongly antiestuarine system (i.e. warm saline bottom waters) it may also reflect local cooling due to transgression. This may be more consistent with current interpretation of the Ireviken Event in a general sense, but perhaps difficult to reconcile with apparently shallower water facies as evidenced by development of the Upper Visby Formation bioherms.

Interestingly, although the overlap in our datasets is less than would be ideal, given the scope for error in correlation on the basis of the *Phaulactis* bed datum, carbon isotope analyses of chitinozoans and scolcodonts indicate an increase in the difference in carbon isotope composition between zooplankton and benthic invertebrates, respectively, prior to the Ireviken carbon isotope excursion (Vandenbroucke et al., 2013). Vandenbroucke and colleagues (2013) attribute the lighter carbon isotope composition

of scolecodonts to the source organisms feeding on a greater proportion of primary producer (as opposed to partially remineralized) organic matter, an interpretation which is consistent with the decrease in hopane/sterane ratios in the Lower Visby Formation. An additional possibility is the incorporation of methanotrophic bacterial biomass by the scolecodont source animals, a circumstance which has been observed with chironomids in modern methane-rich lacustrine settings (see Jones and Grey, 2011). Unfortunately, it was not possible to obtain enough extract for compound specific isotope analysis of these samples.

6.4.3 Whole Dataset and the Late Ordovician "Fingerprint"

Substantial faunal provinciality and endemism are well-recognized in Late Ordovician epeiric seas (e.g. Sheehan, 2001; Melchin et al., 2013). Differentiation within epicontinental seas has also been identified in Nd and other isotope systems, and attributed to formation of disparate water masses in epeiric circulation (e.g. Panchuk et al., 2006). Given the regionalized distributions of heterotrophic macrofauna, both benthic and planktonic, and chitinozoans, a similar localization of microbial communities might be expected, both within and among epeiric seas. In concluding this thesis, we can address these expectations and elaborate upon the Ordovician "fingerprint" introduced in Chapter 1.

The focus of this study on paleotropical environments somewhat hinders what we are able to say about the global diversity of microbial community structures. Unfortunately, the Gondwanan samples (Morocco, from Thijs Vandenbroucke) that were analysed were overmature and did not yield biomarkers. Despite this limitation, we are able to demonstrate that eukaryotic phytoplankton in tropical seas were dominated by green algae, under any nutrient or circulation regime on both Laurentian and Estonian

Shelves from the Katian through Wenlock Stages, and in deep waters of at least Katian through Hirnantian times. That is, "hydrographic" situation (c.f. Melchin et al., 2013) is not sufficient to define algal provinces on the basis of sterane carbon number distribution (Figure 6.9). Variations within this range of environments were likely present but at a taxonomic level below the resolution of our proxies at present. Further statistical treatment of the whole dataset may prove more informative.

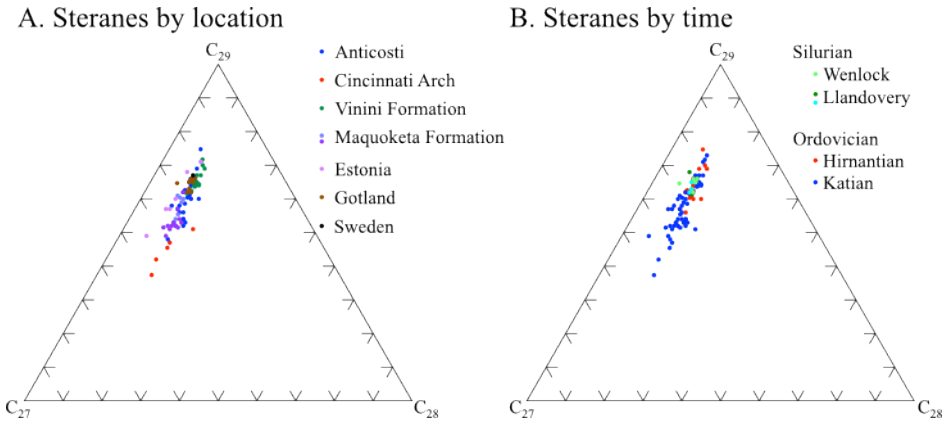

Figure 6.9: Ternary diagrams representing sterane carbon number distribution A. by location and B. through time.

We are also able to demonstrate strong affinities between the balance between bacterial and eukaryotic primary production (H/St) and nutrient regime. H/St, along with 3-MeHI, exhibits the strongest geographic and temporal patterns: lower H/St are observed in upwelling- or runoff-influenced regions, while high H/St is favored by restriction, oligotrophic conditions, and to a lesser degree, in shallower facies. The most extreme H/St ratios, however, are observed in the Hirnantian of Anticosti (up to 19.5), and lowermost Silurian of Estonia (up to 17.2), proximal to the Hirnantian mass extinction intervals. The lowest H/St values are observed in the organic-rich portions of the Maquoketa (as low as 0.1) and Vinini (as low as 0.2) Formations, which both bear phosphatic testimony to elevated nutrient availability. Thus, where high

TOC accumulated in the epicontinental seas, it appears to have been algal-dominated. Bacterially-dominated organic-rich laminae, as in the Nabala stage carbonates of the Viki borehole are an exception. Interestingly, this is also apparently quite different from the hopane-dominated, phosphate-rich shale of the Lower Ordovician Winneshiek Lagerstatte, deposited in a restricted sub-basin formed by meteor impact.

The highest 3β-methylhopane indices are observed in Wenlock-Llandovery rocks of Gotland (up to 21.2), the Maquoketa Formation (up to 18.6), and Estonia (up to 16.2), while the lowest values are observed in the Vinini Formation (as low as 1.7). In fact, in all samples except those from the Vinini Formation, 3-MeHI are in excess of the Phanerozoic average range (Table 5.3, Chapter 2). While 3-MeH are typically taken to reflect contributions from methanotrophic bacteria, a recent study suggests that 3-MeH synthesis plays an important role in cell membrane stabilization and may be a response to oxygen stress (Welander et al., 2012). If that is the case, it might be expected that the locations with the strongest evidence for anoxia might be expected to have the highest 3-MeHI, and that 3-MeH should be abundant in all low oxygen sediments today as well. As this does not appear to be the case, although the CSIA data remain ambiguous, we continue to favor a methanotroph origin for Lower Palaeozoic 3-MeH.

An unanticipated result of this work has been the proposal (Chapter 2) and elaboration of a potential methane cycling feedback on Lower Palaeozoic climate, hypothesized to be particularly effective in periods of Earth history with warm, broadly oligotrophic, low sulfate oceans. On-going work with sulfur isotope geochemistry indicating very low sulfate marine concentration through the Late Ordovician (Jones and Fike, 2013) highlights the importance of a better understanding of the anaerobic oxidation of methane, in addition to better constraining the potential sources of 3β-methylhopane through compound specific carbon isotope analyses as well as catalytic hydropyrolysis

of microbial cultures and enrichments. Although the anaerobic oxidation of methane is likely to be an ancient process and is ubiquitous in ocean sediments today, lipid biomarkers potentially attributable to methanogenic or reverse-methanogenic archaea are seldom reported from non-seep environments. The challenge of developing additional proxies for methane cycling in modern and ancient environments will be the subject of much future work.

A final distinctive characteristic of Late Ordovician microbial communities that we have uncovered is the very low abundance of marine pelagophyte algae in all marine settings studied, as confirmed by only trace or absent levels of the 24-*n*-propycholestane (24-*n*pc)biomarker. Although its absence in the Late Ordovician-Early Silurian cannot be taken to indicate a non-marine origin for sedimentary organic matter or oils, the presence of 24-*n*pc is usually a reliable indicator of marine origin for most time periods including the Neoproterozoic and most of the Phanerozoic eon (discussed in Chapter 4). That said, all the resolvable diastereoisomeric forms of of 24-*n*pc are seldom detected in rocks of this time period despite evidence that pelagophytes had evolved by Ordovician times. We elaborate upon the recognized Ordovician "fingerprint" for rocks and oils with the suggesting that Late Ordovician-derived rocks and oils will, in comparison to Early and Middle Ordovician rocks, have only a minor *G. prisca* signature contribution, trace to no 24-*n*pc, elevated 3β-methylhopane indices (typically 3-MeHI greater than 3.0), C_{28}/C_{29} sterane of less than 0.3 (Table 6.3).

As with macrofauna, the Late Ordovician mass extinction had substantial transient impact upon overall microbial community structure without generating permanent change in dominant clades. Further analysis of the full dataset (in addition to such comparable data as may be derived from literature) incorporating hopane/sterane ratios, methylhopane indices, and other parameters using statistical approaches such as prin-

ciple component analysis is a promising way forward both to identifying un-noticed differentiating parameters and supporting those already apparent.

6.5 Conclusions

With this thesis work we are able to add a view of primary production and microbial community structure to paleoceanographic and paleobiological models of Lower Palaeozoic epicontinental seas. Our results are consistent with the consensus view of the overall evolution of eukaryotic algae and marine biospheric evolution, indicating green algal dominance among eukaryotic primary producers throughout Late Ordovician tropical seas. Furthermore, we demonstrate that expected relationships between upwelling- and weathering-delivered nutrients favored eukaryotic over bacterial primary production in Lower Palaeozoic as well as modern seas. Significantly enhanced abundances of 3β-methylhopane, compounds most likely derived from Type I microaerophilic methanotrophic bacteria, relative to any other interval of time as yet reported for any Proterozoic or Phanerozoic rocks, are found throughout Late Ordovician seas and persist, at least episodically and in some regions, into the Silurian. We interpret these to indicate enhanced production of biogenic methane from sedimentary methanogenesis (from slow diagenesis of sedimentary organic matter) and subsequent enhanced methane release into the marine water column bin these warm, low oxidant seas.

In addition to establishing a baseline for Lower Palaeozoic epicontinental seas, we describe the behavior of microbial community structure during the Hirnantian Stage glacial maximum and mass extinction in both oligotrophic and upwelling-influenced systems and show that eukaryotic production was enhanced during the glaciation, consistent with evidence for enhanced nutrient supply and elevated algal primary production.

Decreases in the abundance of aerobic methanotroph derived compounds during both the Hirnantian Stage glacial maximum and Ireviken Event suggest decreases in methane production; a methane cycling positive feedback on Lower Palaeozoic climate. The patterns of elevated hopane/sterane ratios and high 3β-methylhopane indices in carbonate shelf environments in Laurentian epicontinental seas has been reproduced on the Baltic paleocontinent in both the Late Ordovician and Early Silurian, suggesting these were global features of Late Ordovician tropics that persisted for tens of millions of years through major climatic and geochemical perturbations, and extinctions.

6.6 Acknowledgments

The author would like to acknowledge Thijs Vandenbroucke and Olle Hints for discussion of sampling possibilities, for providing samples of the Viki drill core, and for access to the drill core data repository. Additional thanks are due to Woodward Fischer, Seth Finnegan, and Renata Cummins for the Gotland samples and Ordovician shale sample from Sweden. The author also acknowledges funding support from a University of California, Riverside dissertation year fellowship, a NASA Astrobiology grant to Gordon Love, and Shell.

6.7 References

1. Azmy, K., Veizer, J., Bassett, M., Copper, P., 1998, Oxygen and carbon isotopic composition of Silurian brachiopods: implications for coeval seawater and glaciations: Geological Society of America Bulletin, v. 110, p. 1499-1512.

2. Bickert, T., Ptzold, J., Samtleben, C., Munnecke, A., 1997, Palaeoenvironmental changes in the Silurian indicated by stable isotopes in brachiopod shells from Gotland, Sweden: Geochimica et Cosmochimica Acta, v. 61, p. 2717-2730.

3. Calner, M., Jeppsson, L., Munnecke, A., 2004, Field guide to the Silurian of Gotland - Part I: Review of the stratigraphic framework, event stratigraphy, and stable

carbon and oxygen isotope development: Erlanger Geologische Abhandlunge, p. 113-131.

4. Calner, M., 2008, Silurian global events - at the tipping point of climate change. In: Ashraf, M.T.E. ed. Mass Extinctions, pp. 21-58, Springer-Verlag. Berlin and Heidelberg.

5. Cocks, L.R.M., and Torsvik, T.H., 2002, Earth geography from 500 to 400 million years ago: A faunal and palaeomagnetic review: Journal of the Geological Society, v.159, p.631644, doi:10.1144/0016-764901-118.

6. Cramer, B.D., and Saltzman, M.R., 2005, Sequestration of ^{12}C in the deep ocean during the early Wenlock (Silurian) positive carbon isotope excursion: Palaeogeography, Palaeoclimatology, Palaeoecology, v. 219, p. 333-349.

7. Cramer B.D., and Saltzman, M.R., 2007, Fluctuations in epeiric sea carbonate production during Silurian positive carbon isotope excursions: A review of proposed paleoceanographic models: Palaeogeography, Palaeoclimatology, Palaeoecology, v. 27, p. 37-45.

8. Cummins, R.C., Finnegan, S., Fike, D.A., Eiler, J.M., Fischer, W.W., submitted, Carbonate clumped isotope constraints on Silurian ocean temperature and seawater ?18O.

9. Diaz-Martines, E., and Grahn, Y., 2007, Early Silurian glaciation along the western margin of Gondwana (Peru, Bolivia, and northern Argentina): Palaeogeographic and geodynamic setting: Palaeogeography, Palaeoclimatology, Palaeoecology, v. 245, p. 62-81.

10. Finnegan, S., Fike, D.A., Jones, D., Fischer, W.W., 2012, A temperature-dependant positive feedback on the magnitude of carbon isotope excursions: Geoscience Canada, v. 39, p. 122-131.

11. Harris, M.T., Sheehan, P.M., Ainsaar, L., Hints, L., Mnnik, P., Nlvak, J., Rubel, M., 2004, Upper Ordovician sequences of western Estonia: Palaeogeography, Palaeoclimatology, Palaeoecology, v. 201, p. 135-148.

12. Hints, O., Martma, T., Mnnik, P., Nlvak, J., Pldvere, A., Shen, Y., Viira, V., 2013, Viki drill core - an Ordovician bio- and chemostratigraphic reference section from Saaremaa Island, western Estonia, IGCP abstract.

13. Jeppsson, L., 1983, Silurian conodont faunas from Gotland: Fossils Strata, v. 15, p. 121-144.

14. Jeppsson, L., 1990, An oceanic model for lithological and faunal changes tested on the Silurian record: Journal of the Geological Society of London, v. 147, p. 663-674.

15. Jeppsson, L., 1997, The anatomy of the Mid-Early Silurian Ireviken Event and a scenario for P-S events: In: Brett, C.E., Baird, G.C., (eds.) Paleontological Events: Stratigraphic, Ecological, and Evolutionary Implications, Columbia University Press, New York. pp. 451-492.

16. Laws, E.A., Falkowski, P.G., Smith, W.O. Jr., Ducklow, H., McCarthy, J.J., 2000, Temperature effecs on export production in the open ocean: Global Biogeochemical Cycles, v. 14, p. 1231-1246.

17. Lehnert, O., Mnnik, P., Joachimski, M.M., Calner, M., Fr?da, J., 2010, Palaeoclimate perturbations before the Sheinwoodian glaciation: A trigger for extinctions during the "Ireviken Event": Palaeogeography, Palaeoclimatology, Palaeoecology, v. 296, p. 320-331.

18. Luo, G., Kump, L.R., Wang, Y., Tong, J., Arthur, M.A., Yang, H., Huang, J., Yin, H., and Xie, S., 2010, Isotopic evidence for an anomalously low oceanic sulfate concentration following end-Permian mass extinction: Earth and Planetary Science Letters, v. 300, p.10111.

19. Melchin, M.,J., Mitchell, C.E., Holmden, C., Storch, P., 2013, Environmental changes in the Late Ordovician-Early Silurian: Review and new insights from black shales and nitrogen isotopes: Geological Society of America Bulletin, v. 125, p. 1635-1670.

20. Munnecke, A., and Mnnik, P., 2009, New biostratigrapic and chemostratigraphic data from the Chicotte Formation (Llandovery, Anticosti Island, Laurentia) compared with the Viki core (Estonia, Baltica): Estonian Journal of Earth Sciences, v. 58, p. 159-169.

21. Munnecke, A., Samtleben, C., Bickert, T., 2003, The Ireviken Event in the lower Silurian of Gotland, Sweden - relation to similar Palaeozoic and Proterozoic events: Palaeogeography, Palaeoclimatology, Palaeoecology, v. 195, p. 99-124.

22. Panchuk, K.M., Holmden, C.E., Leslie, S.A., 2006, Local controlson carbon cycling in the Ordovician midcontinent region of North America, with implications for carbon isotope secular curves: Journal of Sedimentary Research, v. 76, p. 200-211.

23. Pldvere, A., 2010, Viki Drill Core: Estonian Geological Sections Bulletin, v. 10.

24. Rohrssen, M., Love, G.D., Fisher, W., Finnegan, S., Fike, D.A., 2013, Lipid biomarkers record fundamental changes in the microbial community structure of tropical seas during the Late Ordovician Hirnantian glaciation: Geology, v. 47, p. 127-30.

25. Stanley, S.M., 2010, Relation of Phanerozoic stable isotope excursion to climate, bacterial metabolism, and major extinctions: Proceedings of the National Academy of Sciences, v. 107, p. 10185-19189.

26. Estonian Geological Survey Database (2013) http://geokogud.info/git. Search term Viki Borehole.

27. Vandenbroucke, T.R.A., Munnecke, A., Leng, M.J., Bickert, T., Hints, O., Gelsthorpe, D., Maier, G., Servais, T., 2013, Reconstructing the environmental conditions around the Silurian Ireviken Event using the carbon isotope composition of bulk and palynomorph organic matter: Geochemistry, Geophysics, Geosystems, v. 14, p. 86-101.

28. Welander, P.V., Summons, R.E., 2012, Discovery, taxonomic distribution, and phenotypic characterization of a gene required for 3-methylhopanoid production: Proceedings of the National Academy of Sciences, v.109, p. 12905-10.

Table 6.1: Organic geochemical data for samples from Estonia and Sweden.

Sample	Formation	Stage	m	tricyclics/ C_{30} αβH	Ts/ (Ts+Tm)	gammacerane/ C_{30} αβH	HHI (%)	C_{31} αβH 22S/ (S+R)	C_{32} αβH 22S/ (S+R)	C_{29} βαH/ (βα+αβ)
BlSh Boda +25		Late Ordovician	Sweden	2.32	0.42	0.02	2.4	0.56	0.56	0.18
OM9-10	Varbola	Juuru	241	0.12	0.06	0.00	0.1	0.11	0.12	0.35
OM9-08	*Adila*	Pirgu	256	3.50	0.39	0.08	4.7	0.46	0.53	0.20
OM9-06	Tudulinna	Vormsi	293	0.15	0.07	0.04	2.2	0.19	0.23	0.40
OM9-5t	*Saunja*	Nabala (tan)	316	0.16	0.06	0.02	0.8	0.16	0.21	0.36
OM9-05b	*Saunja*	Nabala (brown)	316	0.93	0.03	0.00	0.1	0.14	0.11	0.37
OM9-03	Kahula?	Keila	329	0.58	0.10	0.01	0.4	0.13	0.11	0.41
OM9-02	Tatruse?	Halkjala	335	0.33	0.10	0.03	0.2	0.10	0.09	0.37
OM9-01	Pihla	Kukruse	341	0.21	0.12	0.01	0.3	0.13	0.12	0.45

Abbreviations: TOC, total organic carbon; TIC, total inorganic carbon; H, hopane.

Sample	C_{30} βαH/ (βα+αβ)	C_{31} βαH/ (βα+αβ)	C_{29} ββH/ (ββ+βα+αβ)	C_{30} ββH/ (ββ+βα+αβ)	C_{31} ββH/ (ββ+βα+αβ)	Oleanane/ C_{30} αβH	2-MeHI (%)	3-MeHI (%)	H(C_{27}-C_{35}) /St(C_{27}-C_{29})	C_{29}-ene / C_{29} αβH	%C_{27} St (C_{27}-C_{29})	%C_{28} St (C_{27}-C_{29})
BlSh Boda +25	0.10	0.10	0.02	0.00	0.00	0.01	1.3	3.4	0.29	0.01	23	10
OM9-10	0.23	0.19	0.13	0.11	0.05	0.00	0.9	5.4	17.21	0.14	24	8
OM9-08	0.10	0.12	0.05	0.06	0.07	0.01	0.8	7.1	0.43	0.01	30	15
OM9-06	0.21	0.13	0.14	0.17	0.18	0.01	1.6	8.7	0.80	0.09	17	10
OM9-5t	0.19	0.18	0.10	0.07	0.05	0.00	2.9	5.2	1.76	0.22	19	10
OM9-05b	0.26	0.23	0.20	0.22	0.15	0.00	0.8	10.6	5.72	1.09	44	7
OM9-03	0.26	0.24	0.25	0.34	0.26	0.00	2.9	15.1	1.76	0.70	31	9
OM9-02	0.25	0.45	0.28	0.44	0.31	0.01	2.7	14.3	1.57	1.01	35	8
OM9-01	0.24	0.25	0.27	0.35	0.30	0.00	0.5	16.2	1.59	0.98	34	9

Abbreviations: H, hopane; 2-MeHI,2-methylhopane index; 3-MeHI, 3-methylhopane index; St, sterane; -ene, hopene.

Sample	(C_{27}-C_{29})	C_{28}/C_{29} Sterane	C_{29} St αββ/ (ααα+αββ)	C_{27} St αββ/ (ααα+αββ)	C_{29} ααα St S/(S+R)	C_{27} ααα St S/(S+R)	C_{29} Dia/St	C_{27} Dia/St
BlSh Boda +25	67	0.15	0.24	0.17	0.31	0.41	0.38	0.50
OM9-10	68	0.12	0.24	0.10	0.06	0.17	0.12	0.12
OM9-08	55	0.28	0.39	0.38	0.23	0.43	0.78	1.01
OM9-06	73	0.14	0.33	0.10	0.05	0.27	0.03	0.04
OM9-5t	71	0.14	0.31	0.11	0.05	0.23	0.03	0.05
OM9-05b	49	0.15	0.23	0.29	0.06	0.36	0.07	0.05
OM9-03	60	0.15	0.23	0.08	0.05	0.22	0.10	0.12
OM9-02	57	0.14	0.25	0.14	0.06	0.26	0.16	0.16
OM9-01	57	0.16	0.25	0.11	0.06	0.23	0.14	0.13

Abbreviations: St, sterane; dia, diasterane.

Table 6.2: Organic geochemical data for Silurian samples from Gotland, Sweden.

Sample	Formation	m	tricyclics/ C_{30} αβH	Ts/ (Ts+Tm)	HHI (%)	C_{31} αβH 22S/ (S+R)	C_{32} αβH 22S/ (S+R)	C_{29} αβH/ C_{30} αβH	Oleanane/ C_{30} αβH	2MeHI (%)
G8-1.5	Silte		0.07	0.10	0.8	0.33	0.27	0.57	0.00	2
G1+6.0	Upper Visby	6.0	0.12	0.18	1.8	0.42	0.39	0.74	0.00	3.3
G1+4.0	Upper Visby	4.0	0.13	0.14	3.1	0.43	0.37	0.60	0.00	3.4
G1+3.0	Upper Visby	3.0	0.11	0.12	2.1	0.38	0.33	0.59	0.00	2.4
G1+2.0	Upper Visby	2.0	0.16	0.12	1.0	0.39	0.33	0.58	0.00	3.5
G1+1.0	Upper Visby	1.0	0.13	0.12	2.3	0.35	0.29	0.49	0.00	3.1
G1-0.0sb	Upper Visby	0.0	0.18	0.11	0.9	0.30	0.24	0.58	0.00	2.5
G1-0.0lam	Upper Visby	0.0	0.17	0.10	1.3	0.32	0.28	0.56	0.00	2.7
G1-1.0	Lower Visby	-1.0	0.24	0.08	0.7	0.35	0.26	0.51	0.00	2.5
G1-3.0	Lower Visby	-3.0	0.07	0.03	0.0	0.37	0.27	0.55	0.00	3.2

Abbreviations: HHI, homohopane index; H, hopane; 2-MeHI, 2-methylhopane index.

Sample	3MeHI (%)	H(C_{27}-C_{35}) /St(C_{27}-C_{29})	%C_{27} St (C_{27}-C_{29})	%C_{28} St (C_{27}-C_{29})	%C_{29} St (C_{27}-C_{29})	%C_{27} St (C_{27}-C_{30})	%C_{28} St (C_{27}-C_{30})	%C_{29} St (C_{27}-C_{30})	%C_{30} St (C_{27}-C_{30})	C_{28}/C_{29} Sterane	C_{29} St αββ/ (ααα+αββ)
G8-1.5	15.3	2.68	25	11	65	25	11	65	0.2	0.16	0.26
G1+6.0	15.6	1.13	24	10	66	24	10	66	0.3	0.16	0.25
G1+4.0	16.4	1.11	26	12	62	25	12	62	0.6	0.19	0.27
G1+3.0	18.1	0.97	23	11	66	23	11	66	0.4	0.16	0.29
G1+2.0	19.1	0.92	24	11	65	24	11	65	0.6	0.17	0.25
G1+1.0	21.2	1.05	24	11	65	24	11	65	0.8	0.16	0.28
G1-0.0sb	20.2	1.12	27	11	62	26	11	62	0.4	0.18	0.27
G1-0.0lam	20.4	0.97	26	11	63	25	11	63	0.4	0.18	0.27
G1-1.0	19.9	1.50	25	10	65	25	10	65	0.6	0.15	0.27
G1-3.0	19.6	3.81	28	7	64	28	7	64	0.5	0.11	0.21

Abbreviations: 3-MeHI, 3-methylhopane index; H, hopane; St, sterane.

Sample	C_{27} St αββ/ (ααα+αββ)	C_{29} ααα St S/(S+R)	C_{27} ααα St S/(S+R)	C_{29} Dia/St	C_{27} Dia/St
G8-1.5	0.12	0.10	0.24	0.35	0.35
G1+6.0	0.13	0.12	0.29	0.55	0.59
G1+4.0	0.14	0.13	0.30	0.59	0.60
G1+3.0	0.14	0.13	0.29	0.66	0.70
G1+2.0	0.13	0.12	0.27	0.56	0.61
G1+1.0	0.14	0.12	0.29	0.63	0.64
G1-0.0sb	0.11	0.09	0.25	0.57	0.62
G1-0.0lam	0.10	0.10	0.26	0.57	0.60
G1-1.0	0.12	0.09	0.27	0.67	0.71
G1-3.0	0.07	0.06	0.22	0.55	0.44

Abbreviations: St, sterane; dia, diasterane.

n=90	%C_{27} Sterane (C_{27}-C_{29})	%C_{28} Sterane (C_{27}-C_{29})	%C_{29} Sterane (C_{27}-C_{29})	C_{27}/C_{29} Sterane	C_{28}/C_{29} Sterane	3-Methylhopane Index (%)	Hopane/ Sterane
Average	**29**	**11**	**60**	**0.50**	**0.20**	**9.0**	**2.9**
Stdev	**6**	**2**	**7**	**0.18**	**0.05**	**4.9**	**3.6**
Median	**27**	**11**	**61**	**0.45**	**0.19**	**8.3**	**1.6**
Max	**48**	**18**	**74**	**1.29**	**0.39**	**21.2**	**19.5**
Min	**17**	**7**	**37**	**0.23**	**0.11**	**1.7**	**0.1**

Table 6.3: Selected lipid biomarker ratios typical of Late Ordovician and early Silurian rock extracts.